AN INVESTIGATION INTO THE STAND-UP TIME OF STOPES AT THE BIRCHTREE MINE, THOMPSON, MANITOBA

A Thesis Submitted to the College of

Graduate and Postdoctoral Studies

In Partial Fulfillment of the Requirements

For the Degree of Master of Science

In the Department of Civil, Geological and Environmental Engineering

University of Saskatchewan

Saskatoon

By

MATTHEW VIOLOT

PERMISSION TO USE

In presenting this thesis in partial fulfillment of the requirements for a Postgraduate degree from the University of Saskatchewan, I agree that the Libraries of this University may make it freely available for inspection. I further agree that permission for copying of this thesis in any manner, in whole or in part, for scholarly purposes may be granted by the professor or professors who supervised my thesis work or, in their absence, by the Head of the Department or the Dean of the College in which my thesis work was done. It is understood that any copying or publication or use of this thesis or parts thereof for financial gain shall not be allowed without my written permission. It is also understood that due recognition shall be given to me and to the University of Saskatchewan in any scholarly use which may be made of any material in my thesis.

DISCLAIMER

Reference in this thesis to any specific commercial products, process, or service by trade name, trademark, manufacturer, or otherwise, does not constitute or imply its endorsement, recommendation, or favoring by the University of Saskatchewan. The views and opinions of the author expressed herein do not state or reflect those of the University of Saskatchewan, and shall not be used for advertising or product endorsement purposes.

Requests for permission to copy or to make other uses of materials in this thesis/dissertation in whole or part should be addressed to:

Head of the Department of Civil, Geological and Environmental Engineering
University of Saskatchewan
57 Campus Drive
Saskatoon, Saskatchewan S7N 5A9
Canada

OR

Dean
College of Graduate and Postdoctoral Studies
University of Saskatchewan
116 Thorvaldson Building, 110 Science Place
Saskatoon, Saskatchewan S7N 5C9
Canada

ABSTRACT

Open stoping is a common mining method employed in the Canadian mining industry. Extracting large volumes of rock can present stability issues which can affect productivity and safety. Many factors such as changing stress states, rock mass structure, and intact rock strength can contribute to instability. One factor not commonly assessed when examining stope stability is exposure time. With increased exposure time, the rock quality of the opening tends to degrade. Birchtree Mine located in Thompson, Manitoba, is the focus of this study due to the time dependent instability that has been observed.

For the proposed project, an empirical method was chosen since these methods can easily be updated with future case histories to better reflect onsite conditions. Few empirical methods exist for assessing exposure time for open stope mining. The most common method of incorporating time with stability is Bieniawski's 1989 RMR Stand-up Time Graph. As part of this project the original data used to create the RMR Stand-up Time Graph was reinterpreted so it could be plotted on the Stability Graph, which is used for open stope design.

Case histories from the Birchtree mine, along with the original database for Bieniawski's empirical method, have been examined. Comparisons were conducted to evaluate the accuracy and validity of the Bieniawski and Birchtree data. Other factors that may affect stability and exposure time were also discussed. This research has led to the development of a new empirical design method that incorporates exposure time in the prediction of open stope stability.

ACKNOWLEDGEMENTS

I would first like to thank my supervisor Doug Milne for the invaluable guidance and patience and to the committee members for their assistance my research and writing of this thesis.

I would thank Birchtree Mine for providing me with the resources and financial support to complete my thesis and their continued assistance this process. I would also like to thank Wei Wei and Cecile Kelly for taking the time to answer any questions I had and ensuring that I had access to the resources I required during my time spent at the Birchtree Mine.

The following organizations deserve thanks for their financial support:

- Vale Canada
- Natural Sciences and Research Council of Canada (NSERC)

Finally, I would like to thank all the individuals from the Thompson Mines that supported and continue to support my development.

TABLE OF CONTENTS

PERMISSION TO USE AND DISCLAIMER..... i

ABSTRACT..... ii

ACKNOWLEDGEMENTS..... iii

TABLE OF CONTENTS..... iv

LIST OF TABLES..... viii

LIST OF FIGURES..... ix

CHAPTER 1 - INTRODUCTION..... 1

1.1 Mine Background.....1

1.1.1 Mining Method 1

1.1.2 Regional and Local Geology 4

1.2 Thesis Objective.....7

CHAPTER 2 - LITERATURE REVIEW..... 9

2.1 Rock Classification for Rock Mass Strength Estimates.....9

2.1.1 Rock Quality Designation.....9

2.1.2 Rock Quality Tunneling Index (Q) 11

2.1.3 Rock Mass Rating (RMR) 14

2.1.4 INCO Rock Mass Rating.....15

2.2 Stress Based Numerical Modelling Design 22

2.2.1 Stress Based Failure Criteria Phi & C 22

2.2.2 M & S Stress Based Failure Criteria 24
2.2.3 Time Dependant Failure 26
2.3 Empirical Stope Design Techniques 26
2.3.1 Influence of Geometry on Stability 26
2.3.1.1 Opening span/circle span 27
2.3.1.2 Hydraulic radius 27
2.3.2 Modified Stability Graph 28
2.3.3 Design Approaches that Assess the Degree of Failure 33
2.4 Empirical Design Methods Assessing the Effect of Time on Stability 34
2.4.1 Lauffer's Design Method 34
2.4.2 Stand-up Time Graph 35
2.4.3 Revised Stand-up Time Graph 37
2.4.4 Excavation Rate and Exposure Rate 37
2.5 Other Factors Contributing to Stability 38
2.5.1 Blast Damage 39
2.5.2 Undercutting of the Hanging Wall 40

CHAPTER 3 - DEVELOPMENT OF A STOPE STAND-UP TIME GRAPH 42
3.1 Converting Parameters Between Design Methods 42
3.1.1 Conversion of Span to HR 43
3.1.2 Approximating an N/ Value from the Stand-up Time Database 44
3.1.2.1 Rock Mass Rating to Q' 44
3.1.2.2 A, B, and C factors for N' Stability 45
3.2 Modified and Bieniawski RMR Stand-up Time Graph 48
3.3 Comparing the Modified Stand-up Time Graph and the Modified Stability Graph 57

CHAPTER 4 - FIELD DATA..... 60
4.1 Stope Mining Records.....61
4.2 Laboratory Strength Properties.....64
4.3 Geotechnical Data for Stope Analysis.....64
4.3.1 Average Weighted RQD.....65
4.3.2 Peridotite Concentrations.....67
4.3.3 Overbreak and Underbreak.....68
4.3.4 Stress Modelling with Map3D.....69

CHAPTER 5 - CASE HISTORIES..... 72
5.1 Unstable Case Histories.....72
5.1.1 Case History 29-864.1.....72
5.1.2 Case History 30-848.1.....75
5.1.3 Case History 32-872.1.....77
5.1.4 Case History 33-840.1.....80
5.1.5 Case History 33-848.1.....82
5.1.6 Case History 33-848.2.....85
5.1.7 Case History 33-936.2.....87
5.1.8 Case History 33-916.2.....90
5.2 Successful Case Histories.....92
5.2.1 Case History 32-928.1.....92
5.2.2 Case History 33-916.3.....95

CHAPTER 6 - ANALYSIS..... 98
6.1 Birchtree Case Histories.....98

6.2 Actual vs. Predicted Stand-up Time 103
6.3 Birchtree Data vs. Bieniawski Data 105
6.4 Time Factor Analysis 106
6.5 Other Factors that may Affect Stability 107
6.5.1 Peridotite Concentration vs. Stable and Unstable Surfaces 107
6.5.2 Peridotite Concentration vs. RQD 111
6.5.3 Stress Effects on Time to Failure 112

CHAPTER 7 - CONCLUSIONS 114
7.1 Modified Stability Graph and Bieniawski 114
7.2 Other Factors Influencing Stability 116
7.3 Future Work 117
7.4 Summary 117

REFERENCES 118

APPENDIX A SCANLINE DATA 121
APPENDIX B MAP3D OUTPUTS 126
APPENDIX C ROCK MASS CLASSIFICATION DATA FOR CASE HISTORIES 139

LIST OF TABLES

Table 2.1 J_r values for 10cm and 1m joint profiles..... 16

Table 2.2 Joint alteration values..... 16

Table 2.3 RMR_{76} and RMR_{89} failure criteria..... 23

Table 2.4 Rock mass classes for Lauffer's (1958) Stand-up Time Graph..... 35

Table 4.1 Summary of case histories by stable and unstable surfaces..... 62

Table 4.2 Summary of lab testing for massive sulphide and peridotite samples..... 64

Table 4.3 Rock mechanical properties for various rock types at the Birchtree Mine..... 64

Table 4.4 Example of inputs for calculating average weighted RQD..... 66

Table 4.5 Example of excel sheet used to detect peridotite intervals..... 68

Table 4.6 Summary of data inputs for Map3D stress plots..... 71

Table 5.1 Rock classification data for stope 29-864.1..... 73

Table 5.2 Rock classification data for stope 30-848.1..... 75

Table 5.3 Rock classification data for stope 32-872.1..... 78

Table 5.4 Rock classification data for stope 33-840.1..... 80

Table 5.5 Rock classification data for stope 33-848.1..... 83

Table 5.6 Rock classification data for stope 33-848.2..... 85

Table 5.7 Rock classification data for stope 33-936.2..... 88

Table 5.8 Rock classification data for stope 33-916.2..... 90

Table 5.9 Rock classification data for stope 32-928.1..... 93

Table 5.10 Rock classification data for stope 33-916.3..... 95

Table 6.1 Summary of stope surface information for actual and predicted stand-up times..... 102

LIST OF FIGURES

Figure 1.1a) Isometric of an average blast sequence at Birchtree Mine 3

Figure 1.1b) Isometric of an average blast sequence at Birchtree Mine 3

Figure 1.2 Location of the Birchtree Mine 3

Figure 1.3 Longitudinal of the Birchtree Lower 84 Complex 4

Figure 1.4 Geological formations surrounding the Birchtree Orebody 5

Figure 1.5 Regional geology of the Thompson Nickel Belt 5

Figure 1.6 Major faults located in the Birchtree orebody and host rock 7

Figure 2.1 Idealized example of a 3 metre core run for RQD analysis 10

Figure 2.2a Chart for Q Classification from Rocscience document on rock mass classification.. 12

Figure 2.2b Chart for Q Classification from Rocscience document on rock mass classification.. 13

Figure 2.3 Chart for RMR_{76} classification ratings 15

Figure 2.4 Joint roughness profiles for determining JRC using a profile comb 17

Figure 2.5 Chart for 10 centimetre and 1 metre joint profiles for determining JRC 18

Figure 2.6 Example output from the INCO Blocks Program 21

Figure 2.7 Mohr Coulomb Failure Criterion 24

Figure 2.8 Hydraulic radius as a function of the distance from the center of an xxcavation to the supporting abutments 28

Figure 2.9 Modified Stability Graph 29

Figure 2.10 A Factor graph for N' stability 30

Figure 2.11 Favourable and Unfavourable Joint Sets for Stope Backs 31

Figure 2.12 B Factor graph for N' stability 31
Figure 2.13 C Factor grah for N' stability. 32
Figure 2.14 Modified Dilution Graph and illustration of ELOS definition 33
Figure 2.15 Stand-up Time Graph; letters used are described in Table 2.4 35
Figure 2.16 Bieniawski's (1989) RMR Stand-up Time Graph. 36
Figure 2.17 Hutchinson and Diederichs (1996) RMR Stand-up Time Graph 37
Figure 2.18a Short column charge. Energy goes up or down the hole 39
Figure 2.18b Long column charge. Energy moves sideways toward the open void 39
Figure 2.19 Effects of undercutting on HW stability 40
Figure 2.20 Effect of undercutting due to drill hole deviations 41
Figure 3.1 Aspect ratio vs. maximum hydaulic ratio graph 43
Figure 3.2 Stress Factor A graph for N' stability 46
Figure 3.3 Unfavourable joint orientation for shallow dipping sedimentary deposits 47
Figure 3.4 Joint orientation B Factor for N' stability 47
Figure 3.5 Surface dip C Factor for N' stability 48
Figure 3.6 Modified Stand-up Time Graph 49
Figure 3.7 Bieiawski data plotted on the RMR Stand-up Time Graph for RMR values less than 30 50
Figure 3.8 Bieniawski data plotted on the RMR Stand-up Time Graph for RMR values of 31 to 40 51
Figure 3.9 Bieniawski data plotted on the RMR Stand-up Time Graph for RMR values of 41 to 50 51
Figure 3.10 Bieniawski data plotted on the RMR Stand-up Time Graph for RMR values of 51 to 60 52
Figure 3.11 Bieniawski data plotted on the RMR Stand-up Time Graph for RMR values of 61 to 70 52

Figure 3.12 Bieniawski data plotted on the RMR Stand-up Time Graph for RMR values greater than 70 53

Figure 3.13 Bieniawski data plotted on the Modified Stand-up Time Graph for the time interval 0 to 1 day..... 54

Figure 3.14 Bieniawski data plotted on the Modified Stand-up Time Graph for the time interval 1 day to 1 week..... 55

Figure 3.15 Bieniawski data plotted on the Modified Stand-up Time Graph for the time interval 1 week to 1 month 55

Figure 3.16 Bieniawski data plotted on the Modified Stand-up Time Graph for the time interval 1 to 6 months..... 56

Figure 3.17 Bieniawski data plotted on the Modified Stand-up Time Graph for the time interval 6 months to 1 year 56

Figure 3.18 Bieniawski data plotted on the Modified Stand-up Time Graph for time interval greater than 1 year 57

Figure 3.19 Modified Stand-up Time Graph compared to the Modified Stability Graph..... 59

Figure 4.1 Longitudinal of the Birchtree Lower 84 Complex 60

Figure 4.2 General shape of stopes at the Birchtree Mine..... 63

Figure 4.3 Stress contours in the YZ and XZ planes of the major principle stresses for the 33-848.1 Stope from Map3D 70

Figure 5.1 Longsection and cross-section of the 29-864.1 stope..... 73

Figure 5.2 Modified Stand-up Time Graph: 29-864.1..... 74

Figure 5.3 Isometric of standard stope panel at Birchtree Mine showing the location of the 29-864.1 stope in relation to other stopes in the panel 74

Figure 5.4 Longsection and cross-section for the 30-848.1 stope..... 76

Figure 5.5 Modified Stand-up Time Graph: 30-848.1..... 76

Figure 5.6 Isometric of standard stope panel at Birchtree Mine showing the location of the 30-848.1 stope in relation to other stopes in the panel 77

Figure 5.7 Longsection and cross-section of the 32-872.1 stope 78

Figure 5.8 Modified Stand-up Time Graph: 32-872.1 79

Figure 5.9 Isometric of standard stope panel at Birchtree Mine showing the location of the 32-872.1 stope in relation to other stopes in the panel 79

Figure 5.10 Longsection and cross-section of the 33-840.1 stope 81

Figure 5.11 Modified Stand-up Time Graph: 33-840.1 81

Figure 5.12 Isometric of standard stope panel at Birchtree Mine showing the location of the 33-840.1 stope in relation to other stopes in the panel 82

Figure 5.13 Longsection and cross-section of the 33-848.1 stope 83

Figure 5.14 Modified Stand-up Time Graph: 33-848.1 84

Figure 5.15 Isometric of Standard stope panel at Birchtree Mine showing the location of the 33-848.1 stope in relation to other stopes in the panel 84

Figure 5.16 Longsection and cross-section for the 33-848.2 stope 86

Figure 5.17 Modified Stand-up Time Graph: 33-848.2 86

Figure 5.18 Isometric of standard stope panel at Birchtree Mine showing the location of the 33-848.2 stope in relation to other stopes in the panel 87

Figure 5.19 Longsection and cross-section of the 33-936.2 stope 88

Figure 5.20 Modified Stand-up Time Graph: 33-936.2 89

Figure 5.21 Isometric of standard stope panel at Birchtree Mine showing the location of the 33-936.2 stope in relation to other stopes in the panel 89

Figure 5.22 Longsection and cross-section of the 33-916.2 stope 91

Figure 5.23 Modified Stand-up Time Graph: 33-916.2 91

Figure 5.24 Isometric of standard stope panel at Birchtree Mine showing the location of the 33-916.2 stope in relation to other stopes in the panel 92

Figure 5.25 Longsection and Cross-section of the 32-928.1 stope 93

Figure 5.26 Modified Stand-up Time Graph: 32-928.1 94

Figure 5.27 Isometric of standard stope panel at Birchtree Mine showing the location of the 32-928.1 stope in relation to other stopes in the panel 94

Figure 5.28 Longsection and cross-section of the 33-916.3 stope 96

Figure 5.29 Modified Stand-up Time Graph: 33-916.3 96

Figure 5.30 Isometric of standard stope panel at Birchtree Mine showing the location of the 33-916.3 stope in relation to other stopes in the panel 97

Figure 6.1 Birchtree stable case histories 99

Figure 6.2 Birchtree unstable case histories 100

Figure 6.3 Actual stand-up times vs. predicted stand-up times for stable case histories 101

Figure 6.4 Minimum Observed vs. Maximum Predicted Stand-up Time for Stable Case Histories 104

Figure 6.5 Actual vs. Maximum Predicted Stand-up Time for Unstable Case Histories 104

Figure 6.6 Unstable Birchtree Case histories plotted with Bieniawski data points with stand-up times of two weeks or less 105

Figure 6.7 Peridotite concentrations vs. stable surfaces 109

Figure 6.8 Peridotite concentrations vs. unstable surfaces 110

Figure 6.9 Influence of peridotite on time to failure prediction 110

Figure 6.10 RQD comparison for peridotite and combined RQD of remaining rock types 112

Figure 6.11 Influence of stress on time to failure prediction 113

CHAPTER 1
INTRODUCTION

This research involves an assessment of the influence of time on the stability of underground open stopes. Multiple factors can have an influence on stability, and therefore affect the stand-up time. Some of these factors include stress, structure and rock mass properties. During mining, stresses can be shed away from, or can be concentrated around opening surfaces. Both of these situations can reduce rock mass stability. Rock mass structure, as well as intact rock strength will also have a significant impact on overall stability and the stable stand-up time.

The research has been conducted at the Vale Inc. Birchtree Mine in Thompson Manitoba. The mine is located approximately five kilometres southwest of Thompson, Manitoba (Figure 1.1), and is one of three nickel mines currently operating in the area. Birchtree Mine is approximately 1250m deep.

1.1 Mine Background

Birchtree Mine has experienced instability in some of their stopes. The area of concern for this study is called the Lower 84 Complex. It extends from the 2750 to the 4000 foot sublevel (Figure 1.2) (840 to 1230 metres below ground surface). Stope instability at the mine can range from waste dilution to significant failures that have propagated through multiple levels. Consequences of failure include the increased cost of mining dilution to the loss of a significant volume of ore, all of which can significantly increase mining costs and can cause loss of revenue.

1.1.1 Mining Method

The mining method employed at Birchtree Mine is Vertical Block Mining (VBM). This is an open stoping method similar to Vertical Crater Retreat (VCR) mining in that successive layers of the stope are blasted from bottom to top and ore is left in the stope to provide support. Stopes are

mined in a transverse direction. For each crosscut into the orebody, multiple stopes are extracted in a panel (Figure 1.1b). The number of stopes in a panel depends on the thickness of the orebody. Generally, three separate blasts take place to excavate a stope. Initially a raisebore slot is drilled, which creates a void for the rock to break into. The raisebore is drilled from the overcut to the undercut by first drilling a 0.23 metre diameter pilot hole. Once the pilot hole breaks through into the undercut, a 1.1 metre reaming bit is attached to the drill rods. This bit is then pulled up from the undercut, towards the overcut creating the slot. The pilot hole is reamed to within 1.8 metres of the overcut. Each blast within a stope starts around this raisebore to increase the initial void for subsequent blasts. The first blast is normally small and only contains the breakthrough holes. The second blast is generally two to three times larger than the first, as a larger void exists due to the first blast (Figure 1.1a). The third blast is used to remove the remaining ore/rock and generally has the largest tonnage. The goal of each blast is to optimize the tonnage for the final blast, so that the void is completely full with broken ore. This helps support the walls while the ore is being removed.

Since Birchtree Mine is a deep mine in a high stress environment, they use a pyramidal stress shedding mining sequence. The purpose of a pyramidal mining sequence is to push the stress towards the outer boundary (abutment) of the mining area so stress related instability issues can be reduced.

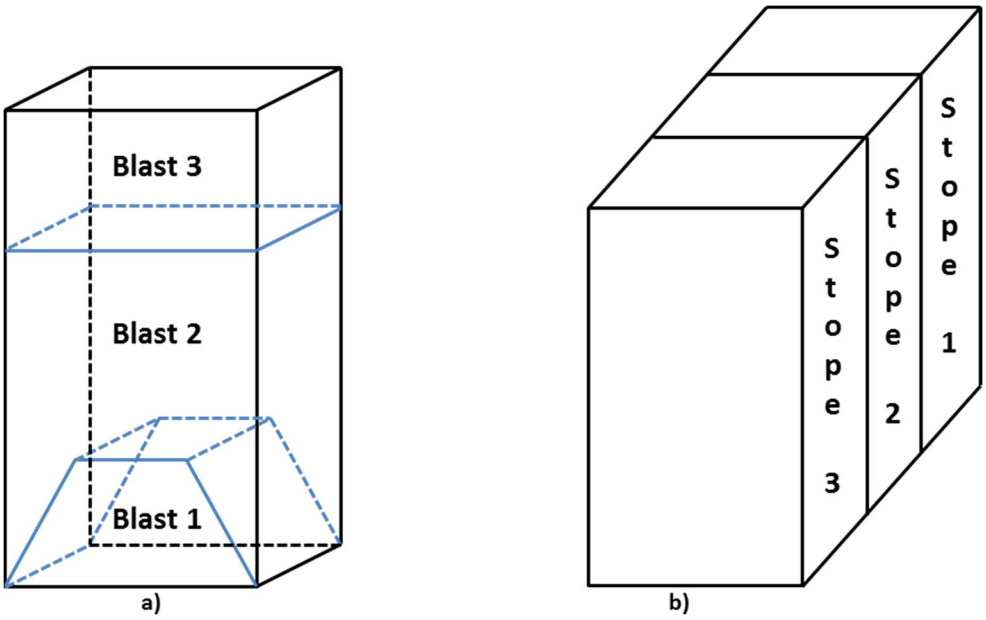

Figure 1.1a) Isometric view of an average blast sequence for Birchtree Mine, b) Isometric view of a panel sequence at Birchtree Mine

Figure 1.2 Location of Birchtree Mine (Google Maps, 2017)

Figure 1.3 Longitudinal of the Birchtree Lower 84 Complex (Birchtree, 2016)

1.1.2 Regional and Local Geology

Birchtree mine is part of the Thompson Nickel Belt (Figure 1.4 and 1.5), which ranges in thickness from 8 to 40km and is approximately 160km long (McDowell et al., 2007). Birchtree Mine is part of the Pipe Formation, which is made up of three separate sub-units (McDowell et al., 2007):

i. P1 – consists of silicate, iron formation, pelitic schist, and quartzite
ii. P2 – consists of sedimentary sulphide and graphite
iii. P3 – iron formation, magnetite, and chert

The Birchtree nickel deposit is located in the P2 schist (Figure 1.5) (Southern, 2017), the host rock for the Birchtree orebody, and ranges in thickness from 3 to 91 metres (Southern, 2011). The ore is classified as a breccia, and is a mixture of sulphide, ultramafic (peridotite), and schist (Southern, 2017). The ore tends to be located between the footwall rocks and the ultramafic peridotite formations, and at times the ore may wrap itself completely around the peridotite formation (Southern, 2011).

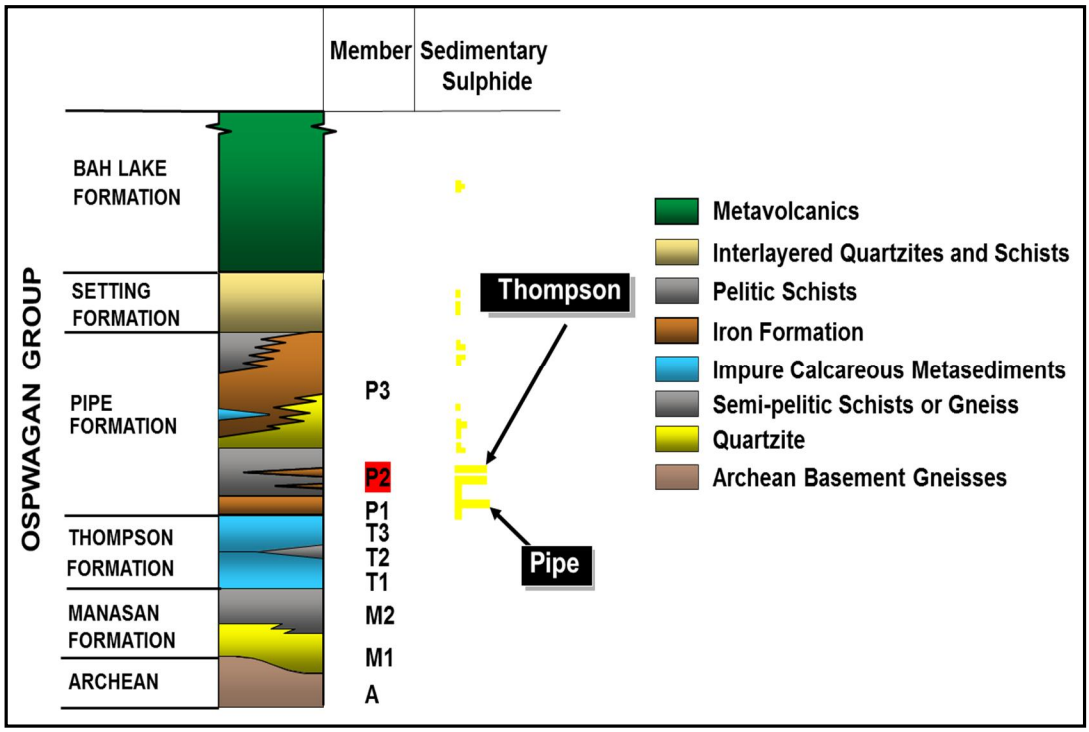

Figure 1.4 Geological formations surrounding the Birchtree orebody (McDowell et. al., 2007)

Figure 1.5 Regional geology of the Thompson Nickel Belt (Eckstrand and Hulbert, 2007)

The ultramafic formations are separated into three categories (Southern, 2011):

i. The core peridotite which consists of the larger formations of peridotite and form the hanging wall of the orebody;
ii. The mineralized peridotite which has sulphide disseminated throughout the formation and can contain nickel grades considered economical to mine and;
iii. The barren peridotite which is classified as a breccia, has little to no associated gradable sulphide material, and is generally the largest contributor of internal dilution within the Birchtree orebody.

The Birchtree orebody is also associated with four major fault zones. The 780 and 1080 faults are located on the footwall side of the orebody (Figure 1.6), and are older than the ore deposit (Southern, 2017). The 1080 fault is the closest of these two structures to the Birchtree ore deposit and is commonly encountered underground. The 1080 fault is generally associated with poor ground conditions, with blocky, wet ground (Southern, 2017). The 609 and 906 faults cross the Birchtree ore deposit, and define the boundaries between the 83, 84, and 85 Complex at the Birchtree Mine (Figure 1.6) (Southern, 2011). The 84 complex is located between these two structures. The 609 and 906 faults are younger than the Birchtree deposit and are generally tightly healed, and associated with dry, competent ground conditions (Southern, 2017).

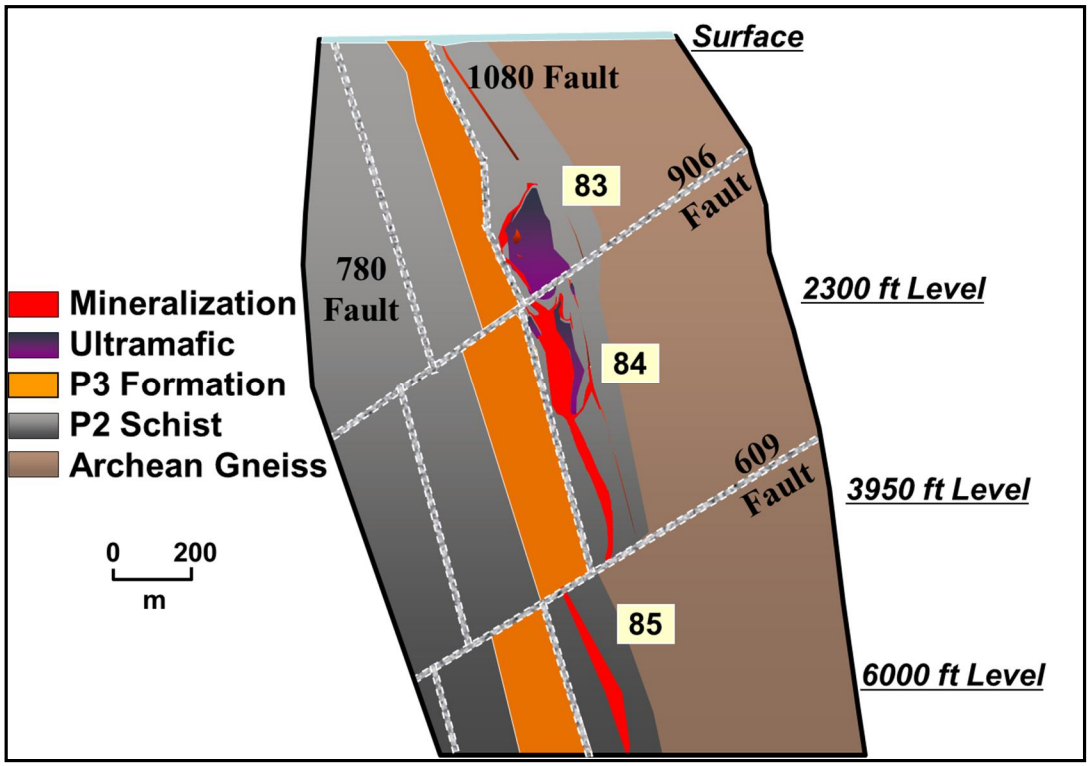

Figure 1.6 Major faults located in the Birchtree orebody and host rock (Birchtree Mine, 2010)

1.2 Thesis Objective

The main objective of this research is to quantify how exposure time affects stope stability at the Birchtree Mine. Many factors simultaneously influence the stability of underground openings including blasting, opening geometry, stress, geology and rock mass conditions.

Exposure time is not commonly assessed when estimating open stope stability, and is defined as the length of time an excavation in left open. The open stopes at Birchtree Mine are backfilled using cemented and uncemented rockfill approximately 2 to 4 weeks after the first blast. This relatively short time between mining and backfilling is due to the significant stope wall instability that can occur at this mine after limited exposure time.

Quantifying the effect of exposure time is accomplished through a case history analysis of multiple stopes including both stable and unstable examples. The case history analysis consists of a compilation of the following information:

- Geology (geological structure and rock types)
- Rock mass classification data (RQD, joint properties, joint orientation)
- Rock mechanical properties (UCS and tensile rock strength, rock density, Young's Modulus)
- Basic stress analysis for each case history to determine stress conditions
- Stope cycle time (exposure time) from the first blast to backfill

Stress modelling programs exist that can account for some of these factors through rock mass classification and factor of safety calculations, however, it can be difficult to determine reliable input data for the programs. Many of the modelling programs require an understanding of the rock mass behaviour before they can accurately reflect mine specific conditions. Empirical methods can more easily be adjusted to mine specific conditions and updated as case histories become available. As the Birchtree project is based on the analysis of case histories, a primarily empirical approach has been taken for analysis.

CHAPTER 2
LITERATURE REVIEW

This section discusses rock mass classification systems and methods that are commonly used for designing underground openings. Both empirical design methods and numerical modelling approaches for underground design are also discussed.

2.1 Rock Classification for Rock Mass Strength Estimates

The rock mass exposed adjacent to tunnels and mined stopes contains joints, shears, and other discontinuities and irregularities that affect the behaviour of the rock mass. Since the volume of rock required to obtain a representative volume of rock for lab testing should be in the order of ten times the joint spacing (Milne, 2016), lab testing has limited application. Rock mass classification has developed into the standard approach used to estimate rock mass properties. There are many different rock classification methods. The main methods applied to Canadian mines are summarized in this section.

2.1.1 Rock Quality Designation (RQD)

The Rock Quality Designation was originally developed by Deere (1963) for use in civil engineering projects. It was later adopted by other geotechnical engineering fields as a way to classify the rock mass (Li et al., 2009). RQD is the most common rock mass classification value used in the mining industry and has been incorporated as a component of the more modern systems.

RQD takes into account the fracture spacing in a rock mass and is defined as the percentage of intact rock that is greater than 10cm in length for a given core run (Equation 2.1). Figure 2.1 shows an idealized drawing of a 3m core run. The blue areas represent intact core greater than 10cm. The RQD for the example in Figure 2.1 would be as follows:

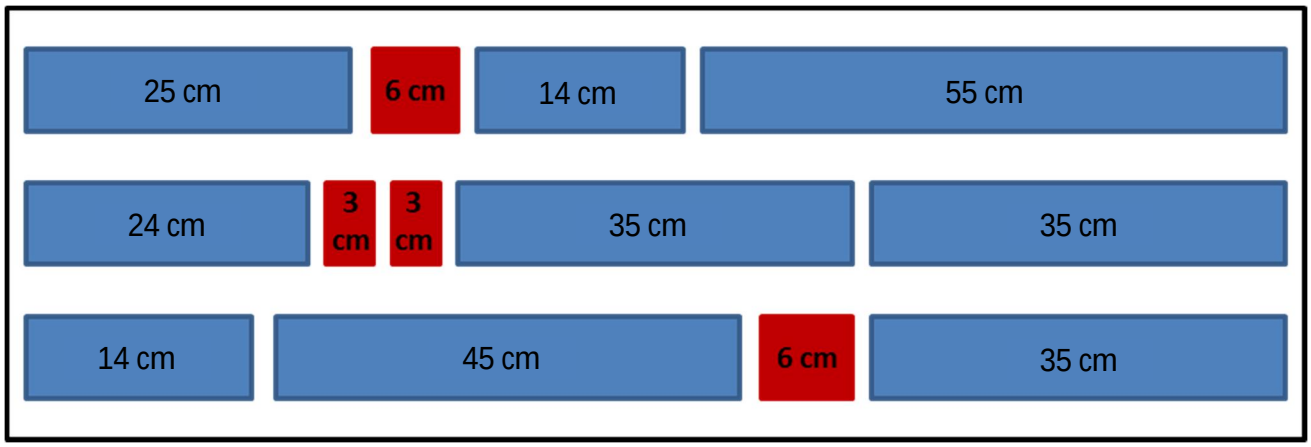

Figure 2.1 Idealized example of a 3 metre core run for RQD analysis

$$RQD = \frac{Length\ of\ Intact\ Core{>}10\ cm}{Total\ Length\ of\ the\ Core\ Run} \times 100 \quad \text{.....(2.1)}$$

$$RQD = \frac{282\ cm}{300\ cm} \times 100$$

$$RQD = 94\%$$

When calculating the RQD, only natural discontinuities are accounted for. Any mechanically induced breaks (i.e. drilling process) are ignored as RQD is used to classify in-situ conditions (Hutchinson and Diederichs, 1996)

Another method for evaluating RQD was introduced by Palmstrom (1982), and is shown in Equation 2.2. This method is used to evaluate RQD based on the number of joints per cubic metre (J_v) and is used to evaluate RQD directly from a given surface exposure.

$$RQD = 115 - 3.3J_v \quad \text{.....(2.2)}$$

RQD can be a very useful value for rock mechanics design, however, it has some drawbacks which include:

- RQD can vary based on the core orientation (Li et al., 2009).
- RQD does not account for joint properties such as alteration, water content, and rock strength (Li et al., 2009).
- RQD is insensitive to changes of joint spacing, if the average joint spacing is over 1m. (Milne et al., 1998).

2.1.2 Rock Quality Tunneling Index (Q)

The Q classification was introduced by Barton et al. (1974) for rock mass classification and tunnel support design. The Q value encompasses many factors which can affect stability and is shown in Equation 2.3, as follows:

$$Q = \frac{RQD}{J_n} \times \frac{J_r}{J_a} \times \frac{J_w}{SRF} \quad \text{.....(2.3)}$$

Where,

Q - rock quality tunnelling index
RQD - rock quality designation
J_n - number of joint sets
J_r - joint roughness
J_a - joint alteration
J_w - joint water
SRF - stress reduction factor

The values of each of the six variables represented in Equation 2.3 are determined based on observed conditions of core or of a rock exposure. Figure 2.2a and 2.2b presents values for each of these variables, based on descriptions of the rock mass.

DESCRIPTION	VALUE	NOTES
1. ROCK QUALITY DESIGNATION	***RQD***	
A. Very poor	0 - 25	1. Where *RQD* is reported or measured as ≤ 10 (including 0),
B. Poor	25 - 50	a nominal value of 10 is used to evaluate *Q*.
C. Fair	50 - 75	
D. Good	75 - 90	2. *RQD* intervals of 5, i.e. 100, 95, 90 etc. are sufficiently
E. Excellent	90 - 100	accurate.
2. JOINT SET NUMBER	J_n	
A. Massive, no or few joints	0.5 - 1.0	
B. One joint set	2	
C. One joint set plus random	3	
D. Two joint sets	4	
E. Two joint sets plus random	6	
F. Three joint sets	9	1. For intersections use ($3.0 \times J_n$)
G. Three joint sets plus random	12	
H. Four or more joint sets, random,	15	2. For portals use ($2.0 \times J_n$)
heavily jointed, 'sugar cube', etc.		
J. Crushed rock, earthlike	20	
3. JOINT ROUGHNESS NUMBER	J_r	
a. Rock wall contact		
b. Rock wall contact before 10 cm shear		
A. Discontinuous joints	4	
B. Rough and irregular, undulating	3	
C. Smooth undulating	2	
D. Slickensided undulating	1.5	1. Add 1.0 if the mean spacing of the relevant joint set is
E. Rough or irregular, planar	1.5	greater than 3 m.
F. Smooth, planar	1.0	
G. Slickensided, planar	0.5	2. J_r = 0.5 can be used for planar, slickensided joints having
c. No rock wall contact when sheared		lineations, provided that the lineations are oriented for
H. Zones containing clay minerals thick	1.0	minimum strength.
enough to prevent rock wall contact	(nominal)	
J. Sandy, gravely or crushed zone thick	1.0	
enough to prevent rock wall contact	(nominal)	
4. JOINT ALTERATION NUMBER	J_a	ϕr degrees (approx.)
a. Rock wall contact		
A. Tightly healed, hard, non-softening,	0.75	1. Values of ϕr, the residual friction angle,
impermeable filling		are intended as an approximate guide
B. Unaltered joint walls, surface staining only	1.0	25 - 35 to the mineralogical properties of the
C. Slightly altered joint walls, non-softening	2.0	25 - 30 alteration products, if present.
mineral coatings, sandy particles, clay-free		
disintegrated rock, etc.		
D. Silty-, or sandy-clay coatings, small clay-	3.0	20 - 25
fraction (non-softening)		
E. Softening or low-friction clay mineral coatings,	4.0	8 - 16
i.e. kaolinite, mica. Also chlorite, talc, gypsum		
and graphite etc., and small quantities of swelling		
clays. (Discontinuous coatings, 1 - 2 mm or less)		

Figure 2.2a Chart for Q classification from Rocscience document on rock mass classification (From Hutchinson and Diederichs, 1996)

4, JOINT ALTERATION NUMBER	J_a	ϕr degrees (approx.)	
b. Rock wall contact before 10 cm shear			
F. Sandy particles, clay-free, disintegrating rock etc.	4.0	25 - 30	
G. Strongly over-consolidated, non-softening clay mineral fillings (continuous < 5 mm thick)	6.0	16 - 24	
H. Medium or low over-consolidation, softening clay mineral fillings (continuous < 5 mm thick)	8.0	12 - 16	
J. Swelling clay fillings, i.e. montmorillonite, (continuous < 5 mm thick). Values of J_a depend on percent of swelling clay-size particles, and access to water.	8.0 - 12.0	6 - 12	
c. No rock wall contact when sheared			
K. Zones or bands of disintegrated or crushed	6.0		
L. rock and clay (see G, H and J for clay	8.0		
M. conditions)	8.0 - 12.0	6 - 24	
N. Zones or bands of silty- or sandy-clay, small clay fraction, non-softening	5.0		
O. Thick continuous zones or bands of clay	10.0 - 13.0		
P. & R. (see G.H and J for clay conditions)	6.0 - 24.0		
5. JOINT WATER REDUCTION	J_w	approx. water pressure (kgf/cm^2)	
A. Dry excavation or minor inflow i.e. < 5 l/m locally	1.0	< 1.0	
B. Medium inflow or pressure, occasional outwash of joint fillings	0.66	1.0 - 2.5	
C. Large inflow or high pressure in competent rock with unfilled joints	0.5	2.5 - 10.0	1. Factors C to F are crude estimates; increase J_w if drainage installed.
D. Large inflow or high pressure	0.33	2.5 - 10.0	
E. Exceptionally high inflow or pressure at blasting, decaying with time	0.2 - 0.1	> 10	2. Special problems caused by ice formation are not considered.
F. Exceptionally high inflow or pressure	0.1 - 0.05	> 10	
6. STRESS REDUCTION FACTOR ***a. Weakness zones intersecting excavation, which may cause loosening of rock mass when tunnel is excavated***		*SRF*	
A. Multiple occurrences of weakness zones containing clay or chemically disintegrated rock, very loose surrounding rock any depth)		10.0	1. Reduce these values of *SRF* by 25 - 50% but only if the relevant shear zones influence do not intersect the excavation
B. Single weakness zones containing clay, or chemically disintegrated rock (excavation depth < 50 m)		5.0	
C. Single weakness zones containing clay, or chemically disintegrated rock (excavation depth > 50 m)		2.5	
D. Multiple shear zones in competent rock (clay free), loose surrounding rock (any depth)		7.5	
E. Single shear zone in competent rock (clay free). (depth of excavation < 50 m)		5.0	
F. Single shear zone in competent rock (clay free). (depth of excavation > 50 m)		2.5	
G. Loose open joints, heavily jointed or 'sugar cube', (any depth)		5.0	

Figure 2.2b Chart for Q classification from Rocscience document on rock mass classification (From Hutchinson and Diederichs, 1996)

A more common form of the Q classification used in mining is known as the modified Q or Q' value which does not apply for the stress reduction factor and is calculated, as shown in Equation 2.4:

$$Q' = \frac{RQD}{J_n} \times \frac{J_r}{J_a} \times J_w \quad \text{.....(2.4)}$$

The above equation can be broken into three terms for classifying a rock mass. The RQD/Jn term represents the block size, Jr/Ja represents the shear strength between the rock joints, and Jw represents the water pressure (Hoek and Brown, 1980).

2.1.3 Rock Mass Rating (RMR)

The Rock Mass Rating system was developed by Bieniawski (1976, 1989). This system classifies rock quality according to five separate categories: rock strength, RQD, joint spacing, joint water and joint condition (Figure 2.3), as well as, a joint orientation term. The correction for joint orientation is not commonly used in mining, and the RMR term is referred to as the modified RMR or RMR' when this correction factor is ignored. The RMR value is the total sum of the ratings from each category. Two RMR systems that are commonly used today are the RMR_{76} and RMR_{89} systems. For the purposes of this thesis, RMR_{76} was used.

RMR_{76} Classification Ratings

Description	*MPA*	*Rating*
Very low	1-25	0-2
Low	25-50	4
Medium	50-100	7
High	100-200	12
Very high	>200	15

Description	*Inflow*	*Rating*
Dry	0	10
Moist	>25L/min	7
under moderate water pressure	25-125L/min	4
sever water problems	>125L/min	0

RQD	*Joints/m^3*	*Rating*
90-100%	0-8	20
75-90%	8-12	17
50-75%	12-20	13
25-50%	20-27	8
<25%	>27	3

Description	*Distance*	*Rating*
very wide	>3m	30
wide	1-3m	25
moderately close	.3-1m	20
close	.05-.3m	10
very close	<.05m	5

Joint Description	**Rating**
• Very Rough, **not continuous,** no separation - hard joint wall rock	25
• Slightly rough surfaces, separation <1mm - **hard joint wall rock**	20
• Slightly rough surfaces, separation < 1mm - **soft joint wall rock**	12
• **Slickensided or gouge**, <5mm thick or Open 1– 5mm	6
• **Soft gouge > 5mm thick** or Joints open > 5mm	0

Figure 2.3 Chart for RMR_{76} classification ratings (After Bieniawski, 1976)

2.1.4 INCO Rock Mass Rating

The INCO Rock Mass Rating (IRMR) system was developed in the early 1990's and tried to use practical aspects of several classification systems currently in use. The IRMR system is a modified RMR_{76} system that combines the Q classification assessment of joint roughness as well as research developed for block size analysis. The IRMR system uses the five basic parameters developed to calculate RMR_{76}, which include factors for RQD, rock strength, joint spacing, joint condition, and groundwater. The weighting for RQD, intact rock strength and groundwater are unchanged from RMR_{76}. The weighting for spacing is based on a block size defined by the average edge length of intact rock blocks (D_{50}) (Folmer, 1992). The joint condition is based upon joint roughness and alteration and uses the terms developed for the rock quality Q classification system.

The joint roughness (Table 2.1) and joint alteration (Table 2.2) values are important classification parameters used for determining rock quality Q (Section 2.1.2). These values are obtained during

scanline surveys that are conducted by geology staff to estimate support requirements at the Birchtree Mine. Joint roughness can be determined using a profile comb to obtain a Joint Roughness Coefficient (JRC) value (Figure 2.4). Joint roughness can also be determined by measuring the 10cm and 1m joint profiles (Figure 2.5) (Barton, 1982). These two values are then multiplied together to obtain J_r (Milne et al., 1991). In the Q classification system, joint alteration values are subjectively determined by evaluating the condition of the joint set (infilling, mineralization, etc.) and comparing that to a set of generally accepted descriptions with associated values (Figure 2.2a).

Table 2.1 Jr values for 10cm and 1m joint profiles (After Milne et al., 1991)

10 cm Profile	Description
1.0	Smooth joint. Joint Roughness Coefficient less than 10
1.5	Rough joint. Joint Roughness Coefficient greater than 1.5
1 m Profile	**Description**
1.0	Planar joint. Amplitude less than 1.0 cm
1.5	Planar to wavy. Amplitude between 1.0 cm and 2.0 cm
2.0	Wavy joints. Amplitude greater than 2.0 cm

Table 2.2 Joint alteration values (After Milne et al., 1992)

Ja Value	Description
1.0 to 1.5	Surface can be scratched with a knife.
2.0	Surface can be scratched with a fingernail. Surface feels slippery.
4.0	Surface can be dented with a fingernail. Surface feels slippery.

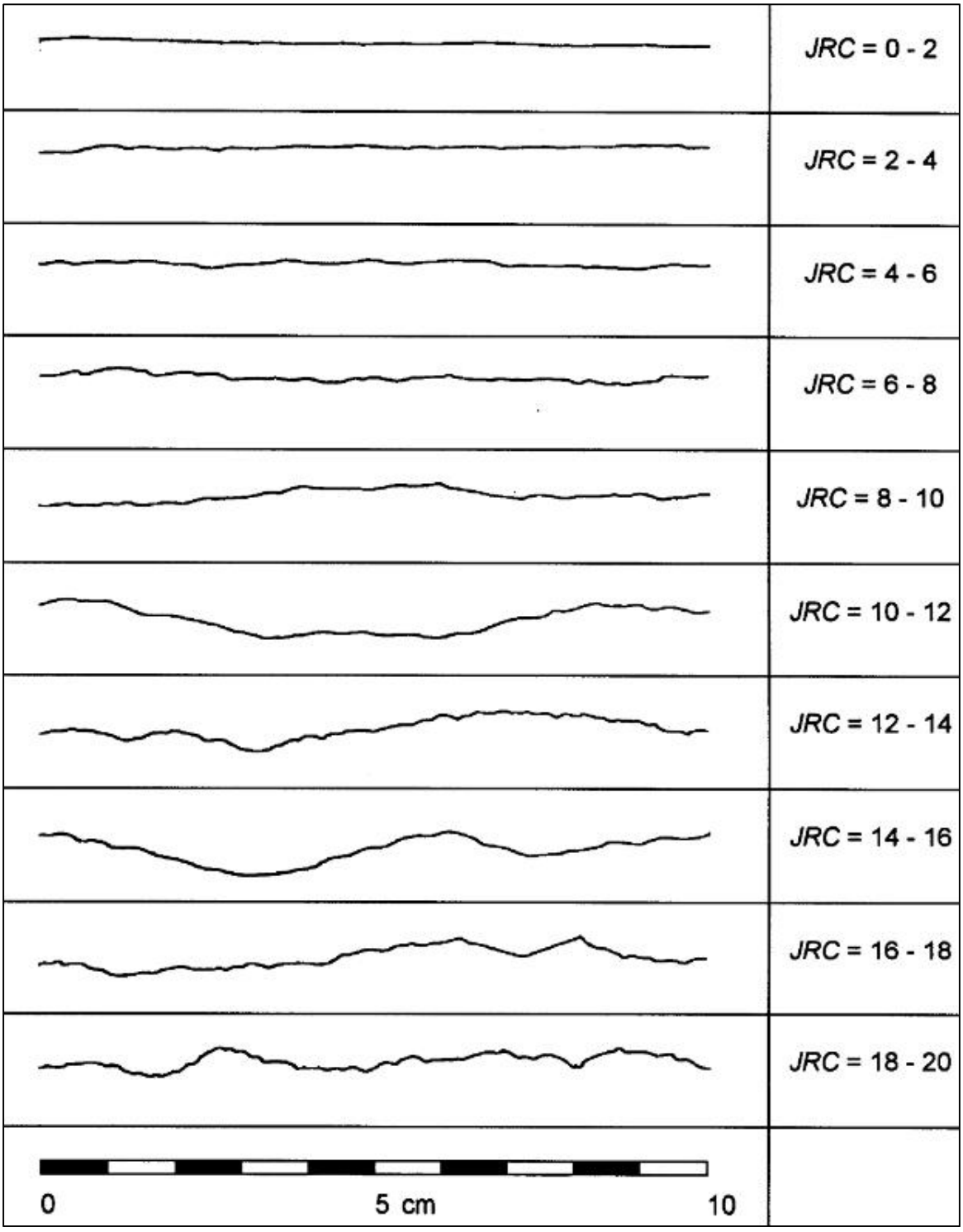

Figure 2.4 Joint roughness profiles for determining JRC using a profile comb (After Barton and Choubey, 1977)

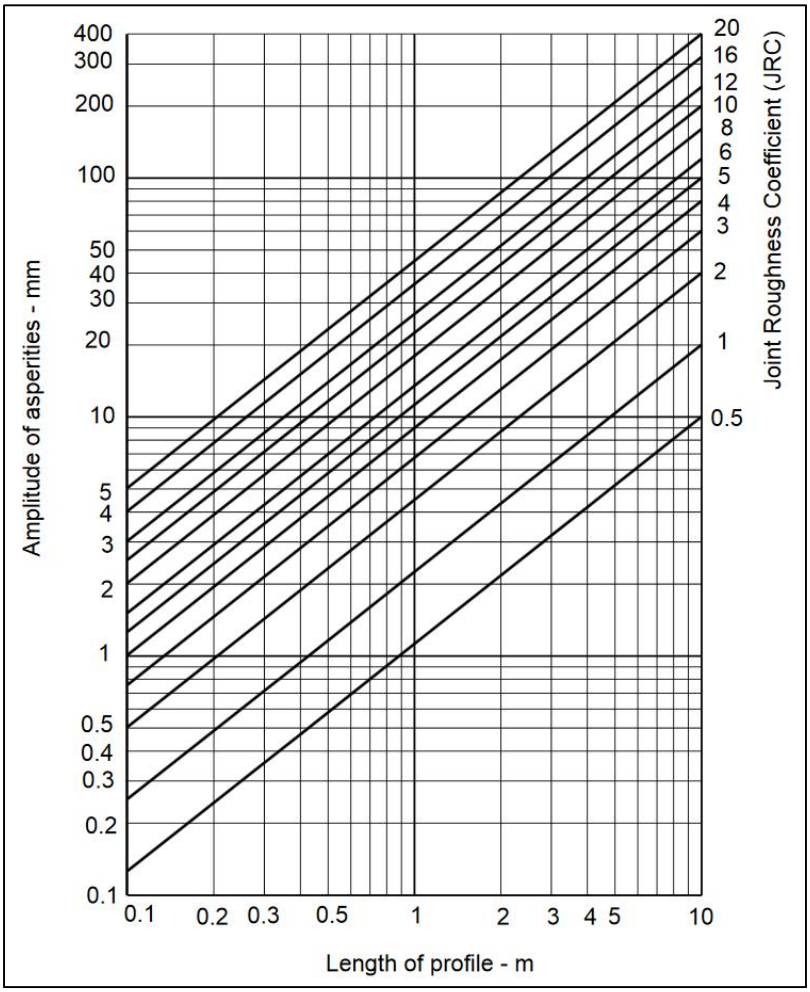

Figure 2.5 Chart for 10 centimetre and 1 metre joint amplitudes for determining JRC (Barton, 1982)

At Birchtree J_r values follow the more commonly used chart for 10 centimetre and 1 metre profile lengths (Figure 2.5), however, their joint alteration values are obtained from a less commonly used method generally associated with areas that have undergone heavy shearing/faulting conditions. For this J_a assessment, the values range from 1-20. The system that Birchtree uses is a modified version of this method that uses joint aperture to determine the J_a value. The Birchtree joint alteration values (J_a) are classified as follows:

i. 0.75 – tightly healed
ii. 1.00 – parting less than 1mm; no infilling
iii. 4.00 – parting between 1mm and 5mm; infilling less than 5mm
iv. 10.00 – parting between 5mm and 10mm; infilling between 5mm and 10mm
v. 20.00 – parting greater than 10mm; infilling greater than 10mm

The second term that differs from a standard RMR_{76} classification is the assessment of joint spacing. In the RMR_{76} system, an average joint spacing is estimated based on the presence of three joint sets. If fewer or more than three joint sets are present, a subjective assessment is made. In the IRMR system at Birchtree Mine, the average block size D_{50}, is calculated using an AutoCAD sub-routine. This sub-routine is called the INCO Blocks program. This program uses information from scanlines that are collected by the geological group at the mine. The data collected from each scanline is input into the INCO Blocks program which generates a three dimensional estimation of jointing in the area of the scanline. It assesses these joints by extending the mapped joint sets into a defined cubic volume of $22.9m^3$. This limited volume is set to avoid creating infinitely long joint sets as they continue to move away from the scanline area.

The final difference between the INCO Rock Mass Rating and the modified RMR_{76} system is in the assessment of RQD. In the IRMR system the weighting for RQD is set to a constant value of 19.5, corresponding to an RQD of 98.5%. This appears to be a significant drawback to the IRMR system because the average RQD for Birchtree's rock mass is significantly lower than this, in the range of 50% to 70%. It may be that the original developers of the IRMR system determined that the overall effect of variable joint spacing at the Birchtree Mine was properly assessed with the D_{50} term and a constant for RQD. Records documenting the early development and application of the IRMR system were not available to verify this.

Equation 2.5 is used to calculate IRMR.

$$IRMR = 19.5 + UCS + D_{50} + J_r + J_a + J_w \quad \text{.....(2.5)}$$

UCS (Unconfined Compressive Strength) represents the rock strength rating, and the J_r, J_a, and J_w terms represent the joint conditions as outlined in Section 2.1.2.

The INCO Blocks program is used to generate the average block size as defined by the D_{50} value (Figure 2.6). This value, along with rock mass classification data collected from scanlines, is then used to generate an IRMR value that is used to determine rock support requirements. Data collected in the scanline includes:

i. Joint Roughness (Jr)
ii. Joint Alteration (Ja)
iii. Rock Type
iv. Structure (joint, shear, schistosity, foliation)
v. Length of feature
vi. Dip, dip direction, and strike

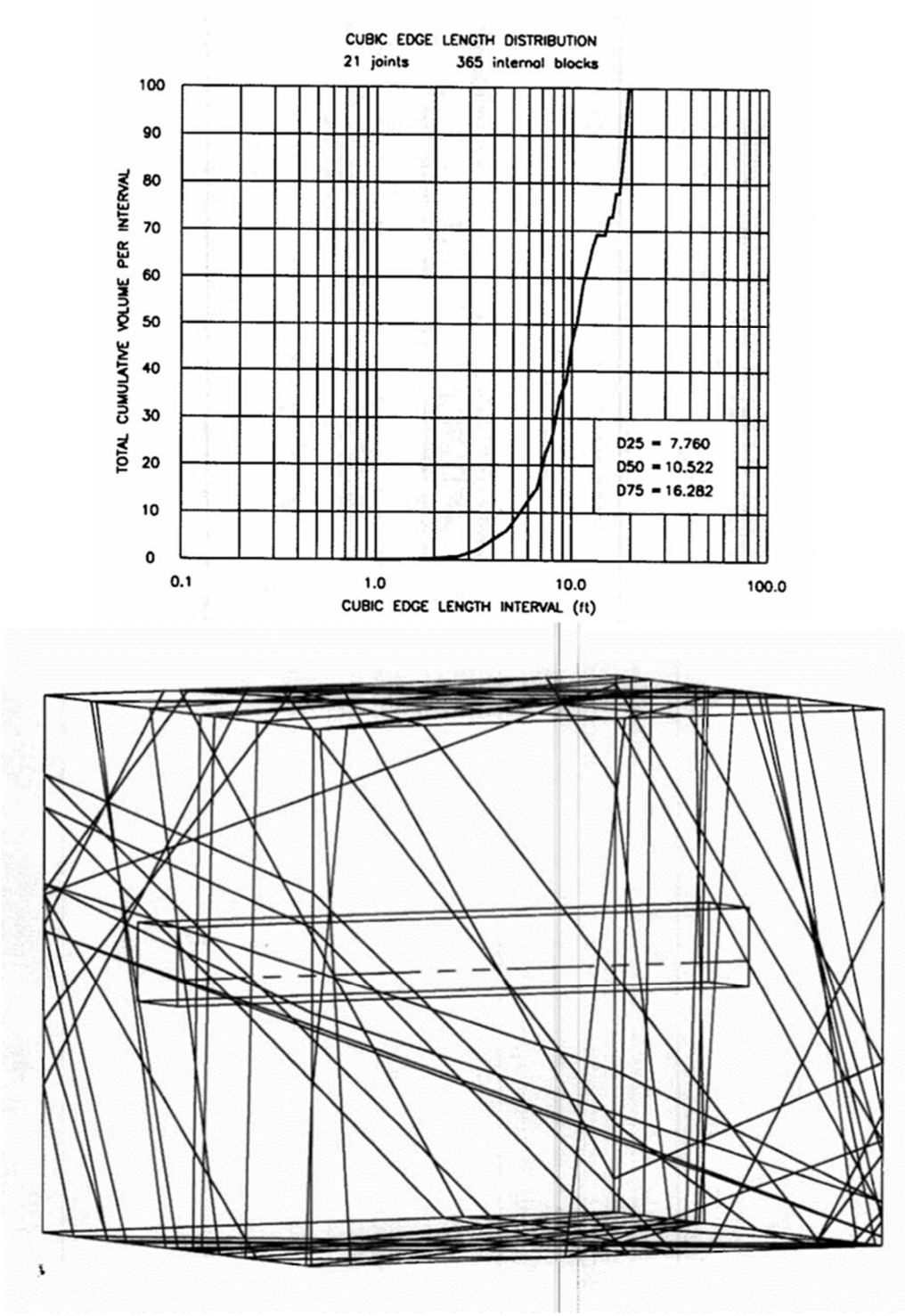

Figure 2.6 Example output from the INCO Blocks program (Birchtree Scanline Binder, 2002)

2.2 Stress Based Numerical Modelling Design

Design techniques for underground mining combine estimated rock mass strength properties with loading conditions acting on the rock mass. Numerical stress modelling based design methods consider stress driven failure and apply primarily empirical based failure criteria (often based on rock classification) to estimate stability. Stresses induced around underground excavations can be modelled with many different stress modelling packages, however, complex stope geometries often require three dimensional stress modelling programs. Detailed input data on the condition of the rock mass, and time related behaviour of the rock was not available so it was felt that a more sophisticated modelling package would not be warranted. Boundary element programs do not need the computer resources that discrete element models require and are generally more user friendly. Two such programs include Map3D and Rocscience's Examine 3D. Map3D is the modelling package used at the mine site, so it was chosen for this research.

Map3D is a three-dimensional boundary element modelling software package. This program allows the importing of stope geometries through the use of AutoCAD and the evaluation of individual stopes, or complete mine complexes, by allowing the input of mine sequences. Map3D allows users to define their stress contours based on equations that reflect mine specific conditions. Once induced stresses are calculated by the Map3D boundary element program, failure can be assessed based on a choice of several failure criteria.

2.2.1 Stress Based Failure Criteria Phi & C

For Mohr Coulomb failure criterion analysis, rock mass classification values are related to phi and c through RMR classification. Table 2.3, developed by Bieniawski (1976 & 1989), related RMR_{76} and RMR_{89} to phi and c. Table 2.3 is separated into five categories, each of which has a corresponding range of cohesion (c) and friction values (φ) based on both RMR_{76} and RMR_{89}.

Table 2.3 RMR76 and RMR89 failure criteria (After Bieniawski, 1976 & 1989)

RMR_{76}	100 - 81	80 - 61	60 - 41	40 - 21	<20
Cohesion (kPa)	> 300	200 - 300	150 - 200	100 - 150	< 100
Friction (^{O})	> 45	40 - 45	35 - 40	30 - 35	< 30
RMR_{89}	100 - 81	80 - 61	60 - 41	40 - 21	<20
Cohesion (kPa)	> 400	300 - 400	200 - 300	100 - 150	< 100
Friction (^{O})	> 45	35 - 45	25 - 35	15 - 25	< 15

The Mohr Coulomb Failure Criterion is one of the more common methods used for evaluating stress based failure for underground design. It is a measure of the peak stress at failure with a given confining pressure (Figure 2.7). When evaluating underground designs with stress modelling software, the Mohr Coulomb Failure Criterion is used to determine a factor of safety (FS) against stress driven failure. The factor of safety is calculated using Equation 2.6.

$$FS = \frac{c+\sigma_3 tan\varphi}{\sigma_1} \quad \text{.....(2.6)}$$

Where:

c is cohesion,

σ_3 is the confining stress,

φ is friction; and,

σ_1 is the peak stress at failure

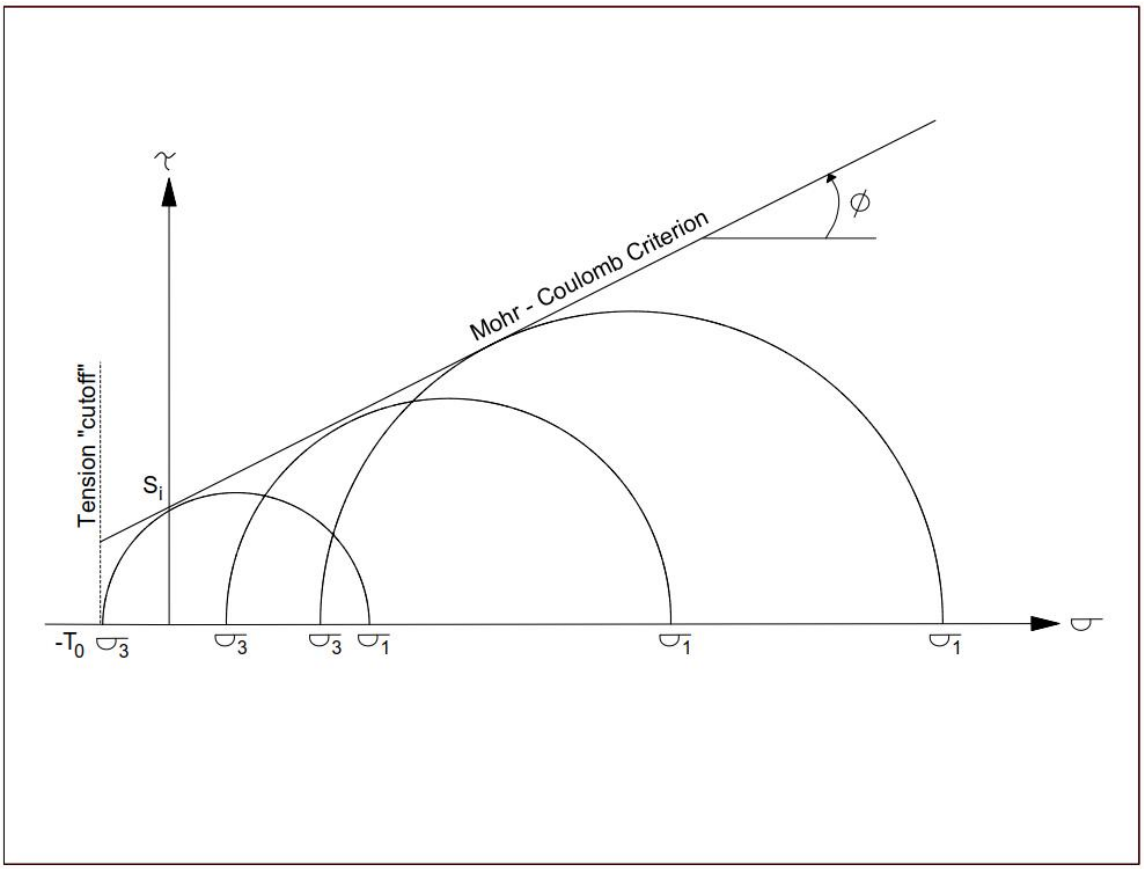

Figure 2.7 Mohr Coulomb Failure Criterion (After Goodman, 1989)

2.2.2 M & S Stress Based Failure Criteria

Hoek and Brown (1980) developed the m & s failure criterion, which calculates a factor of safety for stress based failure in modelling programs. The m & s failure criterion was developed to provide a means of combining laboratory results with field observations for the design of underground openings (Hoek & Brown, 1980). M & s failure criterion is separated into two categories; disturbed (Equations 2.7 & 2.8) (Hoek & Brown, 1980) and undisturbed (Equations 2.9 & 2.10) (Hoek & Brown, 1980). They are calculated with the following equations:

$$\frac{m}{m_i} = exp\left(\frac{RMR-100}{14}\right) \quad \text{.....(2.7)}$$

$$s = exp\left(\frac{RMR-100}{6}\right) \quad \text{.....(2.8)}$$

$$\frac{m}{m_i} = exp\left(\frac{RMR-100}{28}\right) \quad (2.9)$$

$$s = exp\left(\frac{RMR-100}{9}\right) \quad (2.10)$$

Where (Hoek and Brown, 1980):

m is a rock mass constant

s is a rock mass constant

m_i is m for intact rock

In most modern design applications that use the m & s failure criterion, the disturbed equations are no longer considered, as they are too conservative for underground design. The most significant limitation to this evaluation method is that it applies to uniform and isotropic rock masses (Hoek & Brown, 1988). The equations for m & s assume that the material properties are the same in all directions, because they are trying to evaluate a rock mass in a manner similar to soil mechanics, where the m & s criteria are replacing phi and c. The m & s failure criterion is used to determine a factor of safety against stress driven failure. The factor of safety is calculated using Equation 2.11.

$$FS = \frac{\sigma_3 + \sqrt{m\sigma_3 + s\sigma_c^2}}{\sigma_1} \quad (2.11)$$

Where (Hoek and Brown, 1988):

σ'_1 is the major principal stress

σ'_3 is the minor principal stress

σ_c is the UCS for the rock

2.2.3 Time Dependent Failure

Time dependent failure can be thought of as more of a process than a failure criterion. Failure occurs when the stresses around an underground opening exceed the peak strength of the rock mass. When this occurs, the rock mass can no longer support these stresses and they are shed to the surrounding rock mass leaving a zone of failed material around the perimeter of the opening. This zone of failed material will not immediately fall into the opening as the rock mass maintains some residual strength. This is called the post peak strength of the rock mass. The rock mass will continue to undergo failure, pushing the stresses further away from the opening, until the maximum induced stress no longer exceeds the rock mass strength. As stresses are shed further away from the opening, the zone of failed ground will continue to increase, until the residual strength can no support it, and it sloughs into the open void.

2.3 Empirical Stope Design Techniques

As with stress modelling design techniques, empirical design techniques combine estimated rock mass strength properties with loading conditions acting on the rock mass. Most of the commonly used empirical design methods incorporate four key input parameters for design:

i. Rock mass classification (Section 2.1)
ii. Opening geometry
iii. Rock mass factors which influence stability (including stress)
iv. Case histories of stable and unstable stopes

2.3.1 Influence of Geometry on Stability

The geometry of underground openings has a significant effect on stability. As opening size increases, changes to the stress field will extend farther from the opening. For varied opening geometries, the magnitude of stress at the edge of openings will change. Also, as the surface of an opening increases in size, the distance to the supporting abutments increases. Numerical stress modelling design techniques quantify the stress related changes due to opening geometry. Empirical modelling techniques consider the distance to supporting abutments.

2.3.1.1 Opening span / circle span

For the stability of simple excavations, like tunnels, the opening geometry of the roof is defined as the span or width of the tunnel. From the centre of a tunnel, the minimum distance to the supporting tunnel walls, or abutments, is half the span. For more complex excavations, like tunnel intersections, a term called circle span is used to define the geometry. Circle span is the largest sized circle that can be drawn on the plan view of a tunnel without intersecting supporting rock (Lang, 1994). For the intersection of two tunnels, the circle span would be root 2 times the span (~ 1.4 x span).

2.3.1.2 Hydraulic radius

In underground stopes, opening geometry is more complicated than in tunnels and an opening surface often obtains significant support from four walls or abutments, rather than two as in the case of tunnels. The hydraulic radius term can account for support from four abutments and is calculated from the following Equation 2.12 (Laubscher, 1977).

$$HR = \frac{Area}{Perimeter} \quad \text{.....(2.12)}$$

To show how hydraulic radius is a function of the distance from the center of an opening to the four supporting abutments in an excavation, hydraulic radius can be expressed as shown in Equation 2.13 (Milne, 1997)

$$HR = \frac{2}{\frac{1}{0.5a}+\frac{1}{0.5a}+\frac{1}{0.5b}+\frac{1}{0.5b}} \quad \text{.....(2.13)}$$

Where:

a and b is the length of the supporting abutments in an excavation as shown in Figure 2.8.

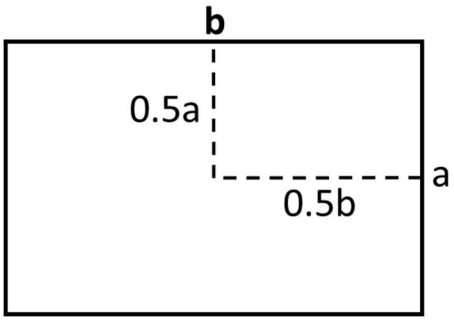

Figure 2.8 Hydraulic radius as a function of the distance from the center of an excavation to the supporting abutments (After Milne, 1997).

The hydraulic radius assesses complex geometries found in underground open stoping, however, this can still be an over simplification of some stope geometries.

2.3.2 Modified Stability Graph

The stability graph method (Figure 2.9) is a commonly used technique for assessing the stability of openings in the Canadian mining industry. Mathews et al. (1981), developed the original Stability Graph. The Modified Stability Graph was further developed by Potvin (1988) and was later updated by Nickson (1992). As of 2010 at total of 483 case histories had been used in its development (Suorineni, 2010). The Modified Stability graph is defined by the following five separate zones:

- Stable zone
- Unsupported transition zone,
- Stable with support
- Supported transition zone
- Unstable zone

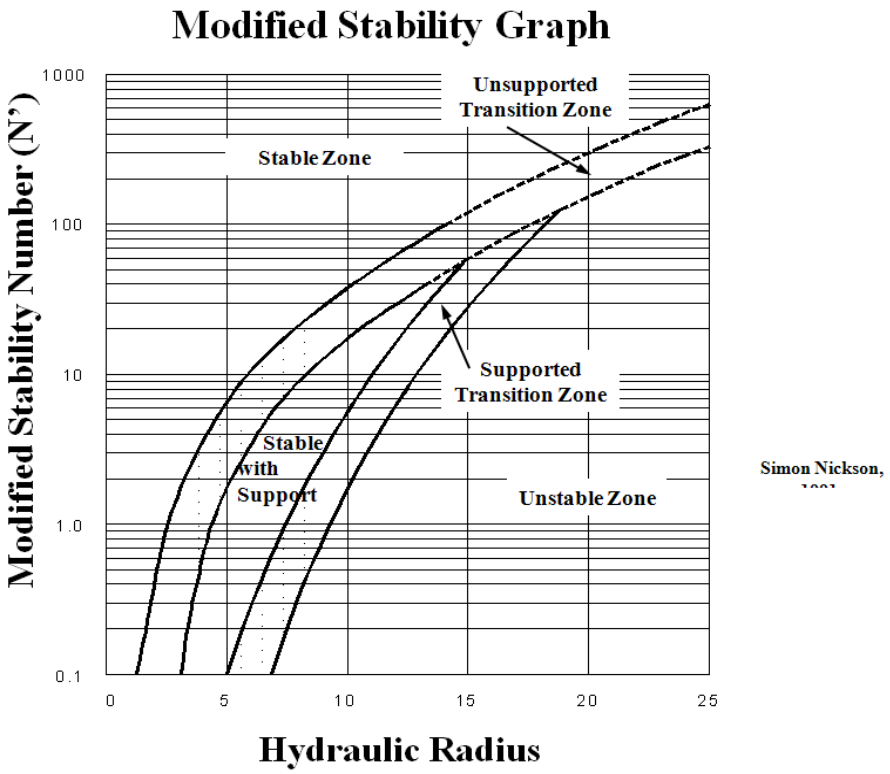

Figure 2.9 Modified Stability Graph (Nickson, 1992)

Each stope surface is classified into a category by two factors: the N' Stability Number and the Hydraulic Radius. The hydraulic radius has been discussed in Section 2.3.1.2. N' is calculated using Equation 2.14.

$$N' = Q' \times A \times B \times C \quad \text{.....(2.14)}$$

Where:

N' - stability number

Q'- rock quality tunnelling index excluding stress reduction factor

A - stress state factor

B - factor based on the angle between the joint orientation and the excavation surface analyzed

C - surface dip correction factor

The A factor assesses the stress state of the surface being examined. The A factor is based on the ratio of induced stress to the unconfined compressive strength of the rock (Figure 2.10) and ranges

between a value of 0.1 and 1. The lower value represents a high stress condition, while the larger value represents a low or relaxed stress condition. To obtain a value of 0.1, the induced stress would be half the UCS or greater. It should be noted that in Yves Potvin's thesis (Potvin, 1988), only 36 of the 154 cases of unsupported wall stability had an A value less than 1.0. This limited amount of data for high stress conditions adds uncertainty to the design methods assessment of high stresses.

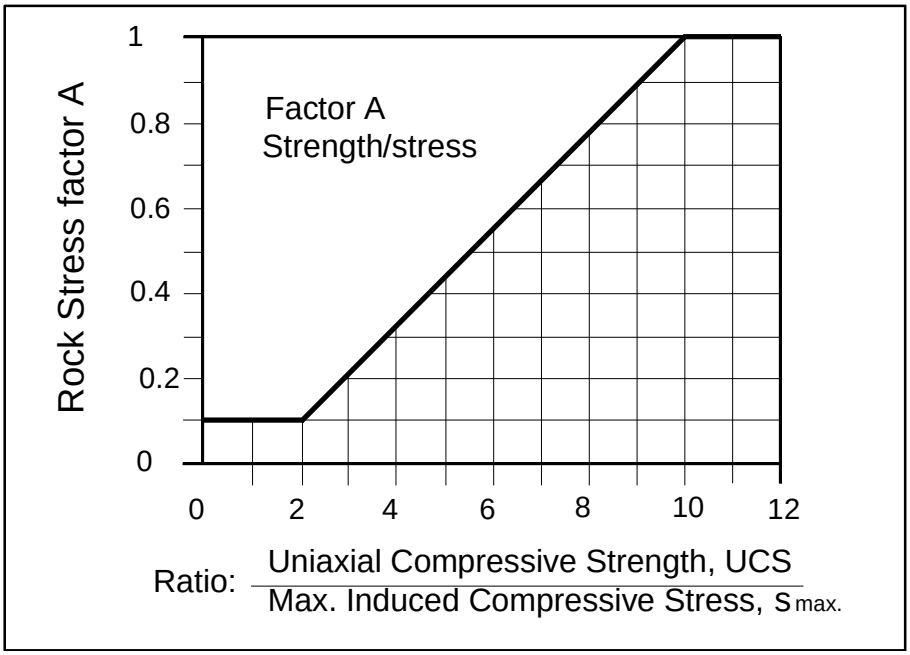

Figure 2.10 A factor graph for N' stability (After Potvin, 1988: from Hutchinson and Diederichs, 1996)

The B factor accounts for the angle between the assessed surface and the joint set most likely to control stability. It is defined as the angle between the controlling joint set and the surface under examination. Figure 2.11 shows a sub-horizontal and vertical joint set that demonstrate the two extremes represented on the B factor graph (Figure 2.12). If assessing back stability, Figure 2.11a would represent the worst case scenario. For the sub-horizontal joint set dipping at 10 to 30 degrees to a surface, the drop in vertical stress normal to the back, would limit the joint clamping stress, and the high horizontal stress would drive shear deformation. For sub-horizontal joints dipping between 20 and 30 degrees, a B factor of 0.2 is used for calculating the N' Stability Number (Figure 2.12). A joint set dipping at 90 degrees to a surface will be the most favourable for stability. For joints sets perpendicular to a surface, the resulting horizontal stress increase would clamp the joint set, giving a B factor of 1 for calculating the N' Stability Number (Figure 2.12).

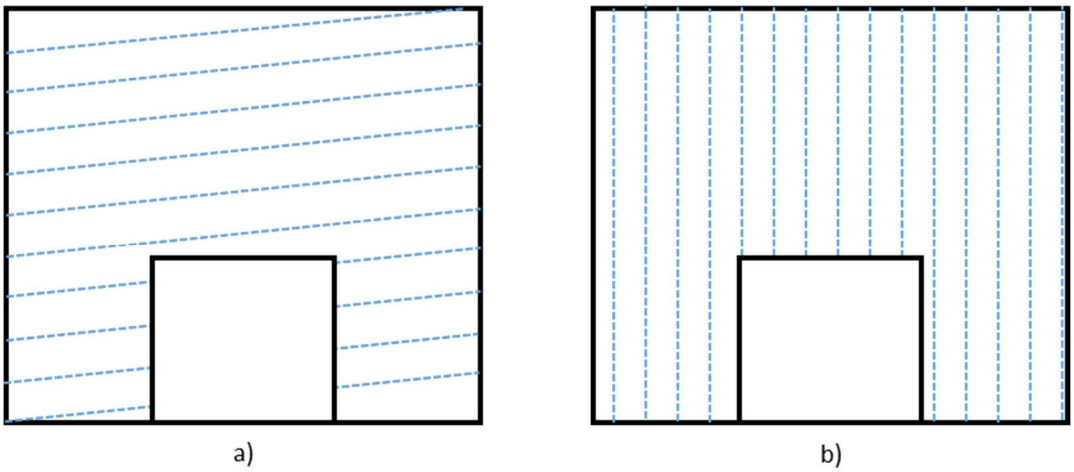

Figure 2.11 Favourable and unfavourable joint sets for stope backs

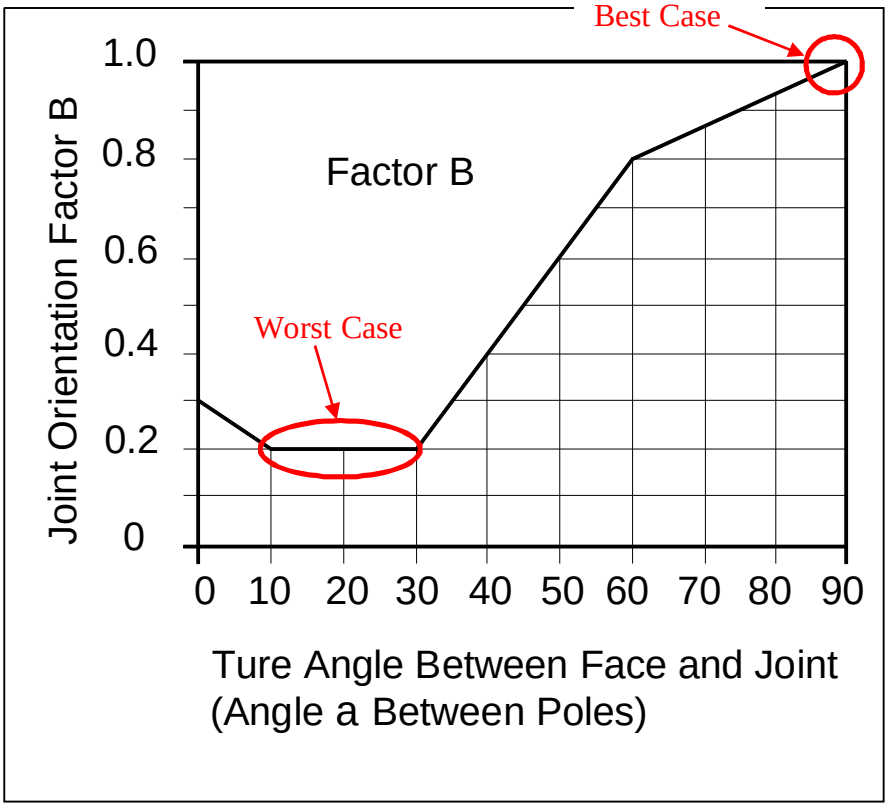

Figure 2.12 B factor graph for N' stability (After Potvin, 1988: from Hutchinson and Diederichs, 1996)

The C factor is a measure of the dip of the surface under examination. The values range from 2 for a horizontal surface, to 8 for a vertical surface (Figure 2.13).

The stability graph method is easy to use and gives a general approximation of how an underground opening will perform; however, some limitations exist. As stated by Suorineni (2010) the main problems that exist with the current Stability Graph method are as follows:

- It does not properly classify complex geometries,
- Faults and other geological structures are ignored,
- Stand-up time is not accounted for and;
- It ignores the effect of blast damage.

Another shortcoming of this approach is that instability or stope failure is not quantified. This is addressed in graphs that look at stope dilution or depth of surface failure.

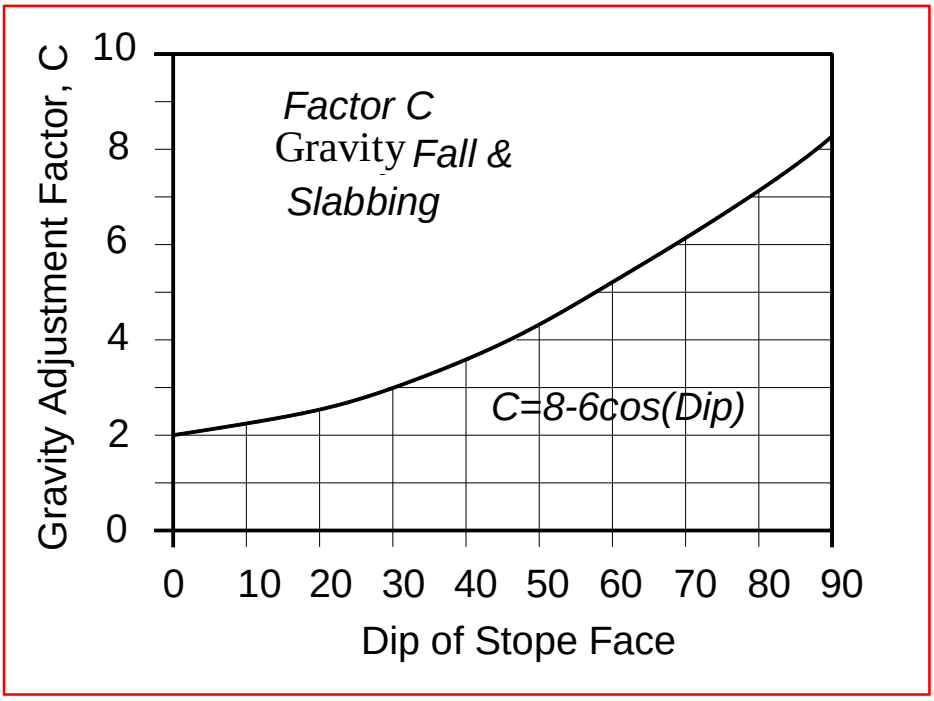

Figure 2.13 C Factor for N' Stability (After Potvin, 1988: from Hutchinson and Diederichs, 1996)

2.3.3 Design Approaches that Assess the Degree of Failure

The Dilution Graph estimates stability based on the total amount of equivalent linear overbreak slough (ELOS) (Clark and Pakalnis, 1997). ELOS represents the total amount of expected dilution based on the average thickness of slough, acting over the stope hanging wall. Based on increased data, in relatively poor ground conditions, the Modified Dilution Graph was developed by Capes (2006). This graph, as well as a representation for ELOS, are illustrated in Figure 2.14. The areas contained by the red zones outside the arc are assumed to be equal to that of the arc's top not encompassed by the rectangle (i.e. even though the shapes are different, the areas will be equal).

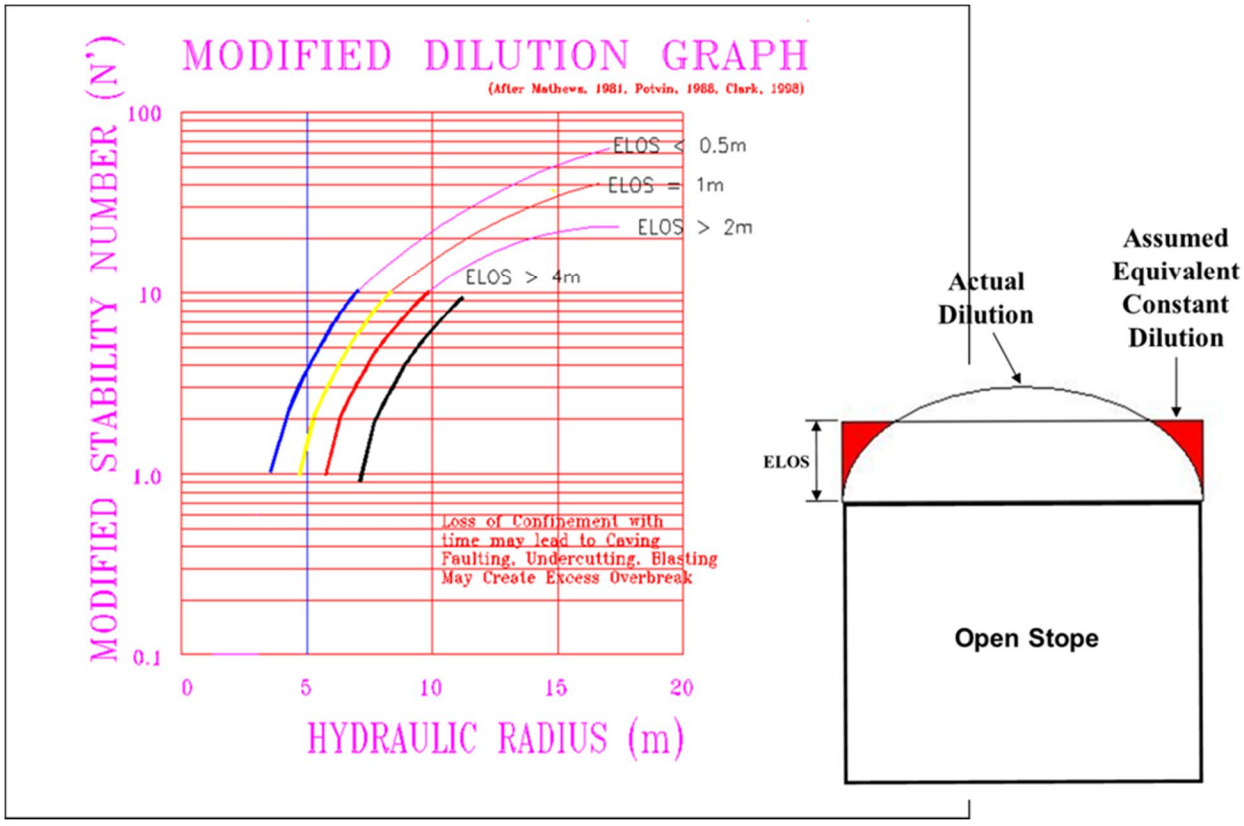

Figure 2.14 Modified Dilution Graph and illustration of ELOS definition (Capes 2006)

2.4 Empirical Design Methods Assessing the Effect of Time on Stability

The Modified Stability Graph and ELOS design approaches are good for determining stability of an underground opening based on some average exposure time, however, they do not take into account the potential change in the rock mass stability over time. These empirical design guidelines are based upon an average exposure time representative of the data base that the empirical design method is based upon. There has been some work done in the past to incorporate exposure time into empirical design methods (Lauffer, 1958; Bieniawski, 1984; Hutchinson and Diederichs, 1996; Pakalnis, 1986; Wang et al., 2003). Most of these methods are based on graphs that rely on span and RMR to determine stand-up time. They have primarily been developed for tunnel applications and they are not widely used in the mining industry.

2.4.1 Lauffer's Design Method

Lauffer (1958) was one of the first to introduce an empirical method for evaluating stand-up time, shown in Figure 2.15. This design method relates stand-up time and rock mass condition to the effective span of an unsupported excavation. In this application, unsupported excavation span is defined as the length of exposed excavation between support elements. The shaded area represents the most common spans and stand-up times encountered in the tunnels used to generate the stand-up time graph (Lauffer, 1958). The letters A-G represent different rock mass conditions (Table 2.4) and are separated by straight lines relating stand-up time to effective span.

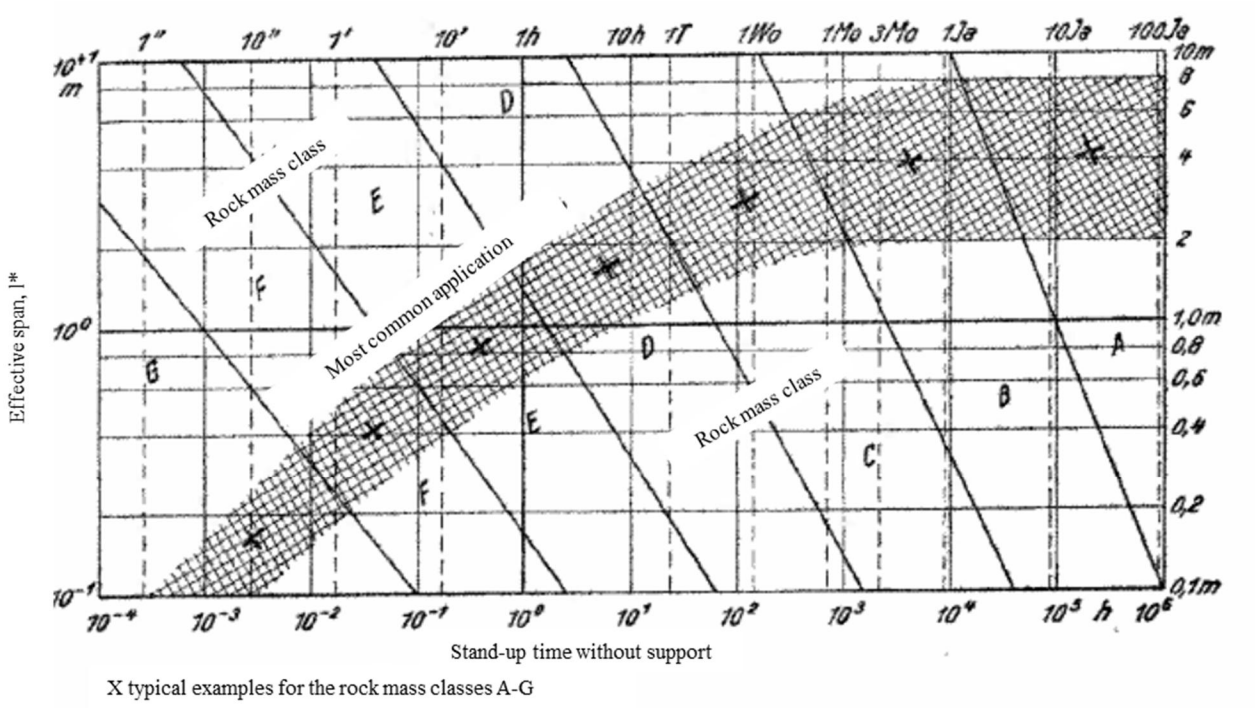

Figure 2.15 Stand-up Time Graph, letters used are described in Table 2.4 (Lauffer, 1958).

Table 2.4 Rock mass classes for Lauffer's (1958) Stand-up Time Graph

Class	Condition
A	Stable
B	Crumbling
C	Very Crumbling
D	Friable
E	Very Friable
F	Subject to Heavy Squeezing
G	Subject to Very Heavy Squeezing

2.4.2 Stand-up Time Graph

The stand-up time graph developed by Bieniawski (1989) was a further development of Lauffer's 1958 empirical method. In developing this graph, Bieniawski added both civil and mining case histories, and applied his own classification system (Figure 2.16). Bieniawski's database is presented in Bieniawski's book, Engineering Rock Mass Classifications (1989). It includes 352 case histories, of which 123 cases include time to failure and the other 229 cases did not fail. Only the 123 points that failed included stand-up times, and are plotted as the rock mass rating RMR_{76} versus the estimated time to failure (Stand-up Time). These 123 points can be further divided into categories: 62 from coal mines, 46 from civil tunnels, and 12 from underground chambers. The

remaining three are from a limestone, metal, and hard rock mine. The majority of the plotted case histories were from sedimentary deposits such as shale, mudstone, sandstone, limestone, and siltstone. The data points are representative of the backs of the excavations, and the majority ranged in depth from 8 to 300 metres.

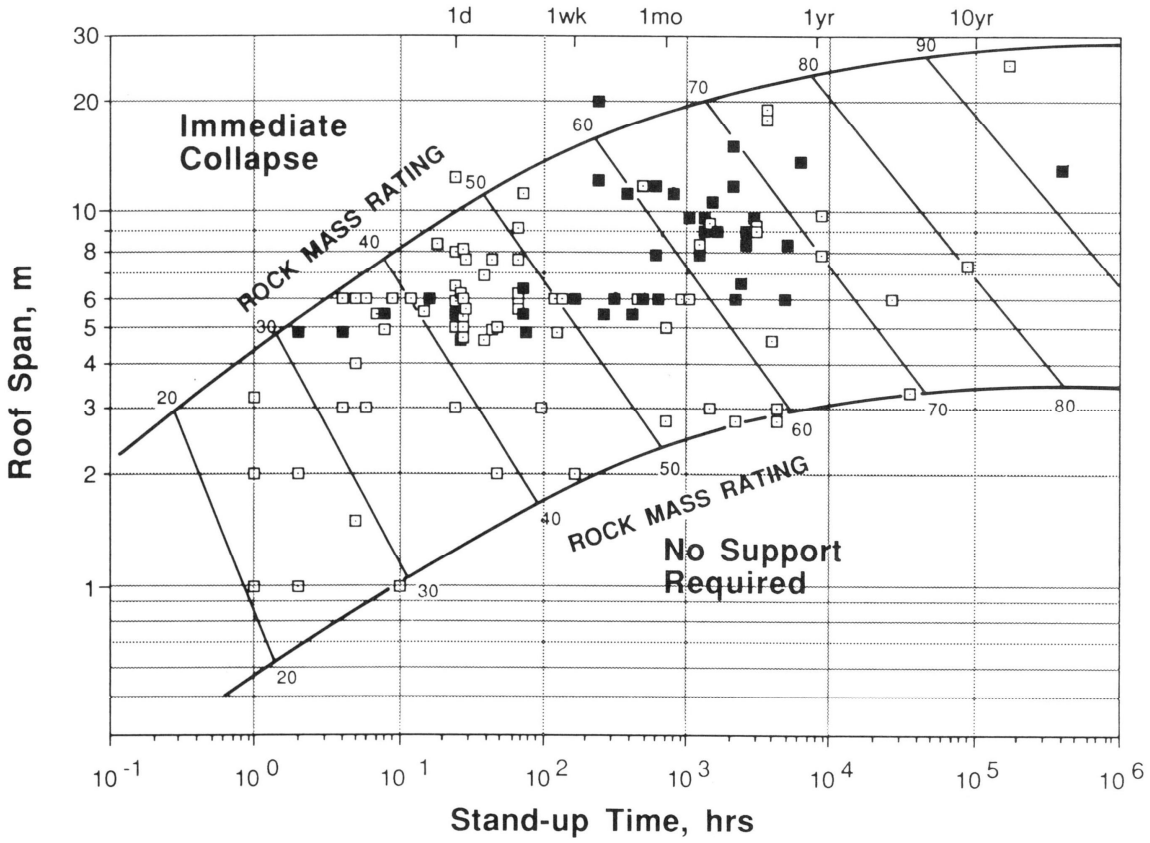

Figure 2.16 RMR Stand-up Time Graph (From Bieniawski, 1989)

2.4.3 Revised Stand-up Time Graph

To further align the stand-up time graph with modern systems, Hutchinson and Diederichs exchanged the x-axis (stand-up time) with the rock mass rating. RMR_{76} is a value that can be collected prior to failure and can be used to predict stand-up time. In most design methods, the measured values are on the axes, while the predicted values are incorporated into the graph. The graph in Figure 2.17, is the most recent iteration of the stand-up time graph. No new data was used to create this version of the graph.

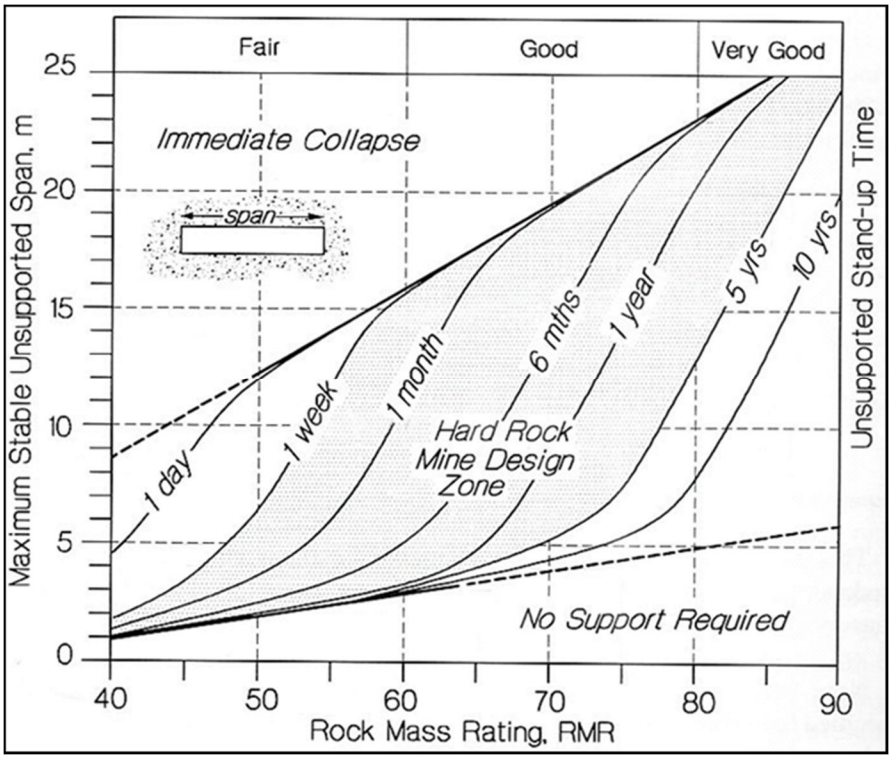

Figure 2.17 RMR Stand-up Time Graph (from Hutchinson and Diederichs, 1996)

2.4.4 Excavation Rate and Exposure Rate

Pakalnis (1986) introduced a new term related to the time taken to excavate a stope. The term excavation rate is a measurement of the square metres of stope hanging wall exposed per month of mining, expressed as thousands of square metres exposed per month (Equation 2.15). This term, as well as the hanging wall RMR value and total area exposed, were combined in an equation that could be used to estimate the total percent hanging wall dilution predicted. This equation was

developed specifically for the Ruttan Mine in northern Manitoba. Equation 2.16 shows this relationship for predicting dilution for isolated stopes (Pakalnis, 1986).

$$Exposure\ Rate = \frac{(L1 \times H)/1000}{months} \quad \text{.....(2.15)}$$

Where:

H is the up dip hanging wall length

L_1 is the stope strike length

$$Predicted\ Dilution = 8.6 - 0.09(RMR) - 13.2\ (Exp.\ Rate) + \text{(Area Exposed)} \quad \text{.....(2.16)}$$

Where:

Predicted Dilution is the average depth of failure expressed as a percent of the ore thickness.

RMR is the Rock Mass Rating (1976)

Exp. Rate is the Exposure Rate

Area Exposed is the final area of the stope hanging wall

2.5 Other Factors Contributing to Stability

Many factors can contribute to the influence of time on stability, as well as the degree of instability or dilution, in open stope mining. In most cases, multiple factors will contribute to any instabilities/slough that is experienced. The design methods presented in the previous sections accounted for factors that include rock strength, joint properties, stress, and opening geometry. Some of the other factors that may contribute to failure, the degree of failure, and time to failure may include:

i. Blast damage – type of explosive and powder factors
ii. Undercutting of a stope's surface
iii. Variable rock mass properties

Of the three points mentioned above, some engineering control exists for undercutting and blast damage.

2.5.1 Blast Damage

Blast damage can be a significant contributor to dilution and potential instability in an open stope. When holes become too confined, a significant portion of the blast energy may impact the surrounding host rock, causing fractures in the surrounding rock mass. Confined holes are created when the break angle towards an open void is less than 60 degrees, or when the burden between the loaded hole, and the open void, is two times greater than the loaded column length (length of powder placed in a production hole) (Figure 2.18). Confined holes may also cause energy to be released up, or down, the production hole, rather than towards the void. This can cause damage to the surrounding rock and lead to potential instability and slough during the blasting process.

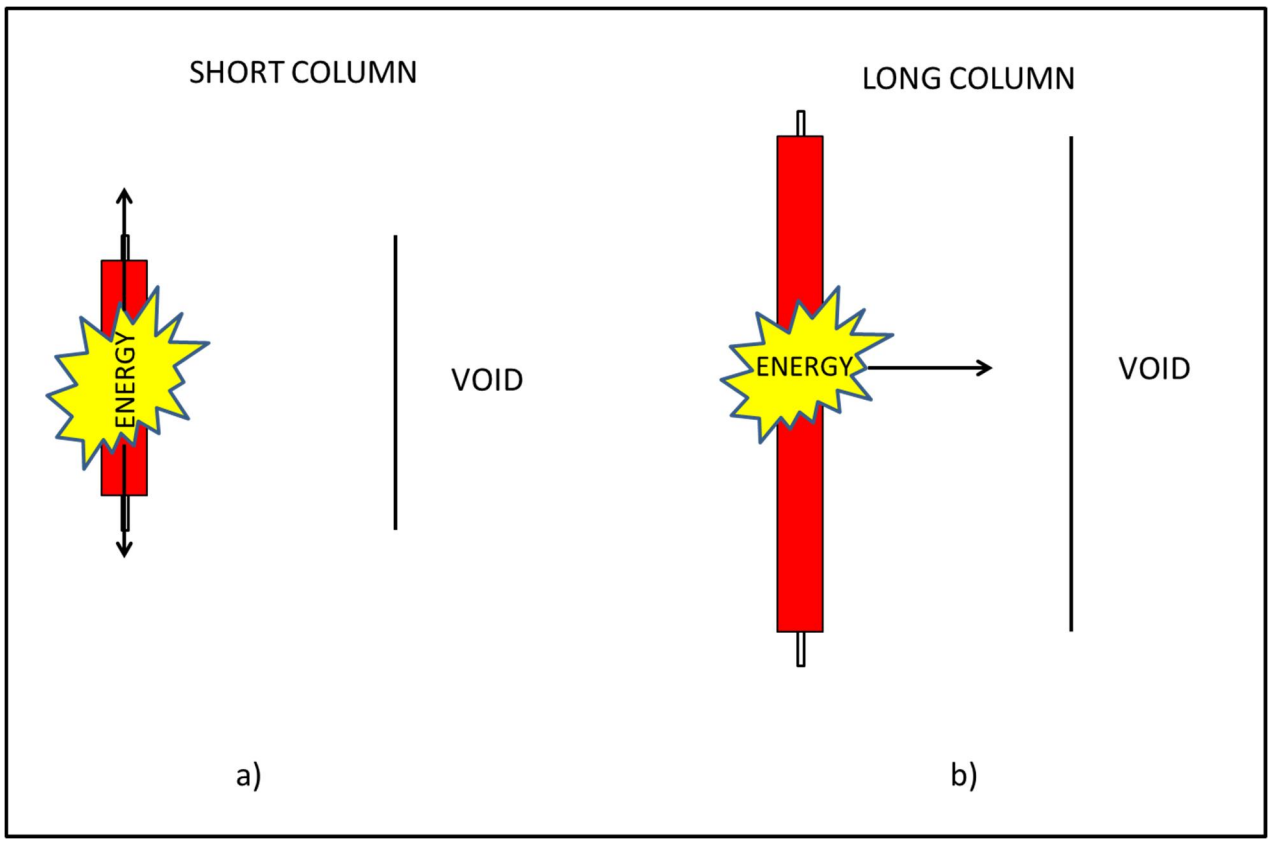

Figure 2.18a) Short column charge. Energy goes up or down the hole. b) Long column charge. Energy moves sideways toward the open void.

2.5.2 Undercutting of the Hanging Wall

Undercutting occurs when the abutment supporting a surface is partially excavated. This primarily refers to the hanging wall of stopes and occurs when the undercut drift for a stope is excavated past the boundary of the hanging wall. When this occurs, the hydraulic radius of the hanging wall may not adequately account for the surface geometry. Undercutting of the hanging wall can cause instability by "increasing the zone of relaxation as well as by reducing abutment support" (Wang, 2004). An example is shown in Figure 2.19. The extent of potential instability and sloughing depends on the degree of undercutting and the condition of the hanging wall rock (Wang, 2004). Deviation of the blasting holes can also lead to undercutting of a stope surface (Figure 2.20)

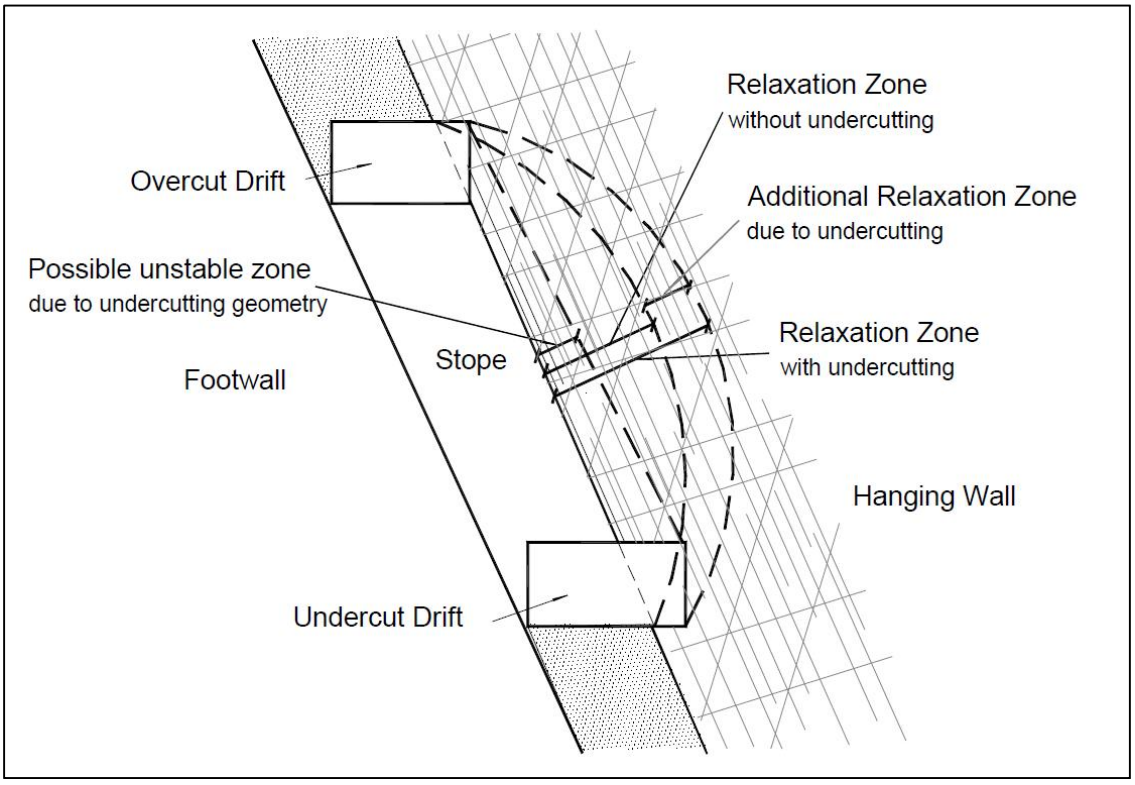

Figure 2.19 Effects of undercutting on HW stability (Wang, 2004)

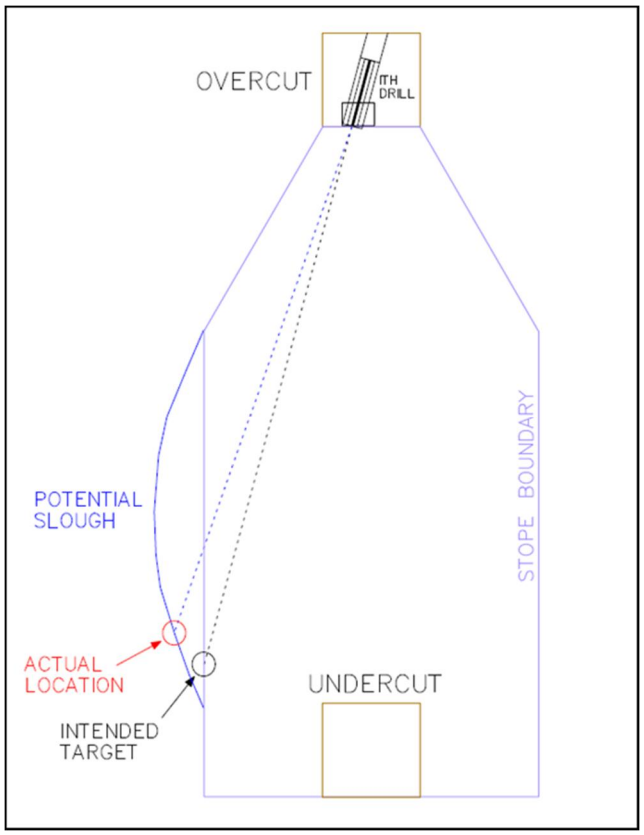

Figure 2.20 Effect of undercutting due to drill hole deviations

CHAPTER 3
DEVELOPMENT OF A STOPE STAND-UP TIME GRAPH

The previous section introduced the stand-up time graph for tunnel or drift stability (Bieniawski, 1989). This method is the most commonly used design approach that incorporates the influence of time on stability. Unfortunately, this approach can only be applied to simple tunnel geometries that can be adequately described with the tunnel span term. The technique cannot be applied to varied surface orientations or stress related instability. The Stability Graph Method for stope design accounts for the factors ignored by the Stand-up Time Graph and has been widely used for underground stope design. Unfortunately, this approach does not account for the length of time exposed.

The following section proposes an empirical design method that applies the advantages of both techniques for the assessment of open stope geometries. To correct the shortcomings to the Stand-up Time Graph, modifications were made to allow the empirical design method to use input parameters applied to the Stability Graph design method for open stoping.

3.1 Converting Parameters between Design Methods

To combine the Stand-up Time Graph with the Open Stope Stability Design approach, some assumptions and simplifications needed to be applied to the database used to develop the Stand-up Time Graph. The Stand-up Time Graph is based on opening span rather than hydraulic radius. The RMR_{76} classification is used instead of Barton's (1974) rock quality Q classification system. Only tunnel backs are designed in the Stand-up Time method and stress is not considered. The following sections discuss conversions, and assumptions, required for converting span and RMR to HR and N' respectively.

3.1.1 Conversion of Span to HR

The Stand-up Time graph uses opening span to quantify the geometry of the tunnel case histories used for design. When openings have a consistent geometry, with the length substantially greater than the width, span adequately assesses opening geometry. When two-way spanning exists, such as most open stope geometries, the hydraulic radius term is required to adequately assess opening geometry. Figure 3.1 shows the relationship between the length and width of an opening surface (aspect ratio) and hydraulic radius. As shown in Figure 3.1, as the length of an opening becomes much greater than the span, the hydraulic radius converges to a value equal to half the span. As the majority of the data points from Bieniawski's RMR Stand-up Time Graph (Figure 2.16) are from backs in coal mining operations and civil tunnel openings, it can be assumed that the aspect ratio (ratio of length to span of the opening) is relatively large. Figure 3.1 suggests that approximating half the span as an estimate for the hydraulic radius for the case histories in the Bieniawski data base will be reasonable.

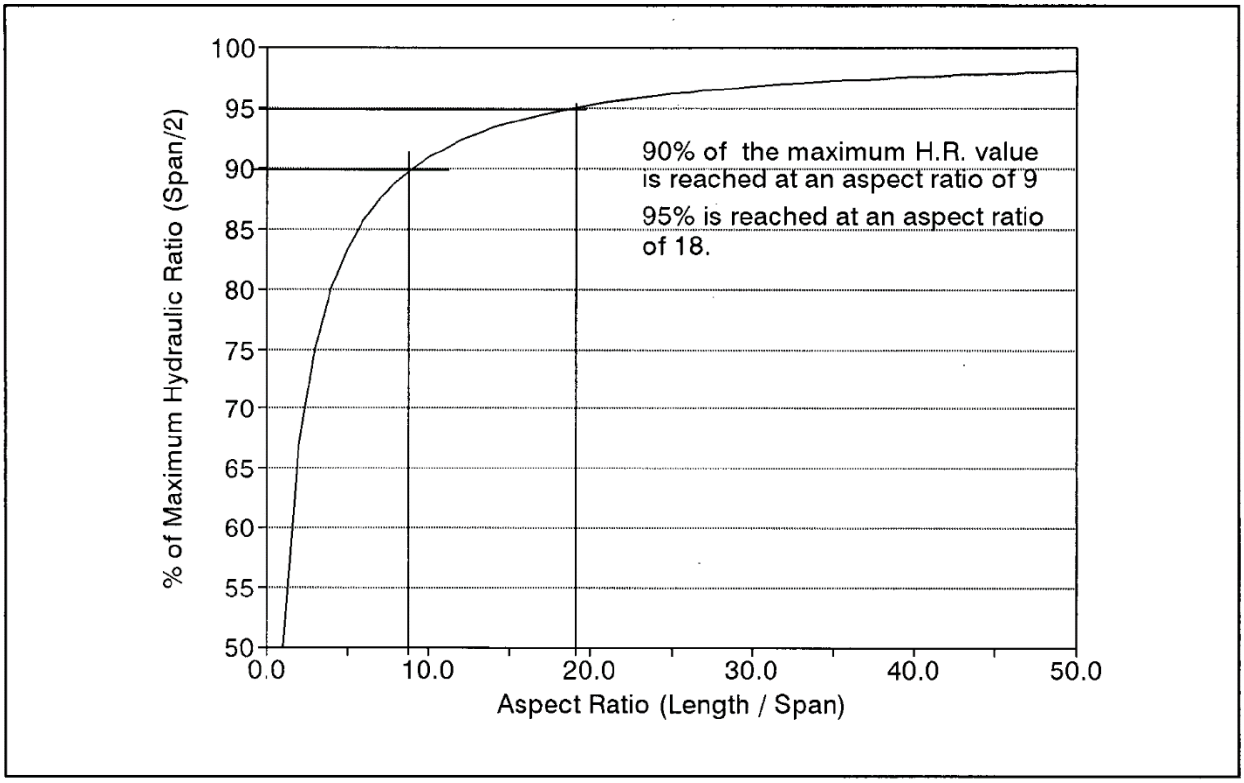

Figure 3.1 Aspect ratio vs. maximum hydraulic ratio graph (Milne, 1997)

3.1.2 Approximating an N' Value from the Stand-up Time Database

To align the RMR Stand-up Time Graph with the Stability Graph design method, data for the calculation of the Modified Stability Number (N') is required. The N' Stability Number, is based on Q' and the A, B, and C factors discussed in Section 2.3.2. Data required to calculate these values was not readily available in the original Bieniawski database. As such, assumptions had to be made about the surface orientation (C factor), joint orientation relative to the opening surface (B factor) and the stress state relative to the strength of the intact rock (A factor). As well, Q' had to be determined using $RMR_{76,}$ as these were the only values available for the case histories in the original database.

3.1.2.1 Rock Mass Rating to Q'

The Stand-up time graph uses RMR_{76} to estimate rock mass conditions, whereas, the Stability Graph is based upon Q'. To calculate N', the Q' value is required. The Q' value is calculated by converting RMR_{76} to Q'. For this conversion, the following equation is used (Bieniawski, 1984):

$$RMR = 9ln(Q') + 44 \quad \text{.....(3.1)}$$

$$Q' = e^{\frac{RMR-44}{9}} \quad \text{.....(3.2)}$$

The use of this equation for equating RMR_{76} and Q is not ideal (Milne et al., 1998) and an assumption that stresses are not influencing the Q' value (Q ~ Q') is required. Since the empirical database does not have the data upon which the RMR_{76} value was based, Equations 3.1 and 3.2 are the only options for estimating values for Q'.

3.1.2.2 A, B, and C factors for N' Stability

The other components required to estimate N' include the stress (A), critical joint (B), and surface dip (C) factor. To estimate the A, B, and C factors, the following assumptions were made:

i. Low stress conditions are present as all but five of the unstable openings in Bieniawski's graph were from openings at a depth of less than 300 metres (A factor ~ 1);
ii. The majority of the data points are for openings in civil tunnels and coal mines, commonly in shallow dipping sedimentary deposits, where the major controlling joint set would be parallel to the backs (B factor ~ 0.3) and;
iii. Case histories were for near horizontal backs (C factor = 2.0)

The A factor requires an estimate of both the average intact rock strength and the induced stresses near the opening surface. To estimate average rock strength, the Bieniawski database was reviewed. Since 95 of the 123 cases of failure were in sedimentary rocks, an approximate UCS of 75 MPa was estimated based on general strength values for sedimentary rocks from Goodman (1989).

To estimate an A value for the case histories, it was assumed that low stress conditions were present, as all but one of the case histories for sedimentary rocks were from a depth of 300 metres or less. Assuming an average specific gravity of 2.5 for sedimentary rock, the stress state at an average depth of 150 metres would be approximately 3.8 MPa. If the hydrostatic virgin stresses are assumed, an induced stress in the drift backs would be approximately twice the virgin stress levels for a value of 7.6 MPa (based on Kirsch equations for stresses induced around a cylindrical tunnel, (Kirsch, 1898). This is shown in the example below. From this example, the ratio of Uniaxial Compressive Strength to Induced Compressive Stress is approximately 10, corresponding to an A Factor value of approximately 1 for average depths and rock strengths for 96 of the 123 case histories (Figure 3.2).

$$\sigma = SG\rho_w gh \quad \text{.....(3.3)}$$

$$\sigma = (2.7)(1000kg/m^3)(9.8m/s)(300m)$$

$$\sigma = 7.9\ MPa$$

$$A = \frac{75\ MPa}{7.9\ MPa} \approx 9.5 \quad \text{.....(3.4)}$$

Where:

σ=stress

SG = specific gravity

ρ_w = unit weight of water

g = gravity

h = depth

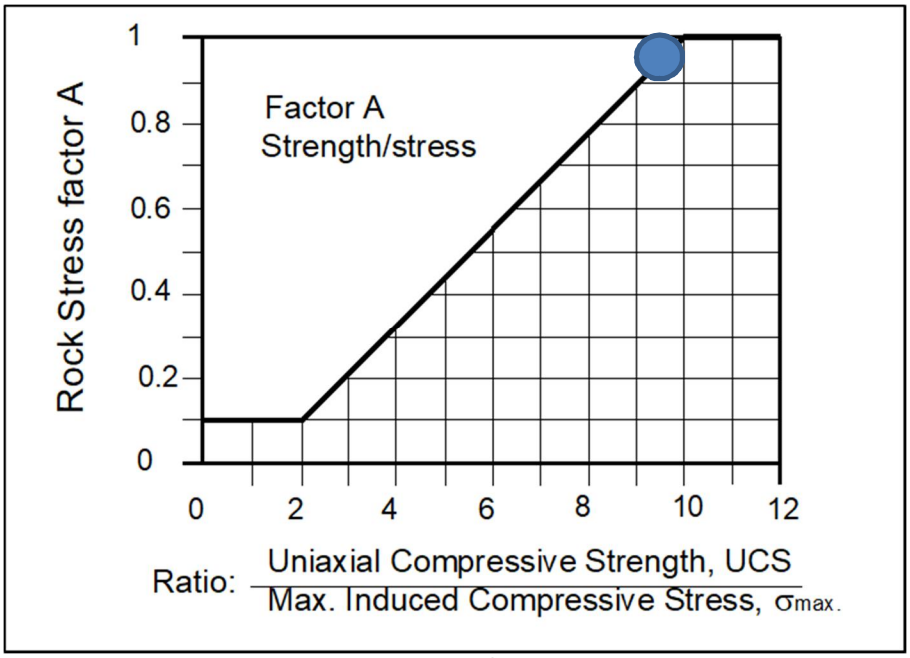

Figure 3.2 Stress Factor A graph for N' stability (Potvin, 1988)

To estimate the B factor for the N' Stability Number, it was assumed that the major controlling joint set in most of the case histories is horizontal, as many sedimentary deposits have horizontal or near horizontal bedding. Figure 3.3 shows the assumed conditions for the B factor conversion. From the B factor graph (Figure 3.4), the joint orientation corresponds to a B factor of 0.3. Sub-horizontal joint sets ranging from 10 to 30 degrees will have a slightly larger effect on stability with a B factor rating of 0.2. It is likely that many drifts would assume a shanty back geometry (parallel to jointing), if a joint set was present at an angle of 10 or 20 degrees to horizontal. Since the joint sets were assumed to be horizontal, the value of 0.3 was used for the derivation of the N' Stability Number.

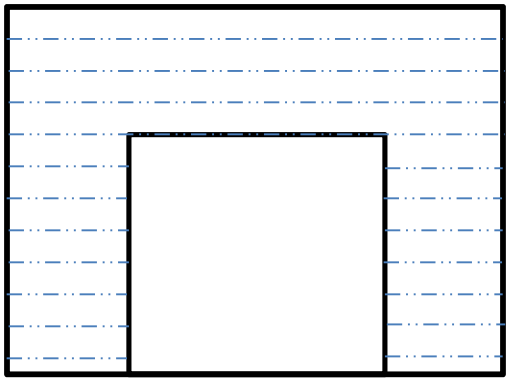

Figure 3.3 Unfavourable joint orientation for shallow dipping sedimentary deposits

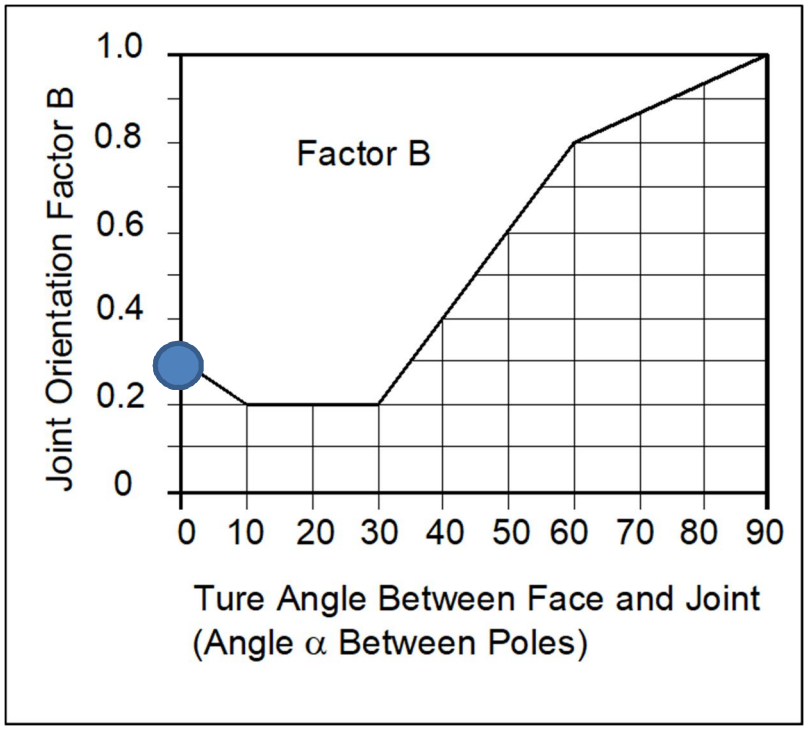

Figure 3.4 Joint orientation B Factor for N' stability (Potvin, 1988)

The C factor is based on the dip of the surface being examined. For shallow excavations in flat lying sedimentary deposits, shallow dipping backs can be assumed. A C value of 2 was used based on these assumptions (Figure 3.5). If a shanty back, dipping at 10 to 20 degrees from horizontal was in the data base, this would not have a significant effect on the C value.

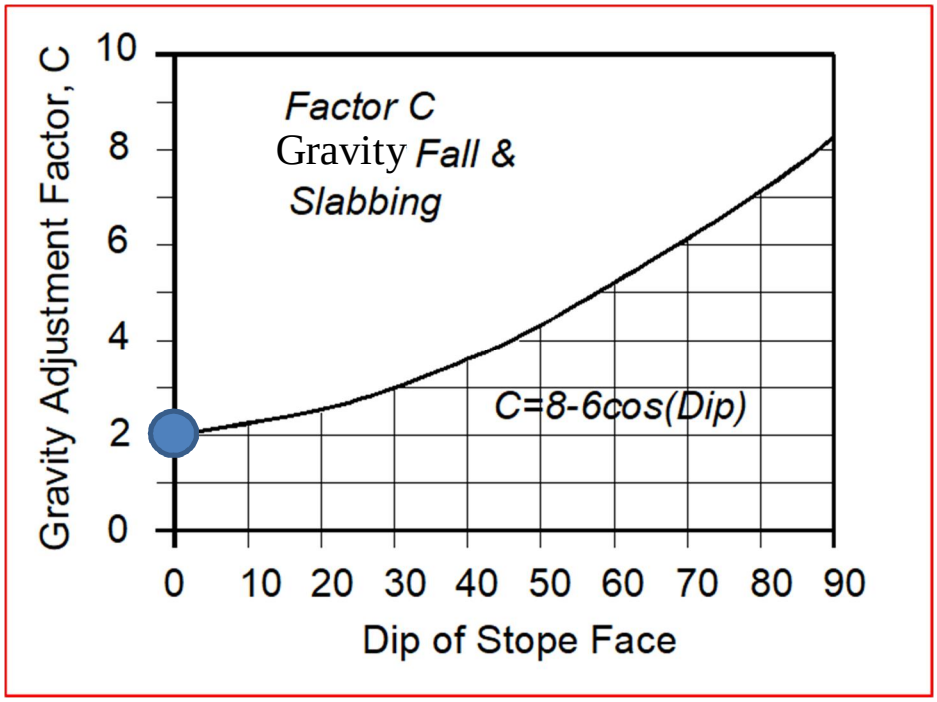

Figure 3.5 Surface dip C Factor for N' stability (Hutchinson and Diederichs, 1996)

3.2 Modified and Bieniawski RMR Stand-up Time Graph

Based on the assumptions and correlations described in the preceding sections, the axes on the Bieniawski RMR Stand-up Time Graph (Figure 2.17) were changed to correspond to the Modified Stability Number N' vs. Hydraulic Radius as shown in Figure 3.6. This new graph is called the Modified Stand-up Time Graph. The lines on the graph were transferred to the Modified Stand-up Time Graph using the procedure described in the previous section.

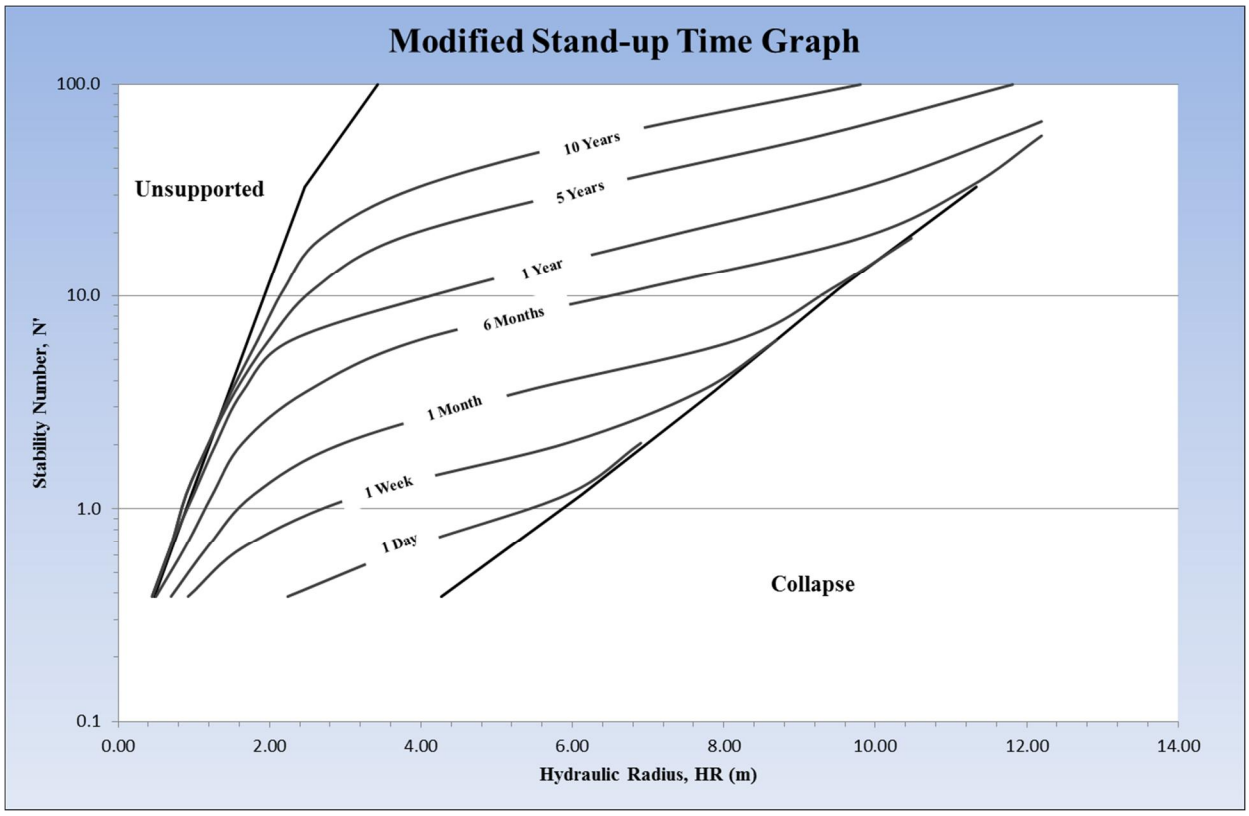

Figure 3.6 Modified Stand-up Time Graph

The original Stand-up Time Graph is a plot of tunnel span versus stand-up time, with predicted RMR zones delineated on the graph. The Modified Stand-up Time Graph plots the Stability Number N' versus the hydraulic radius, with the predicted stand-up time delineated on the graph. The new Modified Stand-up Time Graph follows the graphing convention used by the Modified Stability Graph (Figure 2.9) (Potvin, 1988) and the re-plotted Stand-up Time Graph (Figure 2.17) (Hutchinson and Diedrichs, 1996).

A comparison has been made between Bieniawski's data plotted on the original RMR Stand-up Time Graph and the same data plotted on the Modified Stand-up Time Graph. The original RMR Stand-up Time Graph was plotted on individual graphs representing six RMR intervals ranging from less than 30, increasing in intervals of 10, to values greater than 70 on the final graph (Figures 3.7 to 3.12). These graphs highlight the scatter in RMR values for measured spans and stand-up times. It is interesting to note that the data supporting the original Stand-up Time graphs were never previously plotted with the RMR data shown.

The Graph originally created by Bieniawski has zones defined by RMR rather than stand-up time. Each zone exists for a range of stand-up times and spans. For example, an RMR of 40 to 50 (Figure 3.9) is defined by stand-up times ranging from 8 hours for larger spans, to 29 days for smaller spans. The way in which Bieniawski presents the data, the scatter indicates how well the RMR value corresponds to the predicted range of values for the span and stand-up time.

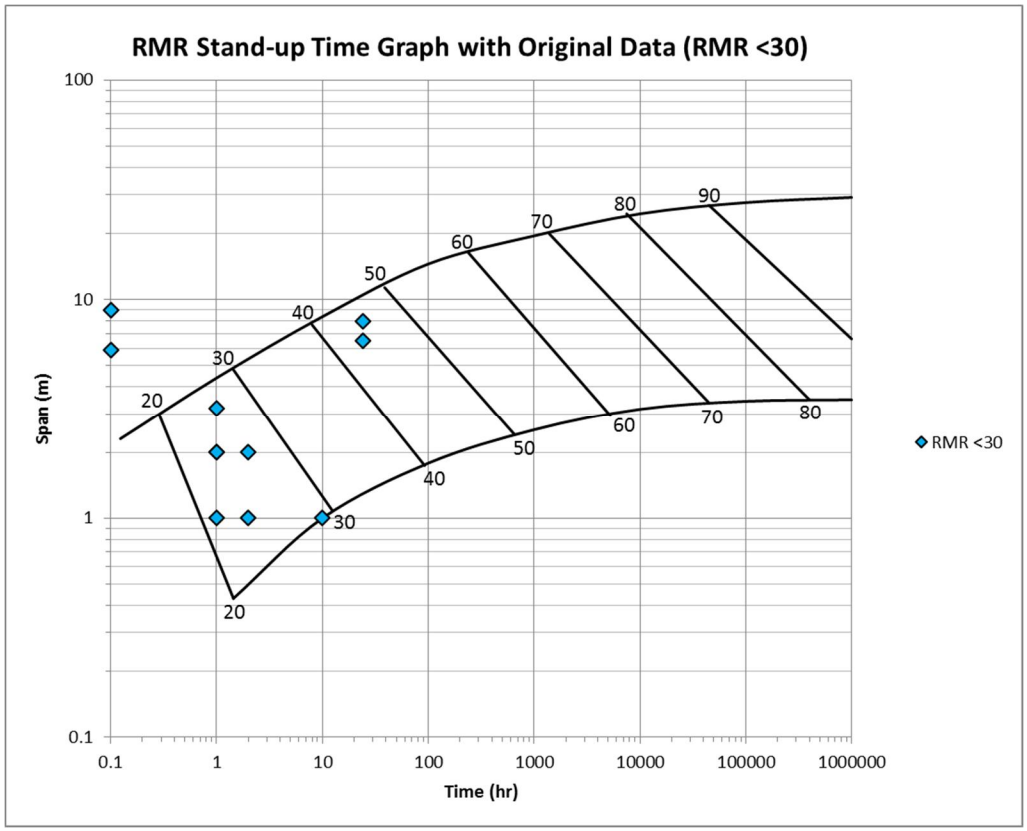

Figure 3.7 Bieniawski data plotted on the RMR Stand-up Time Graph for RMR values less than 30

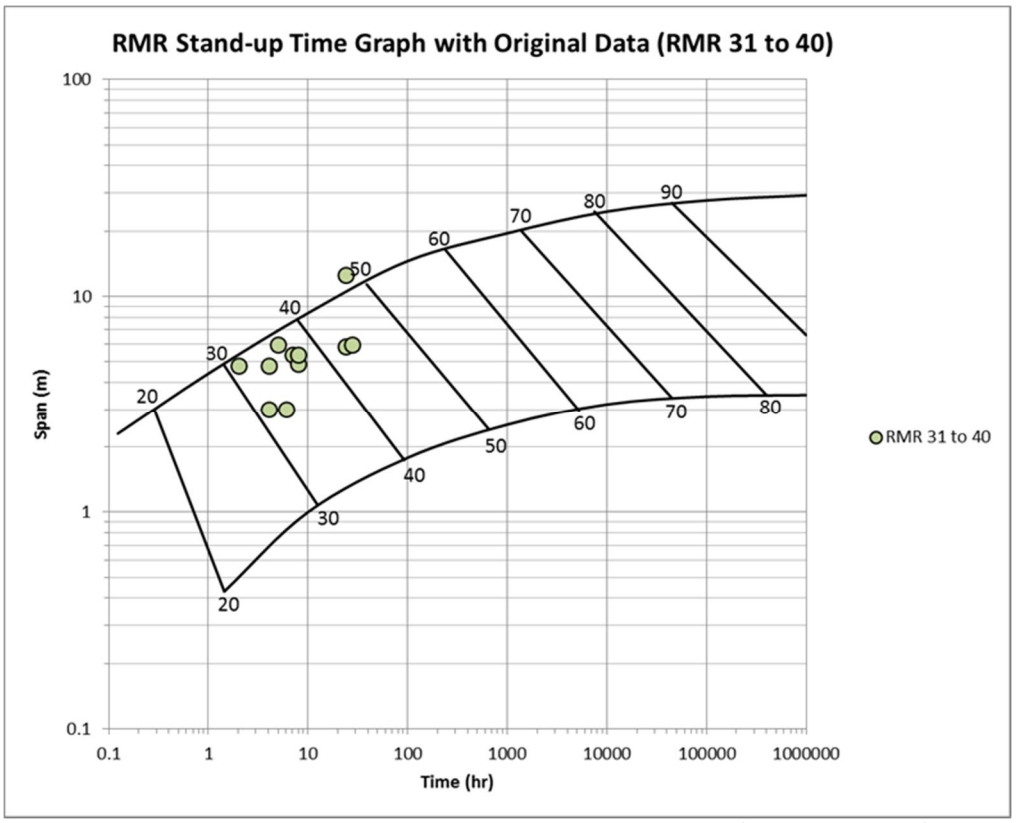

Figure 3.8 Bieniawski data plotted on the RMR Stand-up Time Graph for RMR values of 31 to 40

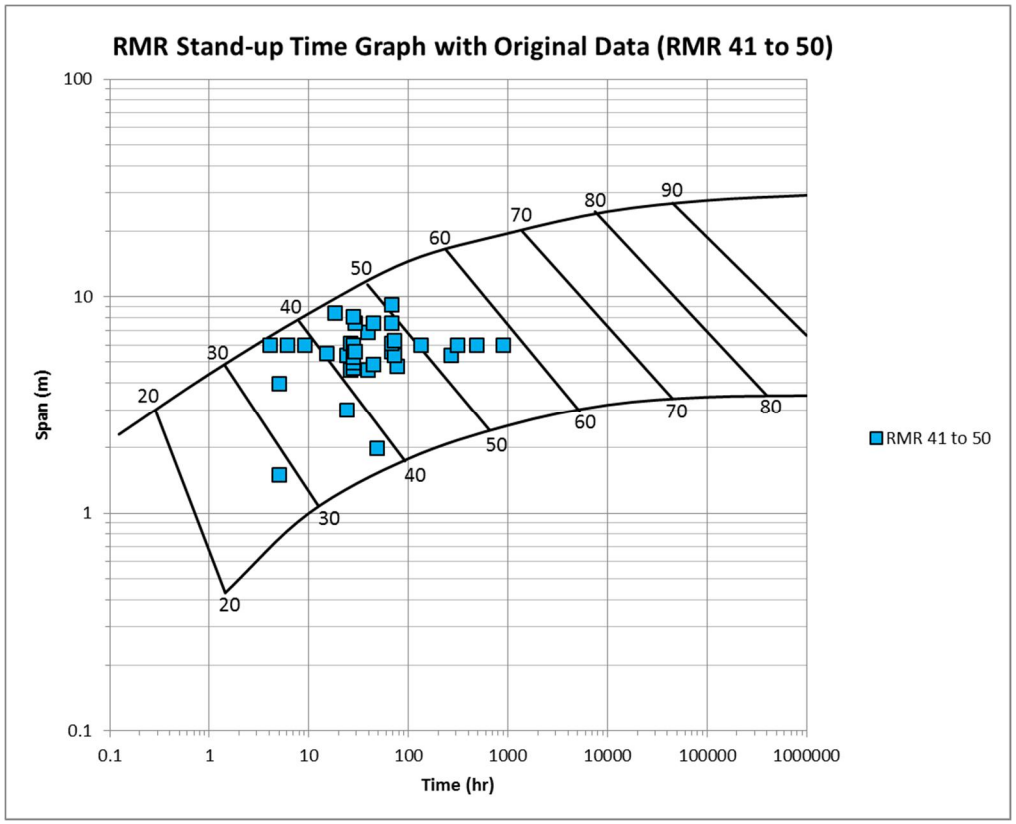

Figure 3.9 Bieniawski data plotted on the RMR Stand-up Time Graph for RMR values of 41 to 50

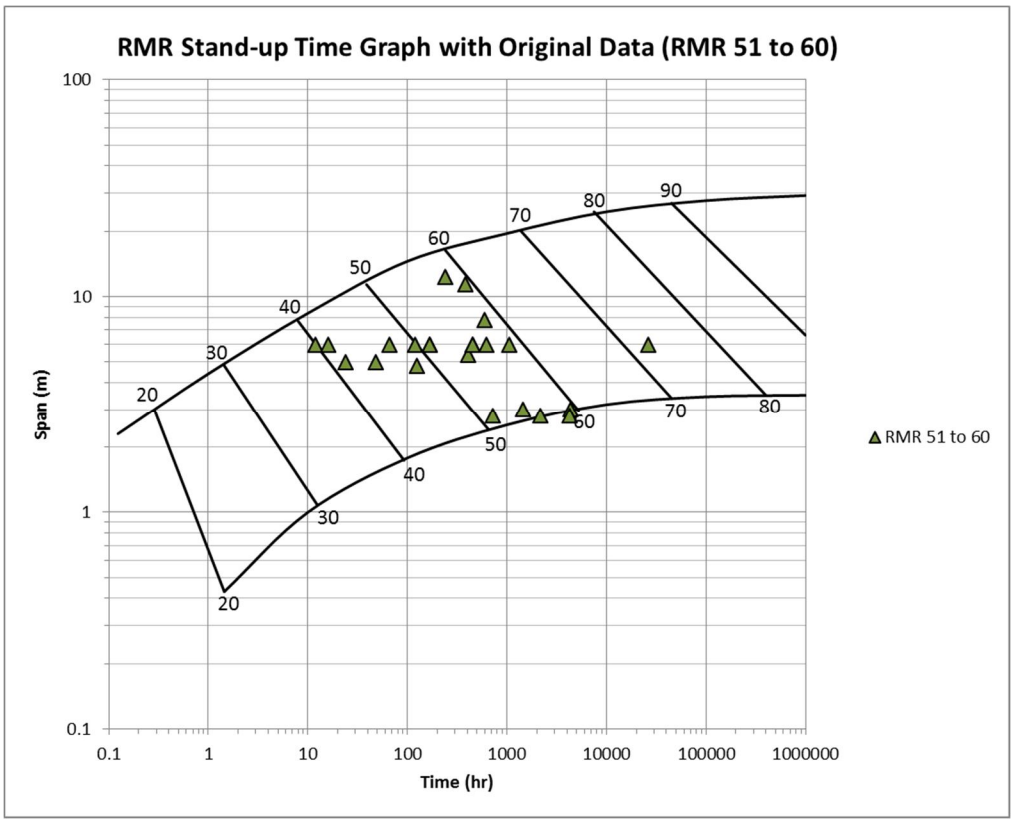

Figure 3.10 Bieniawski data plotted on the RMR Stand-up Time Graph for RMR values of 51 to 60

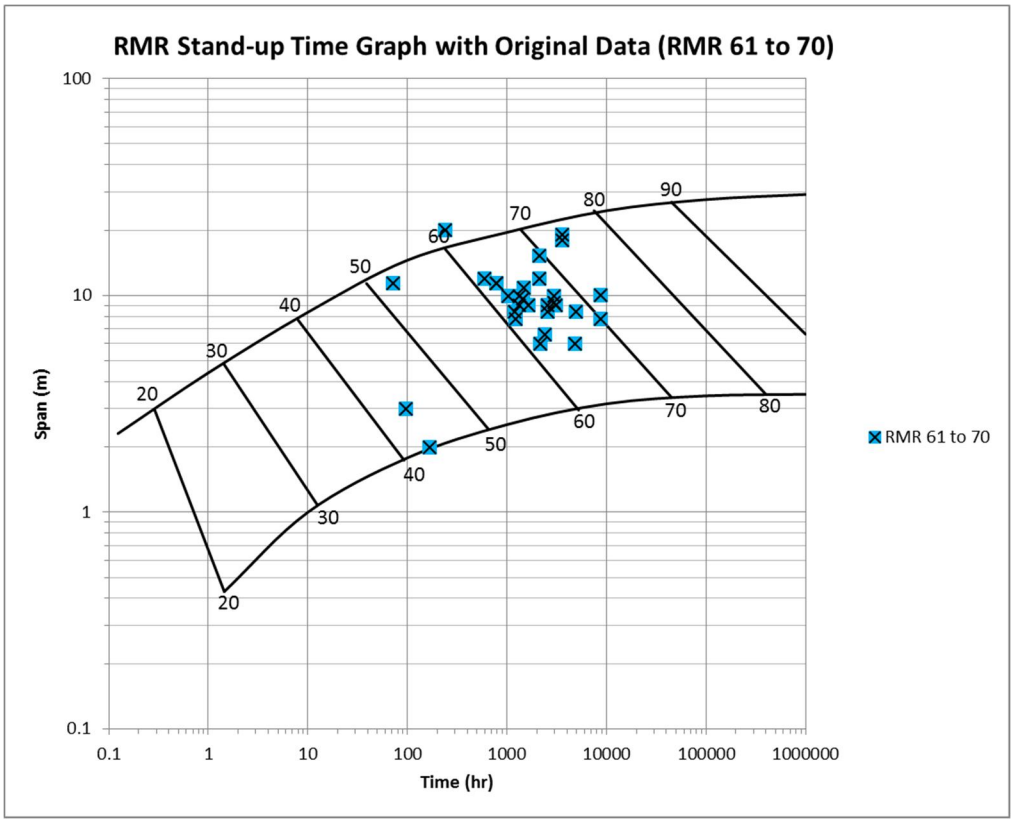

Figure 3.11 Bieniawski data plotted on the RMR Stand-up Time Graph for RMR values of 61 to 70

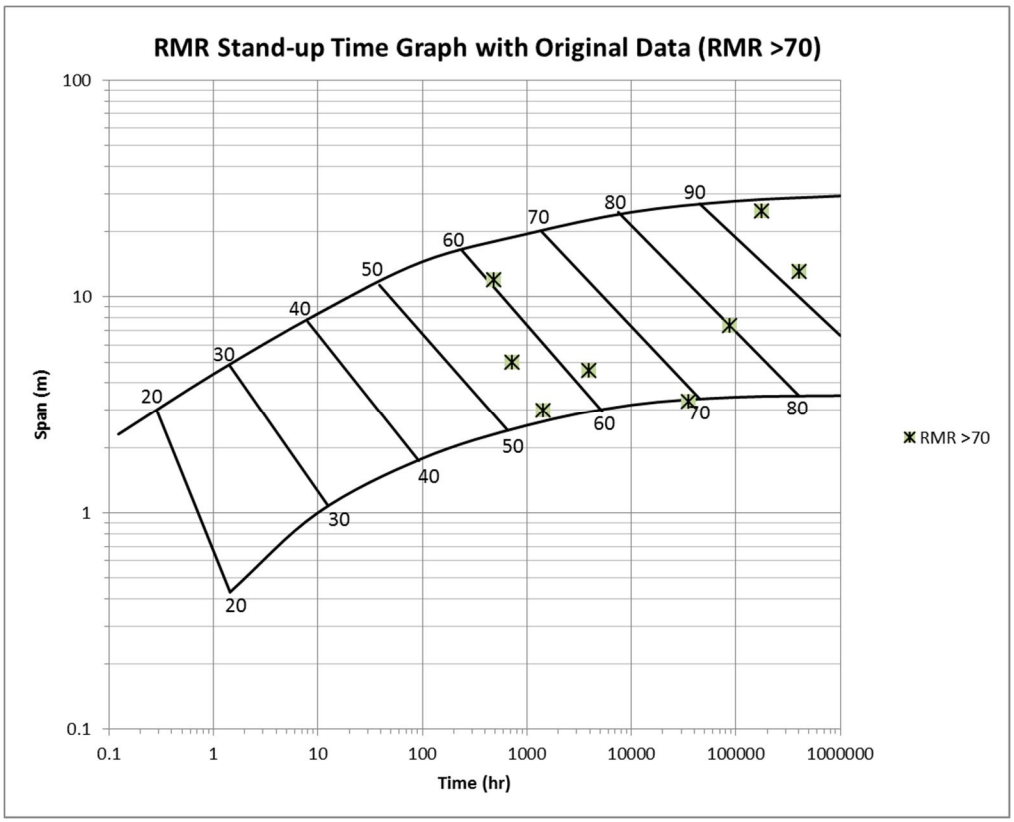

Figure 3.12 Bieniawski data plotted on the RMR Stand-up Time Graph for RMR values greater than 70

Some of the scatter in the plotted data may be attributed to other factors that influence failure that are not accounted for in RMR and span. Introducing N' and Hydraulic Radius is an attempt to help account for more factors influencing failure, and potentially reduce the scatter of future data sets.

To plot the data points on the Modifed Stand-up Time Graph (MST Graph), N' and HR had to be calculated. A few of the case histories had associated Q' values, but for the majority, Q' had to be calculated using Equation 3.2.

Figure 3.13 to Figure 3.18 show that there appears to be a significant amount of scatter in the data points, however, the individual graphs warrant discussion. Figure 3.13 shows cases of failure that occurred in one day or less. Only 20 of the cases plotted such that failure would be predicted in 1 day or less, however, a total of 38 of the 46 cases plotted such that failure could be expected in 1 week or less. Figure 3.14 shows 24 cases where failure occurred between 1 day and 1 week. Of these 24 cases, 15 plotted within the expected failure lines. Figure 3.15 shows 15 cases that failed between 1 week and 1 month. Of these 15 cases, only 4 plotted in the expected stand-up time limits

and there is significant scatter. Figure 3.16 supports the proposed design lines as the 6-month line approximates the median of the data cluster.

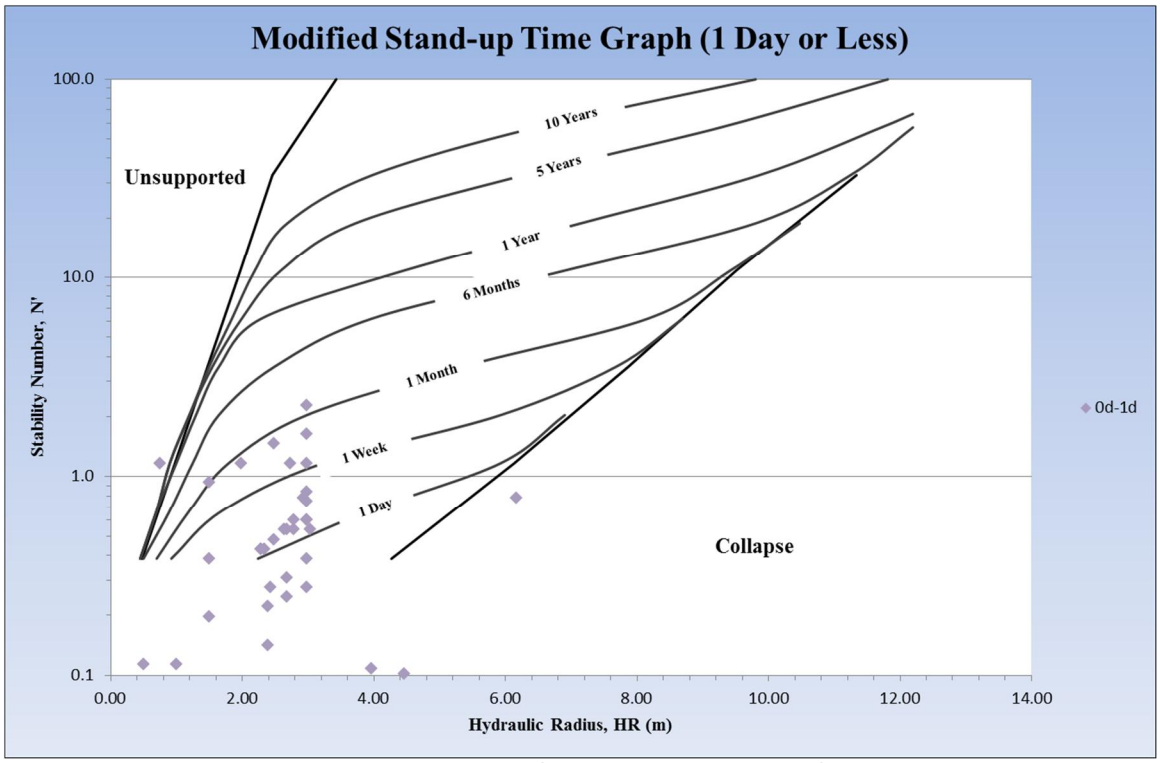

Figure 3.13 Bieniawski data plotted on the Modified Stand-up Time Graph for the time interval 0 to 1 day

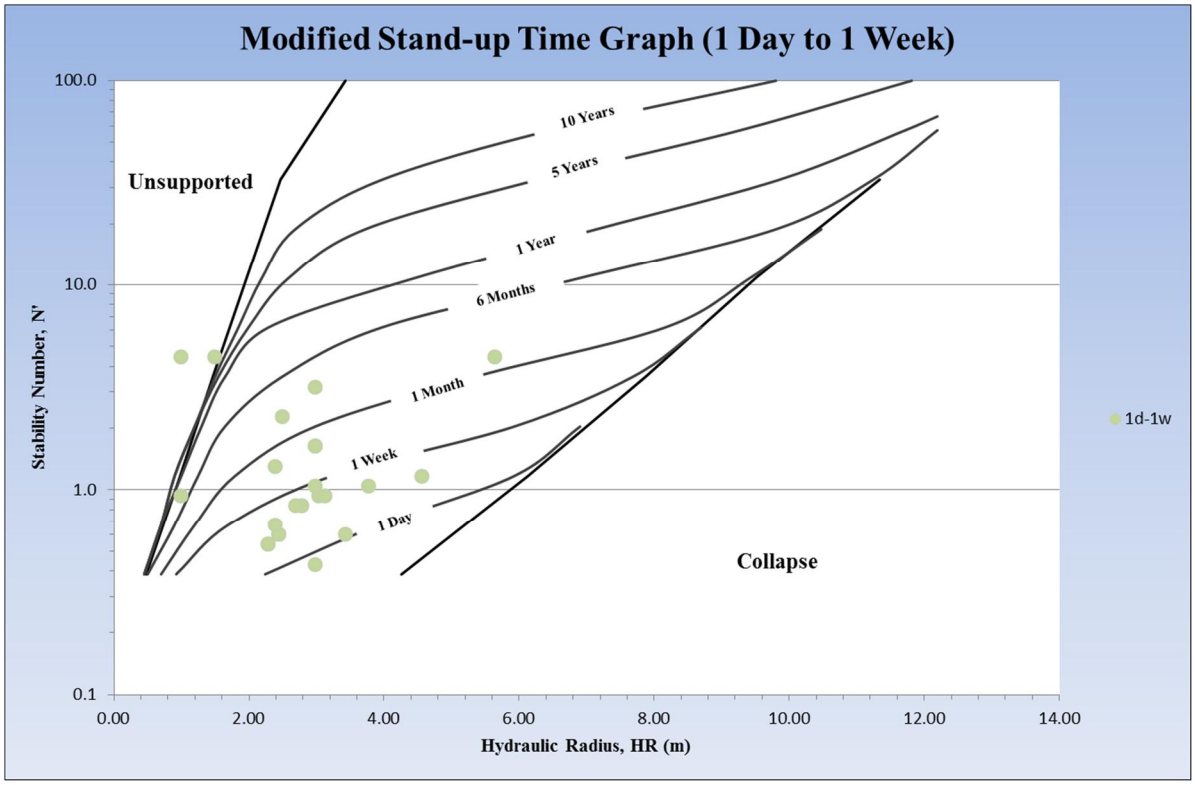

Figure 3.14 Bieniawski data plotted on the Modified Stand-up Time Graph for the time interval 1 day to 1 week

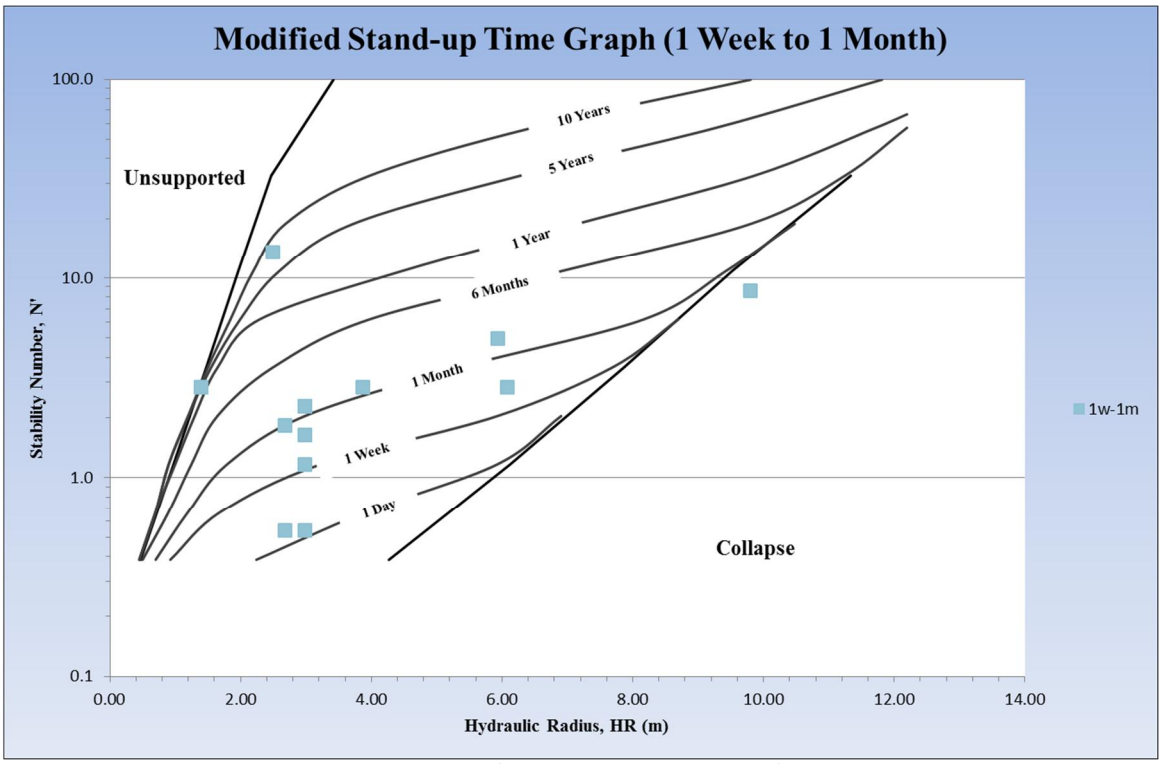

Figure 3.15 Bieniawski data plotted on the Modified Stand-up Time Graph for the time interval 1 week to 1 month

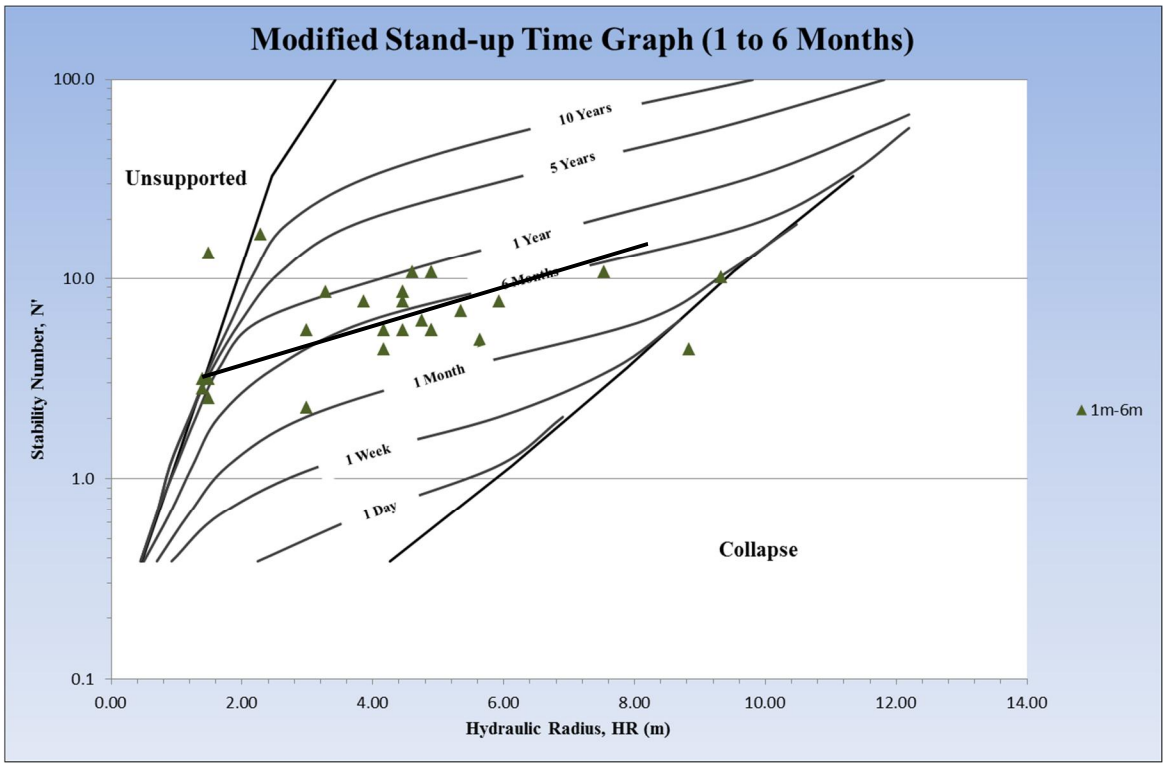

Figure 3.16 Bieniawski data plotted on the Modified Stand-up Time Graph for the time interval 1 to 6 months

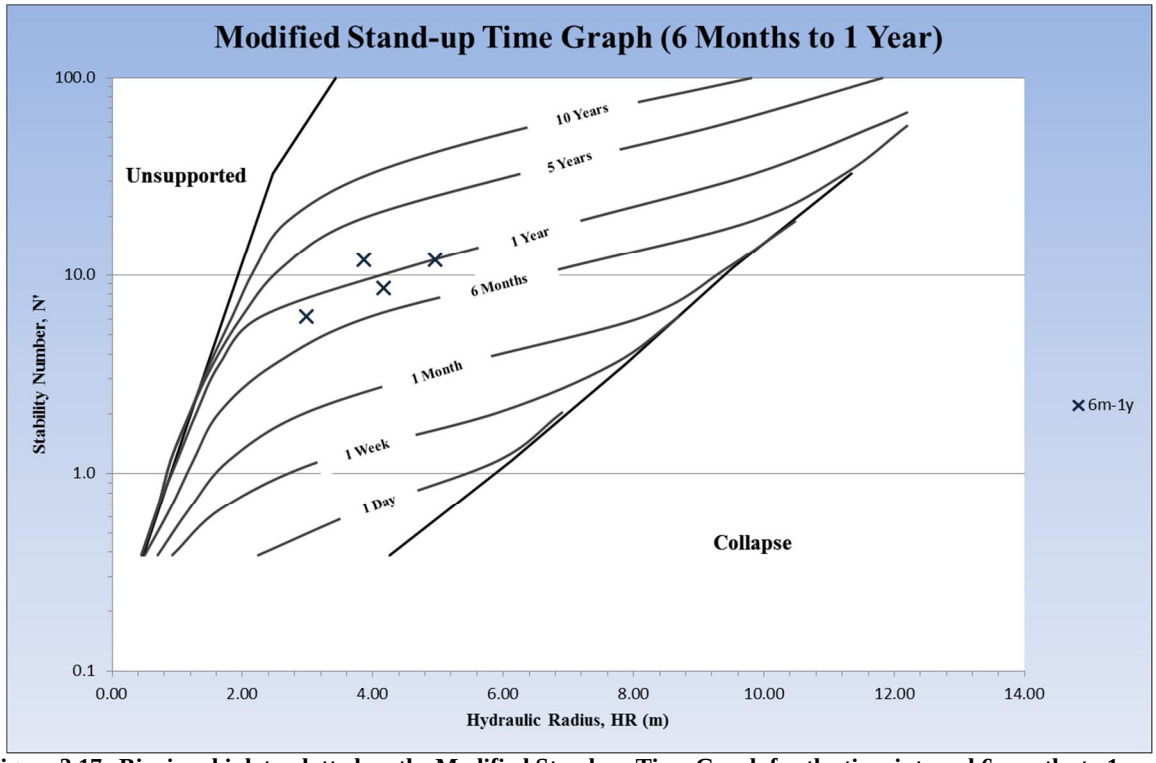

Figure 3.17 Bieniawski data plotted on the Modified Stand-up Time Graph for the time interval 6 months to 1 year

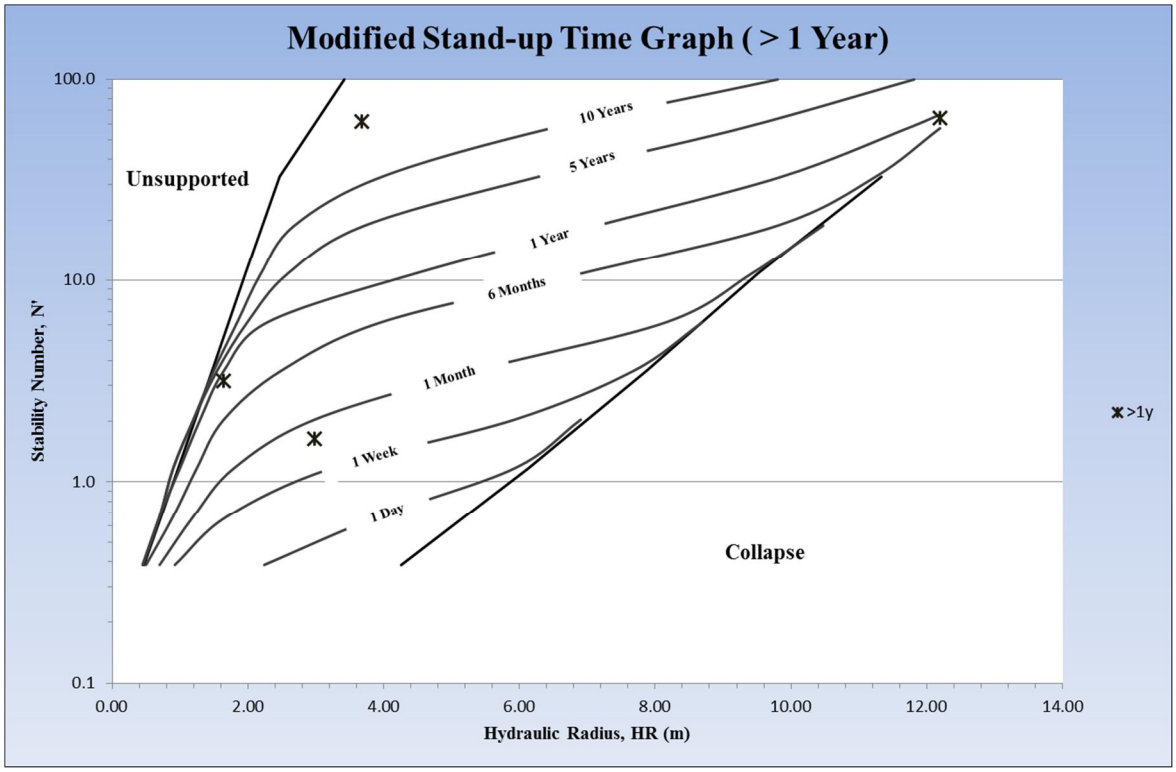

Figure 3.18 Bieniawski data plotted on the Modified Stand-up Time Graph for time interval greater than 1 year

There is very little data supporting the lines representing stand-up times greater than 6 months (Figures 3.17 and 3.18). A total of only seven data points were available in the original data. The four data points that help define the 1 year trendline support it very well, however, more data would be required to justify any trend based on this data alone. For the remaining 5 and 10 year time lines, none of the data supports the trend lines for this time period. It is likely that trend lines greater than 6 months were drawn to resemble trends observed for the 1 day to 6-month trend lines.

3.3 Comparing the Modified Stand-up Time Graph and the Modified Stability Graph

As part of the study, the Modified Stand-up Time Graph was compared to the Modified Stability Graph. The original Bieniawski RMR stand-up time graph is based on both civil and mining case histories, has been applied only to excavation backs, and is primarily based on case histories under a depth of 300 metres. The Modified Stability Graph was developed solely based on mining case histories for use in the mining industry, primarily considers stope hanging walls and backs, and is based on case histories at depths over 500 metres. To make it easier to compare the two design graphs, they are superimposed in Figure 3.19. Three zones are defined in the graph; zone 1 includes

HR values less than 4 metres, zone 2 has HR values between 4 and 8 metres and zone 3 has HR values greater than 8 metres. Within each zone, the Modified Stability Graph and the Modified Stand-up Time Graph are compared:

- In zone 3, the unsupported transition zone on the Modified Stability Graph corresponds to a stand-up time between a few months to one year, and the hydraulic radius exceeds 8 metres. This suggests that a stope with an HR of 8 metres or more requires at least a few months, to a year to mine.
- In zone 2, the unsupported transition zone on the Modified Stability Graph corresponds to a stand-up time under one week to one year and the hydraulic radius is between 4 and 8 metres. This suggests that a stope with an HR of 4 to 8 metres requires at least a week to just under a year to mine.
- In zone 3, the transition zone on the Modified Stability Graph corresponds to a stand-up time of under one month and the hydraulic radius is less than 4 metres. This suggests that a stope with an HR of less than 4 metres requires less than a month to mine.

In general, larger stopes, with a larger hydraulic radius, will require a longer time to complete mining. The unsupported transition zone within the modified stability graph method incorporates a rough measure of exposure time with the surface hydraulic radius. The Modified Stand-up Time Graph appears to be a promising approach for combining the need for assessing the stability of mining openings, with the addition of exposure time from the combined civil and mining database

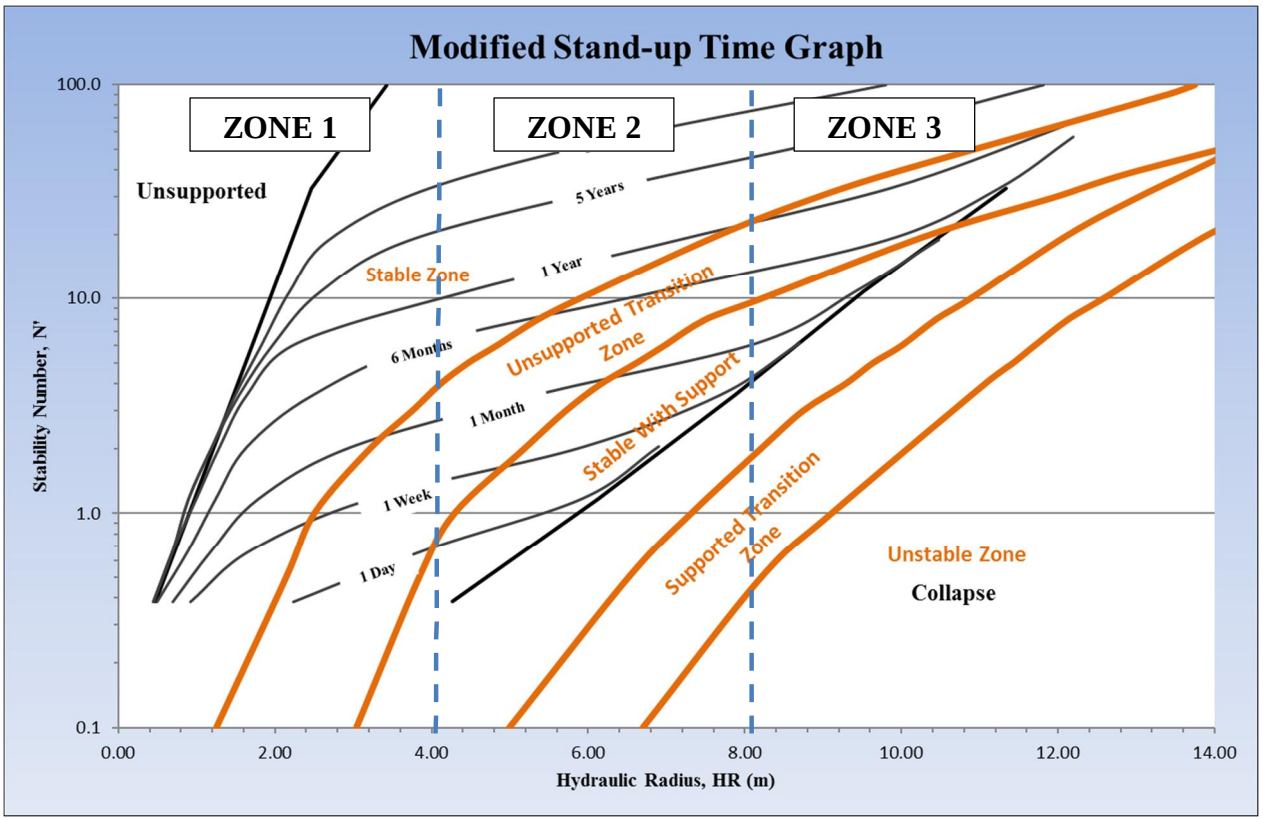

Figure 3.19 Modified Stand-up Time Graph compared to the Modified Stability Graph

CHAPTER 4
FIELD DATA

Field data on the mining and stability of open stopes was collected from a total of ten case histories from various areas of the Birchtree Lower 84 Complex (Figure 4.1). The purpose of collecting the field data was to help determine factors influencing stability of open stopes, and the exposure time prior to the stope experiencing instability.

Figure 4.1 Longitudinal view of the Birchtree Lower 84 Complex (Birchtree, 2016)

4.1 Stope Mining Records

At the Birchtree Mine, paper copies of information relating to each mined stope are kept in what are called block books. These block books contain information which can include:

- Blast letters à includes information such as total feet loaded, powder factor, energy factor, blast timings, charge length information for each production hole, a long-section of the stope, and cross-sections of each ITH (in the hole) blasting ring.
- Cablebolt summaries à includes information pertaining to total footage drilled, length of cables, total footage completed per shift, number of cables and straps installed, grouted and tensioned.
- Dilution assessments à includes information on total tons extracted, grade, total pounds of nickel, tons of planned and unplanned dilution, total dilution, and minability.
- Blast hole length à after each blast, holes are cleaned and measured for depth. This allows the mine engineer to determine if there was any underbreak/overbreak, and make adjustments to the blasting plan accordingly.
- ITH summary sheets à includes information on which blast holes were drilled, total feet drilled, feet drilled per shift, and total feet cleaned per shift after a blast.
- Muckbase report à contains a summary of total tons of ore and waste removed from the block on a daily basis. Also includes information on planned tons, actual tons, and it may also contain notes from engineers and geologists pertaining to the stope.
- Fill letters à contains information on type and amount of fill required to backfill the stope. It will also contain instructions for each stage of the filling process.
- Stope cavity monitoring survey data (CMS data) à this data records the geometry of the blasted stopes, which may be conducted more than once during the blasting of a stope.

It should be noted that the block books can contain a mixture of the above information, however, all this data is not necessarily contained in each record of the stope's history. The information most commonly found in these block books are the Blast Letters, in the hole percussion drilling summaries (ITH), cablebolt summaries, muckbase reports, and fill letters.

The ten case histories used for the study contained all the necessary information for classifying the stopes using common empirical design methods. This includes information that could be used to calculate the N' Stability number and hydraulic radius. For these ten case histories, eight were considered to be unstable, while two were considered stable. The case histories are summarized in sections 5.1 and 5.2. Each case history is labelled by the level, the last 3 numbers of the northing coordinate, and then the stope number (i.e. 29-864.1 would be the 2950 level on an 864 northing, and it will be the first stope out of the block).

To classify stability for each case history, five different surfaces were examined. These surfaces included the back, hanging wall, footwall, and the north and south shoulders. Table 4.1 summarizes the case histories used for this project. It should be noted that a back instability can also include the lift back (i.e. after blast 2, when the stope is not yet fully open, and the temporary back sloughs). Figure 4.1 summarizes the location of each case history within the Lower 84 Complex.

Table 4.1 Summary of case histories by stable and unstable surfaces

Stope	Stable/Unstable	Failure Surface
29-864.1	Unstable	Back
30-848.1	Unstable	Raisebore
32-872.1	Unstable	S. Shoulder
32-928.1	Stable	N/A
33-840.1	Unstable	S. Shoulder
33-848.1	Unstable	FW
33-848.2	Unstable	Back
33-916.2	Unstable	N. Shoulder
33-916.3	Stable	N/A
33-936.2	Unstable	Back

The north and south walls were not considered as possible surfaces for the case histories as the shoulders for Birchtree stopes have an average dip of approximately 78 degrees to the north or south. This means that the majority of the north and south walls are considered as part of the shoulders (Figure 4.2).

This study considers exposure time from the point at which the last blast is taken in an open stope. This is a reasonable approach when considering the back of an open stope. For the case of a stope hanging wall, foot wall, and shoulders, it can be argued that the exposure time should be measured from the time when the stope walls are exposed by mucking (removing the broken ore from the stope) as the broken material provides confinement to the stope walls. This broken material will generally not fill the block enough to support the back. Mucking records were available for this study, but they were not accurate enough to properly track the incremental exposure of the stopes surface. The mucking records rely on bucket factors (tons per bucket removed from the stope) which can vary based on the grade of the block and operator mucking from the stope. The muck (broken ore) is also not drawn down at a consistent rate along each wall and can vary over time. It would be recommended that any future study use cavity monitoring scans (CMS) at various intervals of the mucking process, to gather accurate data on the effect of incremental exposure of the stope walls.

Additional sources of data include lab testing, geotechnical data, and peridotite concentrations, and are presented in the following sections.

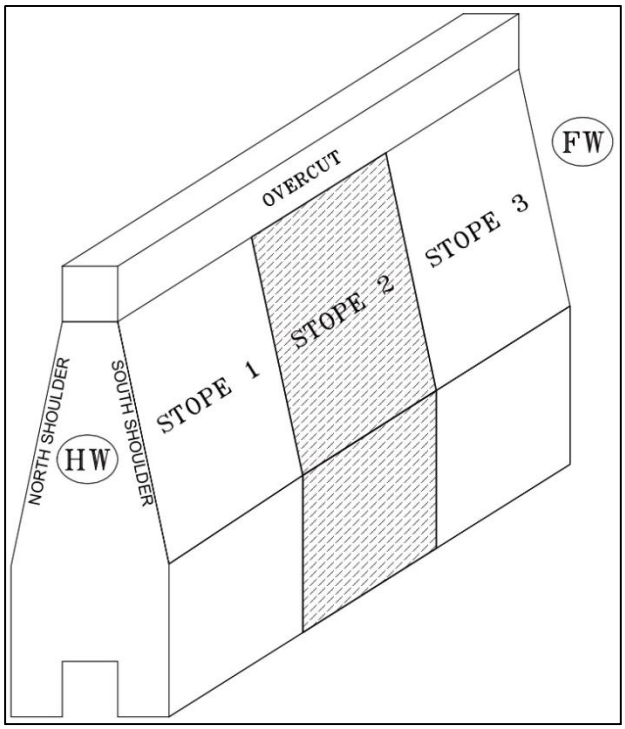

Figure 4.2 General Shape of Stopes at the Birchtree Mine

4.2 Laboratory Strength Properties

For this research, a small lab testing program was conducted on two separate rock types. These rock types included ore samples labelled MASU (massive sulfide) and peridotite samples labelled PRDT. The results for the UCS testing are shown in Table 4.2. A summary of historic rock testing values used at the Birchtree Mine area shown in Table 4.3.

Table 4.2 Summary of unconfined compressive strength (UCS) testing for massive sulphide and peridotite samples

Core ID	Sample #	Rock Type	UCS (MPa)
742	**UCS1**	Sulphide	56.7
743	**UCS3**	Sulphide	51.0
743	**UCS2**	Sulphide	55.7
762	**UCS2**	Peridotite	151.6
746	**UCS3**	Peridotite	33.3
746	**UCS1**	Peridotite	113.5

Table 4.3 Rock mechanical properties for various rock types at the Birchtree Mine (After Birchtree Material Properties Table, 2010)

		Material Properties					Rock Mass Properties	
Mine	Rock Type	Density (g/cm^3)	Tensile Strength (MPa)	UCS (MPa)	Young's Modulus (GPa)	Poisson's Ratio	Average IRMR	m_i
Birchtree Lower 84	Sulphide Matrix (Sumx)	3.5	11	67	52	0.30	61	25
	Massive Sulphide (Masu)	4.5	4.5	74	58	0.25	-	-
	Ultramafic	3.1	8.1	158	60	0.30	60	17
	Biotite Schist	2.8	10	72	49	0.29	66	10
	Quartzite	2.7	9.4	214	72	0.25	68	15

4.3 Geotechnical Data for Stope Analysis

For each case history, the joint sets were determined using scanline data collected for the 84 Complex at Birchtree. Scanlines are not completed for each stope, so available data is limited. The closest scanlines on the adjacent level or levels above/below are used to define an area. Determining the major joint sets is required to estimate the B factor used to calculate N'. Refer to Appendix A for scanline data used for each stope.

Stope specific geotechnical data to differentiate conditions between the stope case histories could only be collected when data was available. Geotechnical information is dispersed throughout the mine, and data on the variability of properties between stopes, such as joint information, was not

available. General average properties for most stopes were used for case histories. The only comprehensive geotechnical data that could be used to differentiate between stopes included RQD, peridotite concentrations within stopes, and modelled stress conditions. The assessment of these properties is described in the following sections and summarized for individual case histories.

4.3.1 Average Weighted RQD

As discussed is Section 2.1, RQD is the percentage of intact core longer than 10 centimetres in length, measured for a core run, which is often three metres long. RQD can also be categorized within each rock type. If two RQD measurements are available for a rock type, an average RQD can be based simply on the average of the two values; however, this may not be representative. For example, one RQD value may represent one metre of core, while the other core run may be two metres long. The RQD for the two metre length will have a larger impact on the overall rock quality as it represents a greater percentage of the length of core drilled. To account for the various lengths of the possible RQD intervals, a weighted average system was used to calculate the average RQD for each case history.

For each stope, the diamond drill holes will generally extend well beyond the stope boundaries. To ensure the RQD data is representative, RQD data is obtained up to a maximum of six metres outside the stope boundaries. RQD values are separated into ten different category ranges from 1 to 100 (i.e. 0-10, 11-20, 21-30…91-100). For each of these ranges, weighted average values for RQD are calculated and multiplied by the total length of core within that range to obtain the RQD factor (Equation 4.1). To obtain the average weighted RQD, the sum of the RQD factors for all ranges is divided by the total length of core (Equation 4.2). Data from the 32-872.1 case history is shown in Table 4.4. An example calculation for the RQD range of 11 to 20 is shown in Equations 4.1 and 4.2.

Table 4.4 Example of inputs for calculating average weighted RQD

RQD Range	Total Metres	Percentage of Total Core	Average RQD within Range	Factor
0-10	30.8	23%	1	43
11-20	10.3	8%	15	154
21-30	6.9	5%	25	175
31-40	7.4	5%	35	256
41-50	14.1	10%	45	630
51-60	23.5	17%	55	1300
61-70	12.6	9%	67	843
71-80	10.6	8%	77	823
81-90	10.5	8%	85	899
91-100	9.3	7%	97	903
Total	**136.0**			**6026**
Average RQD				**44**

$$RQD\ Factor = \left[\frac{(\sum RQD\ in\ each\ range)}{\#\ of\ RQD\ Measurements}\right] \times Total\ Length\ of\ RQD \quad \text{.....(4.1)}$$

$$RQD\ Factor = \left[\frac{(12 + 15 + 16 + 17)}{4}\right] \times 10.3m$$

$$= 15 \times 10.3m$$

$$= 153.8m$$

$$Weighted\ Average\ RQD = \frac{\sum RQD\ Factor}{Total\ Core\ Length} \quad \text{.....(4.2)}$$

$$= \frac{6026m}{136m}$$

$$= 44$$

4.3.2 Peridotite Concentrations

Peridotite is an ultramafic rock that can be found at the Birchtree Mine, often within the ore zone. It has been observed that excavations in peridotite tend to experience instability. To quantify the effect of peridotite on stability, peridotite concentrations were determined for each case history using magnetic probe data from production drill holes.

The magnetic probe is normally used to identify intervals of nickel within each stope to help refine block designs and estimate stope grades. Higher positive readings indicate areas of ore, while low to zero readings indicate intervals of waste rock. Intervals of peridotite are identified by negative readings of 1000 or less. The probe takes a reading every 0.09 meters. To determine the peridotite concentrations for each stope surface, holes parallel to that surface (hanging wall, footwall, south shoulder, and north shoulder) were used. Peridotite concentrations for the stope backs could not be collected as no holes were drilled normal to these surfaces. Data from these holes were copied into an MS excel sheet to identify peridotite intervals. An example of this spread sheet is shown in Figure 4.1. If a peridotite reading is detected, the MS excel sheet indicates this with a value of 1. The concentration of peridotite is determined by dividing the total number of detected peridotite intervals by the total number of readings recorded by the probe. For example, if there was 90 metres of data recorded, a total number of 1000 data points would be reviewed in the spread sheet. If 600 of these data points were identified as peridotite, the concentration for that surface would be (Equation 4.3):

$$Concentration\ of\ Peridotite\ (\%) = \frac{600}{1000} x100 \quad \text{.....(4.3)}$$

$$= 60\%$$

Table 4.5 Example of Excel sheet used to detect peridotite intervals

	From	To				
Interval	0	200				
Total Peridotite Readings Present Within Interval			288			
Total Readings Within Interval			439			
% Peridotite Contained Within Interval			65.60%			
Hole ID	Memory	From	To	MAG	Peridotite Present Within Interval	Reading Present Within Interval
		0.16	0.49	-42	0	1
		0.49	0.82	-1044	1	1
		0.82	1.15	-896	0	1
		1.15	1.48	-2418	1	1
		1.48	1.8	-1951	1	1
		1.8	2.13	-1463	1	1
		2.13	2.46	-516	0	1
		2.46	2.79	0	0	1

4.3.3 Overbreak and Underbreak

After each blast, holes are cleaned to ensure that they are open and ready to load for the next blast. As part of this process, hole measurements are taken, and that information is given to the stope planner, so he/she can design their next blast, making adjustments as required due to the differences in designed depths and actual measurements. From these measurements, overbreak and underbreak can be measured. Various factors can contribute to either overbreak or underbreak, some of which include:

i. Overloading or under loading a production drill hole
ii. Geological contacts
iii. Rock properties (RQD, joint alteration)
iv. Blast design shapes. The most stable shape is a dome-like structure. If the blast is designed to have a flat back with no taper, as the boundaries are reached, the blast shape will tend to round out and form the dome-like shape.
v. If one of the production holes do not break to the top of charge, it may cause any remaining holes behind it to underbreak as the open void in front is now smaller.

vi. Drill hole deviations. If two holes deviate too close to one another, one hole may cut the other off, not allowing it to blast properly, if at all. This may in turn create larger burdens for holes behind it to break, increasing the distance between the open void and the proceeding production hole.

4.3.4 Stress Modelling with Map3D

Map3D is the stress modelling program that is currently used at the Manitoba Vale Operations for evaluating the predicted levels of stress surrounding their mining stopes. This program is a three dimensional boundary element program. To determine an A factor for N' stability, a stress evaluation was done for each case history (Sections 5.1 and 5.2). A linear elastic model was chosen because no data exists for estimating non-elastic parameters.

For each case history, data was imported from Vulcan. Vulcan is a three-dimensional mine design program that allows users to draft various mine related activities, and compute ore grades, volumes, masses, and various other material properties. From the data, stopes for each case history were constructed in Map3D. To determine the magnitude of stress acting on the individual surfaces in a stope, stress grids intersecting the stope were constructed in the YZ and XZ planes as seen in Figure 4.3. The stress grids were divided into 0.6 metre intervals. The initial stress state at depth, for a particular case history, was determined using Equation 3.3 from Section 3.1.2.2. For the purposes of this study, principal stresses were assumed to be horizontal and vertical with a horizontal to vertical stress ratio of 2. This is a common average value for the Canadian Shield. Stresses in the horizontal plane were assumed to be uniform. For each case history the sulphide material properties were used for model input (Referred to as Sumx in Table 4.3, Section 4.2). The ore bearing sulphide has a density of 3.4, which was used to calculate the model's vertical stress gradient. A summary of the input data for each case history is shown in Table 4.6.

Stress modelling was conducted to determine the maximum induced compressive stress acting on the five potential surfaces. This value was used to determine the A factor for the N' Stability Number (Section 2.5). To account for past mining, all stopes mined within a four stope radius, up to two levels above and below the stope of concern, were accounted for. It was assumed that any

stopes outside this zone would have minimal effect on the induced stresses around the stope of concern.

An example output from Map3D for the 33-848.1 Stope is shown in Figure 4.3. Refer to Appendix B for stress plots of each case history.

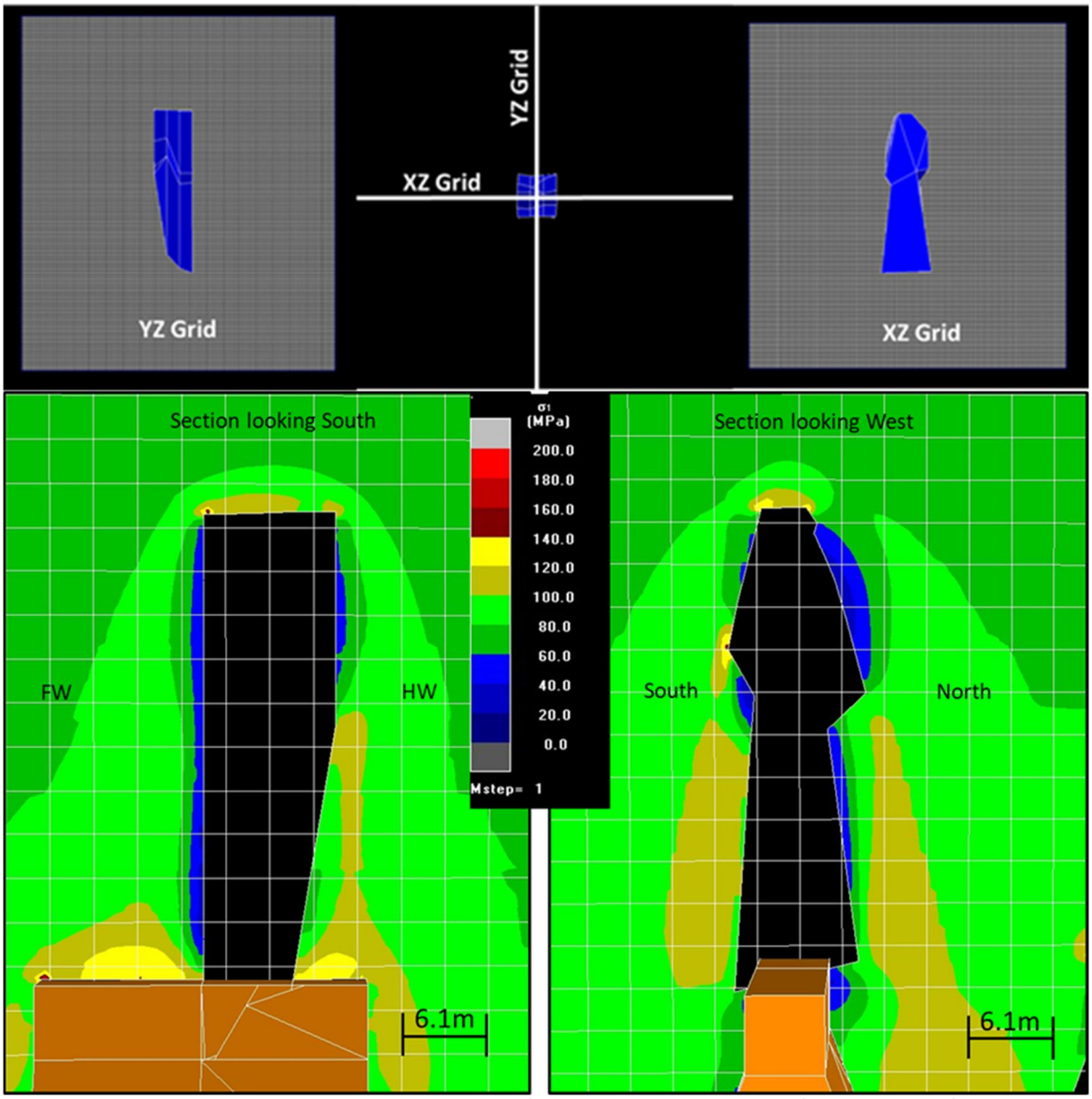

Figure 4.3 Stress contours in the YZ and XZ planes of the major principle stresses for the 33-848.1 from Map3D

Table 4.6 Summary of data inputs for Map3D stress plots

Stope	Material	UCS (MPa)	Young's Modulus (GPa)	Poisson's Ratio	Sigma 1 = Sigma 2 (MPa)	Sigma 3 (MPa)	Sigma 1 = Sigma 2 Gradient (MPa/metre)	DSigma 3 (MPa/metre)
29-864.1	Sulphide	67	51.7	0.3	62	31	0.069	0.034
30-848.1	Sulphide	67	51.7	0.3	64	32	0.069	0.034
32-872.1	Sulphide	67	51.7	0.3	67	33	0.069	0.034
33-840.1	Sulphide	67	51.7	0.3	69	35	0.069	0.034
33-848.1	Sulphide	67	51.7	0.3	69	35	0.069	0.034
33-848.2	Sulphide	67	51.7	0.3	69	35	0.069	0.034
33-936.2	Sulphide	67	51.7	0.3	69	35	0.069	0.034
33-916.2	Sulphide	67	51.7	0.3	69	35	0.069	0.034
32-928.1	Sulphide	67	51.7	0.3	69	35	0.069	0.034
33-916.3	Sulphide	67	51.7	0.3	69	35	0.069	0.034

CHAPTER 5
CASE HISTORIES

5.1 Unstable Case Histories

Instability in stopes may occur at any point in the mining process. Instabilities can occur as the overcut and undercut are being driven, in the raisebore before blasting has begun, during the blasting process, or at any point once the stope is completely excavated. In most cases, instability will occur during the mining process, or immediately after the stope is fully exposed. Depending on the extent, and severity of the instability, the stope may continue to be mined as long as it is safe to do so, and the ore being extracted is economical. The following sections summarize a few examples of stable and unstable stopes that were excavated at the Birchtree Mine. For additional rock classification data for refer to Appendix C.

5.1.1 Case History 29-864.1

The 29-864.1 stope was classified as unstable. Following the first blast in this block, rows 5 and 6 were measured during hole cleaning and it was discovered that they had begun to slough as hole measurements came back shorter than designed for the first blast (Figure 5.1). When measurements of the production hole depths after the blast were taken, it was found that rows 5 and 6 had sloughed to 5.2 and 0.6 meters respectively below the drillroom bench. The remaining ore was later recovered using the remaining blast holes, and no further issues were encountered. As this stope experienced instability after only one blast was taken, the unstable surface was a temporary back. A summary of the rock mass and stress conditions for the temporary back is presented in Table 5.1 and a plot of the predicted stand-up times is shown in Figure 5.2. Figure 5.3 is an isometric sketch showing the relative location of the stope in the mining panel.

Table 5.1 Rock classification data for stope 29-864.1

29-864.1	N. Shoulder	S. Shoulder	Hanging Wall	Footwall	Back
Critical Joint Orientation (º)	45	45	45	25	5
Maximum Induced Stress (MPa)	59	59	62	58	96
Unconfined Compressive Strength (MPa)	67	67	67	67	67
Q'	9.0	9.0	9.0	9.0	9.0
A Factor	0.1	0.1	0.1	0.1	0.1
B Factor	0.2	0.2	0.5	0.85	0.25
C Factor	5.8	6.1	8	8	2
N' Stability Number	1.0	1.1	3.6	6.1	0.5
Hydraulic Radius (m)	3.7	3.8	2.5	3.7	2.4
Peridotite Concentration (%)	66	51	61	35	-
Surface Condition	Stable	Stable	Stable	Stable	Unstable
Exposure Time	> 1 day	> 1 day	> 1 day	> 1 day	< 1 day

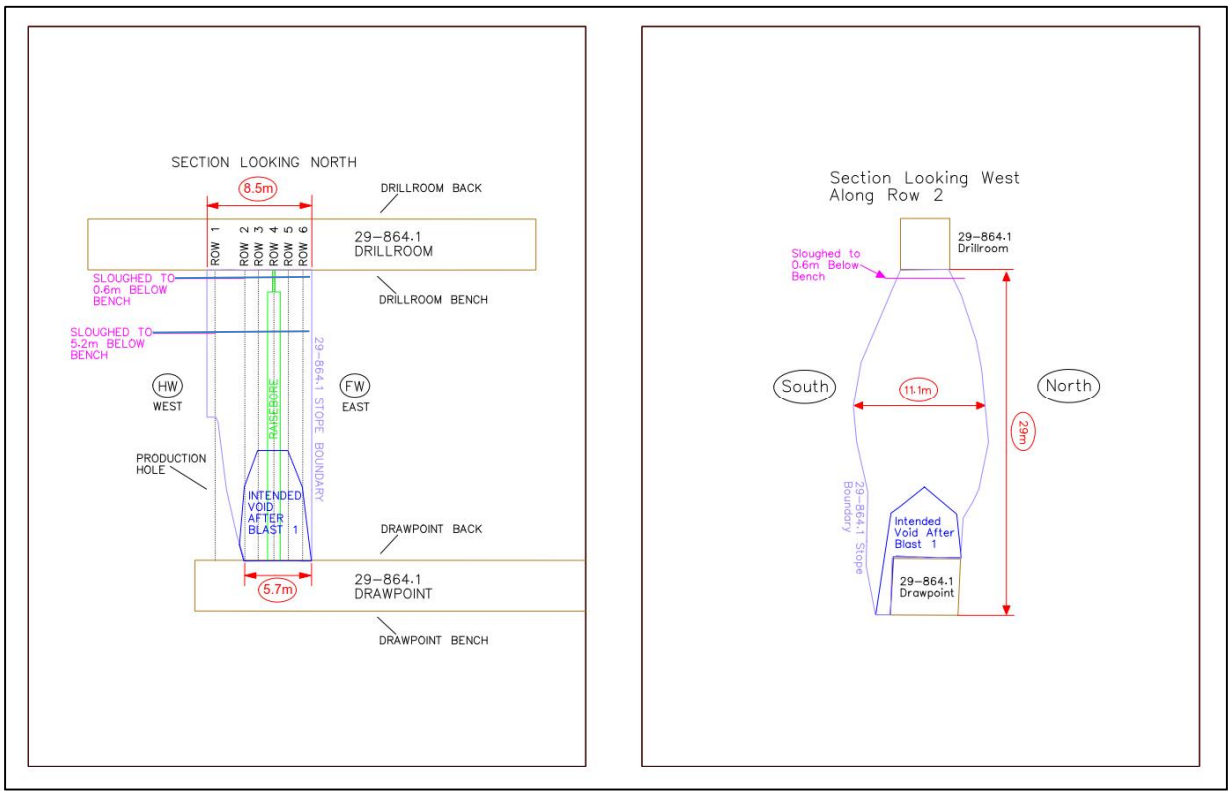

Figure 5.1 Longsection and cross-section of the 29-864.1 stope

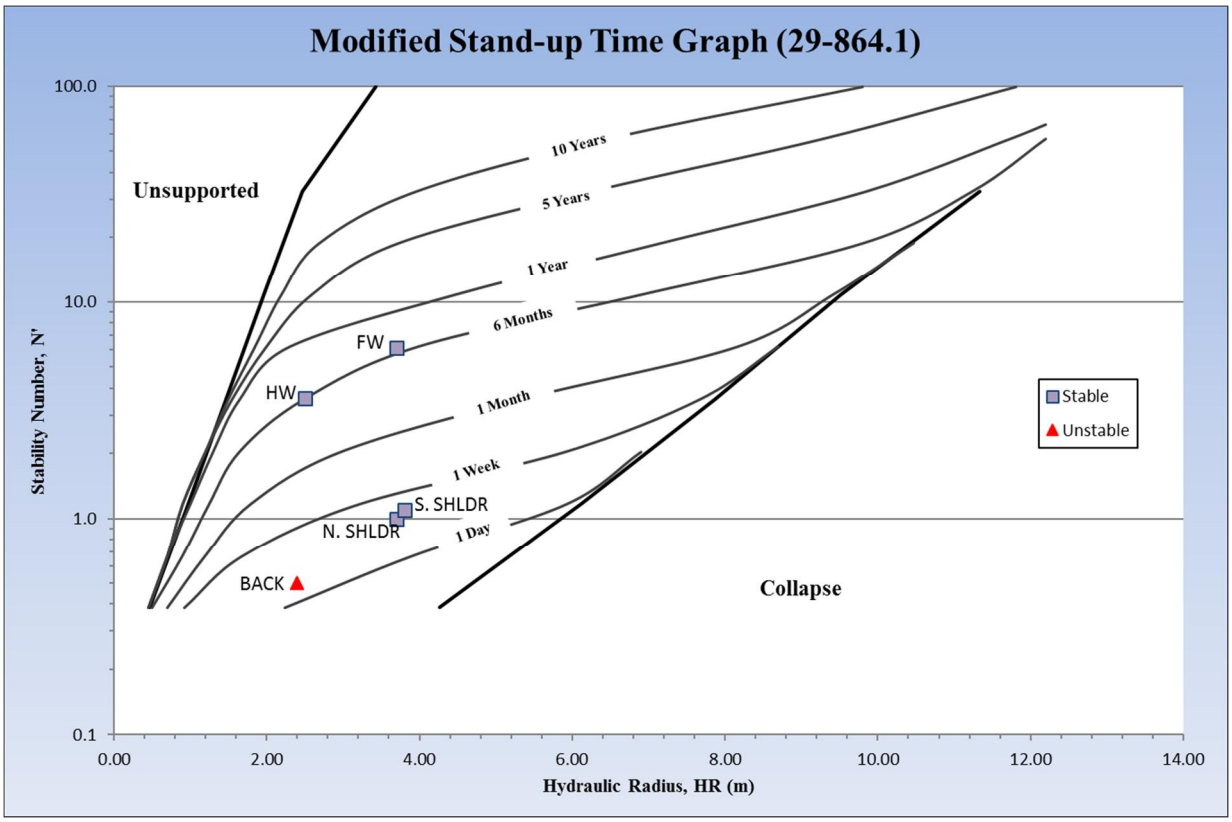

Figure 5.2 Modified Stand-up Time Graph: 29-864.1

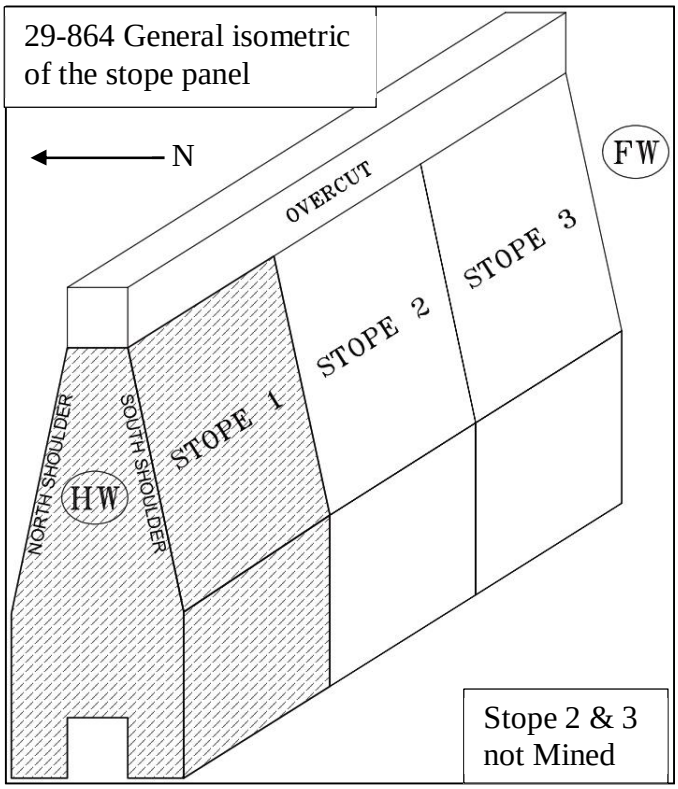

Figure 5.3 Isometric of the standard stope panel at Birchtree Mine showing the location of the 29-864.1 stope in relation to other stopes in the panel

5.1.2 Case History 30-848.1

The 30-848.1 stope was classified as unstable. While drilling the In The Hole (ITH) blast rings in the stope, the driller heard noise coming from the raisebore and decided to check the holes on row 7. After checking these holes, the driller found that a void was encountered at approximately 12.8 metres. The driller reported that the raisebore had begun to slough. The raisebore sloughed to approximately 6.1 metres wide (Figure 5.4). Poor ground conditions were also reported in rows 8 and 9 during the drilling of ITH blast rings for the stope and geology noted that the block consisted mostly of massive peridotite. For additional information on all the stopes surfaces, refer to Appendix C. Table 5.2 summarizes the rock classification data for the 30-848.1 Stope and a plot of the predicted stand-up times is shown in Figure 5.5. Figure 5.6 is an isometric sketch showing the relative location of the stope in the mining panel.

Table 5.2 Rock classification data for stope 30-848.1

30-848.1	N. Shoulder	S. Shoulder	Hanging Wall	Footwall	Back	Raisebore
Critical Joint Orientation (°)	81	81	81	81	8	81
Maximum Induced Stress (MPa)	74	63	82	78	91	74
Unconfined Compressive Strength (MPa)	67	67	67	67	67	67
Q'	9.3	9.3	9.3	9.3	9.3	9.3
A Factor	0.1	0.1	0.1	0.1	0.1	0.1
B Factor	0.3	0.3	0.2	0.2	0.2	0.2
C Factor	7.1	7.1	8	8	2	8
N' Stability Number	2.0	2.0	1.5	1.5	0.4	1.5
Hydraulic Radius (m)	4.3	3.5	3.7	3.5	3.2	1.7
Peridotite Concentration (%)	-	-	-	-	-	-
Surface Condition	Stable	Stable	Stable	Stable	Stable	Unstable
Exposure Time	> 3 days	> 3 days	> 3 days	> 3 days	> 3 days	< 3 days

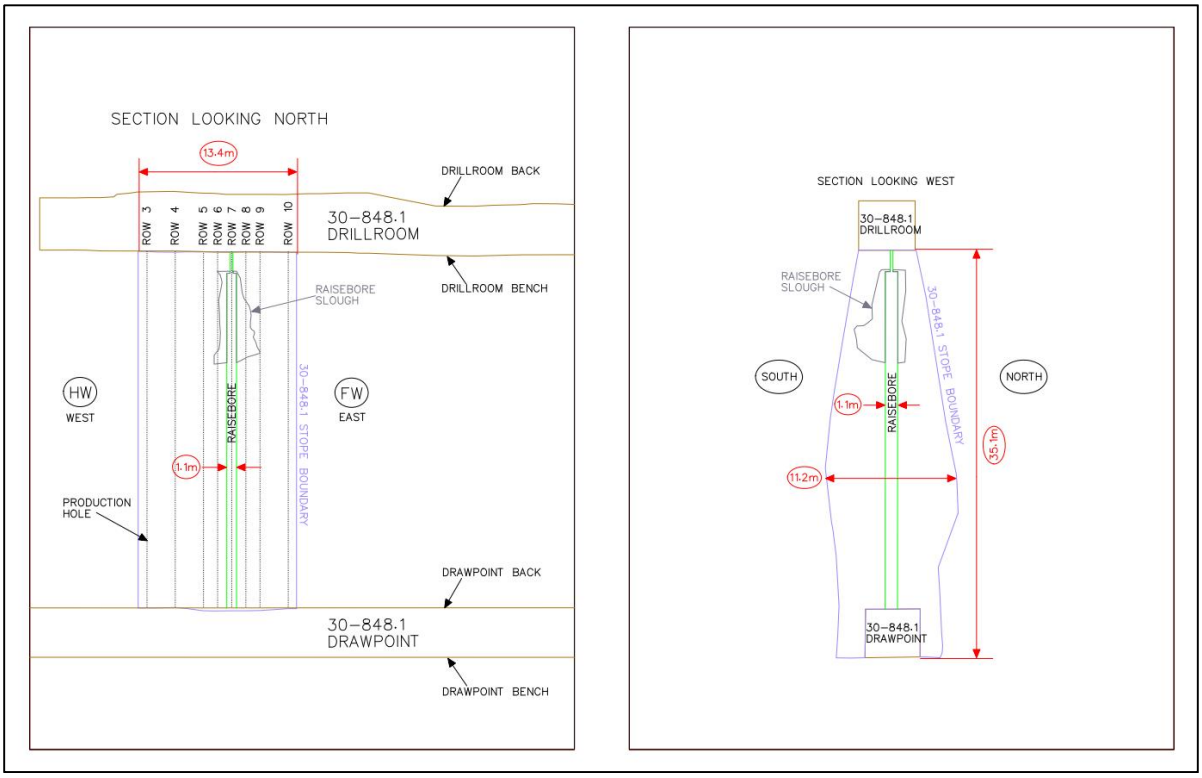

Figure 5.4 Longsection and cross-section for the 30-848.1 stope

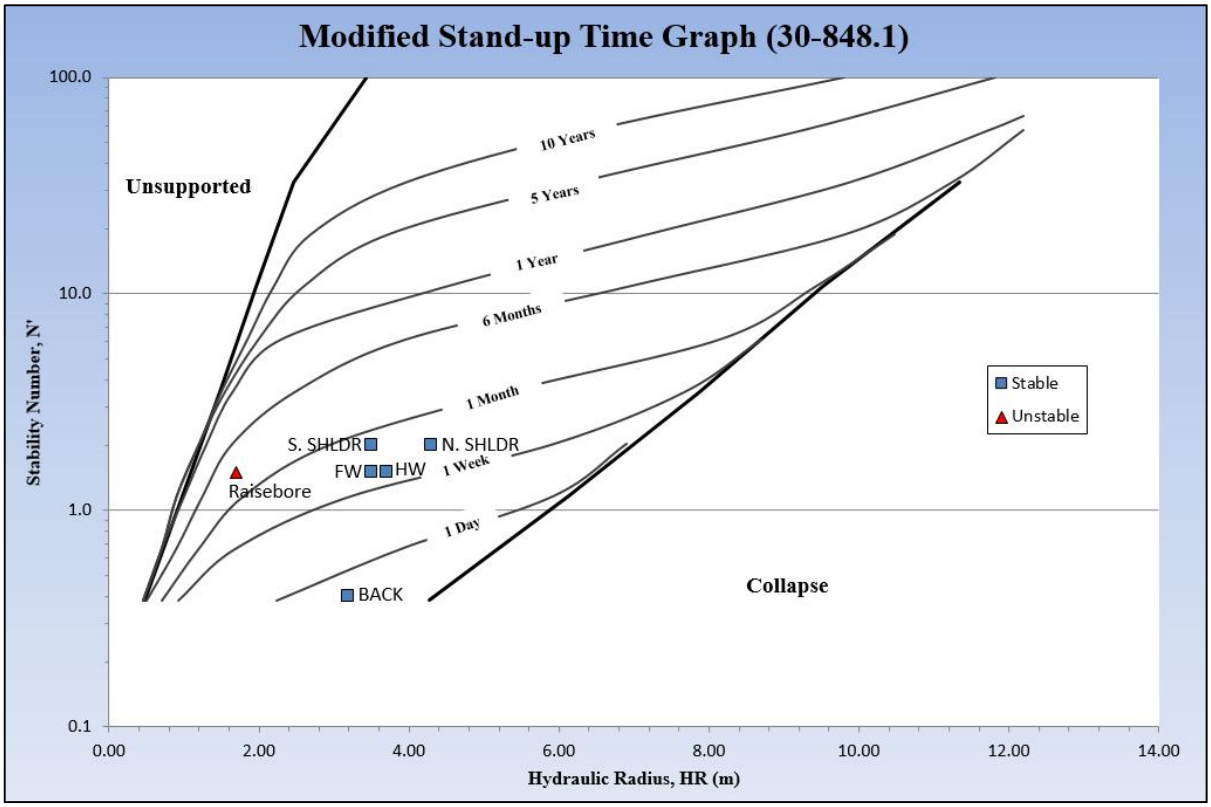

Figure 5.5 Modified Stand-up Time Graph: 30-848.1

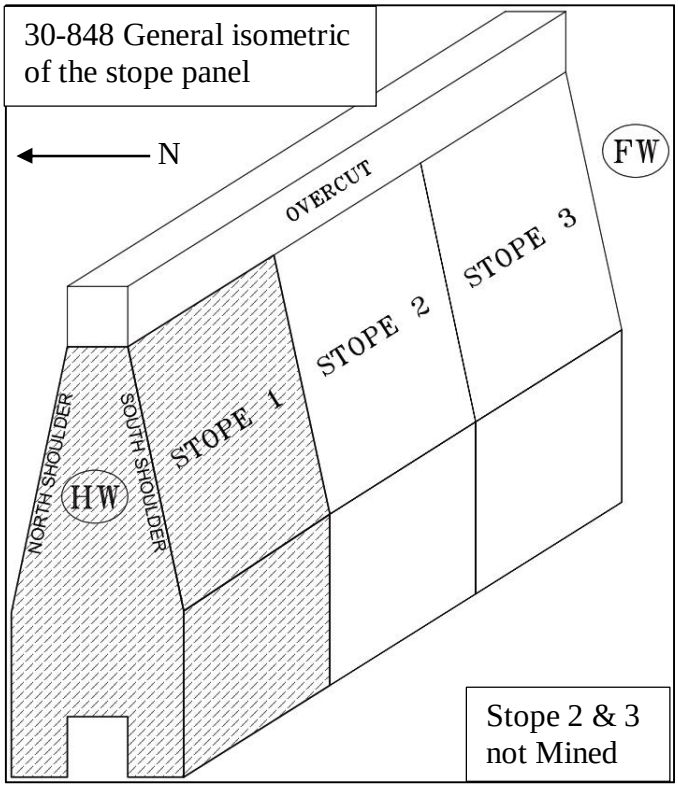

Figure 5.6 Isometric of standard stope panel at Birchtree Mine showing the location of the 30-848.1 stope in relation to other stopes in the panel

5.1.3 Case History 32-872.1

The first blast letter for this block was issued on December 6th, 2009. There was a total of three blasts for this stope, with the last blast letter issued on December 17, 2009. After the final stope blast, the south shoulder sloughed approximately 4.6 metres; as such, this block was classified as an unstable case history. Rock classification data for the stope is summarized in Table 5.3 and Figure 5.8 shows a plot of the predicted stand-up times. Figure 5.7 is a longsection and cross-section showing the 32-872.1 stope. Figure 5.9 is an isometric sketch showing the relative location of the stope in the mining panel.

Table 5.3 Rock classification data for stope 32-872.1

32-872.1	N. Shoulder	S. Shoulder	Hanging Wall	Footwall	Back
Critical Joint Orientation (°)	81	75	75	81	22
Maximum Induced Stress (MPa)	66	66	83	72	104
Unconfined Compressive Strength (MPa)	67	67	67	67	67
Q'	7.0	7.0	7.0	7.0	7.0
A Factor	0.1	0.1	0.1	0.1	0.1
B Factor	0.02	0.3	0.25	0.2	0.2
C Factor	5.8	6.3	6.1	8	2
N' Stability Number	0.8	1.3	1.1	1.1	0.3
Hydraulic Radius (m)	2.8	3.9	3.2	3.3	2.4
Peridotite Concentration (%)	40	68	56	64	-
Surface Condition	Stable	Unstable	Stable	Stable	Stable
Exposure Time	> 3 days	< 3 days	> 3 days	> 3 days	> 3 days

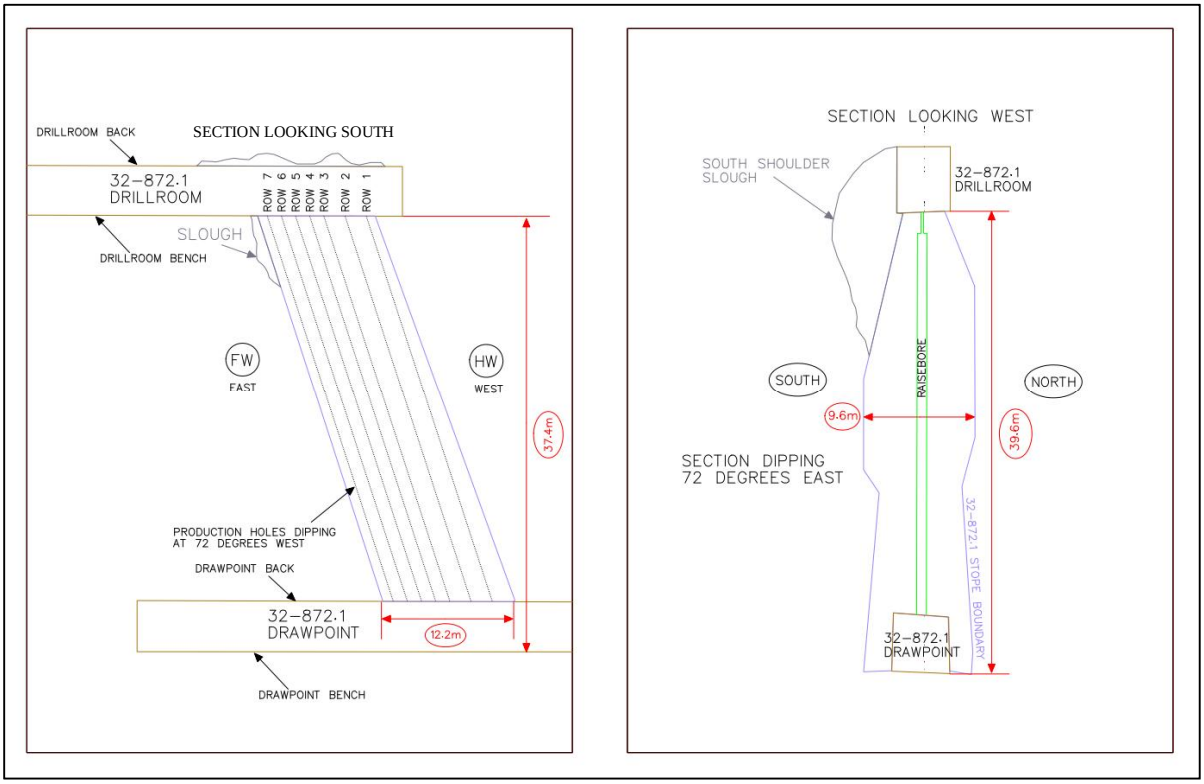

Figure 5.7 Longsection and cross-section of the 32-872.1 stope

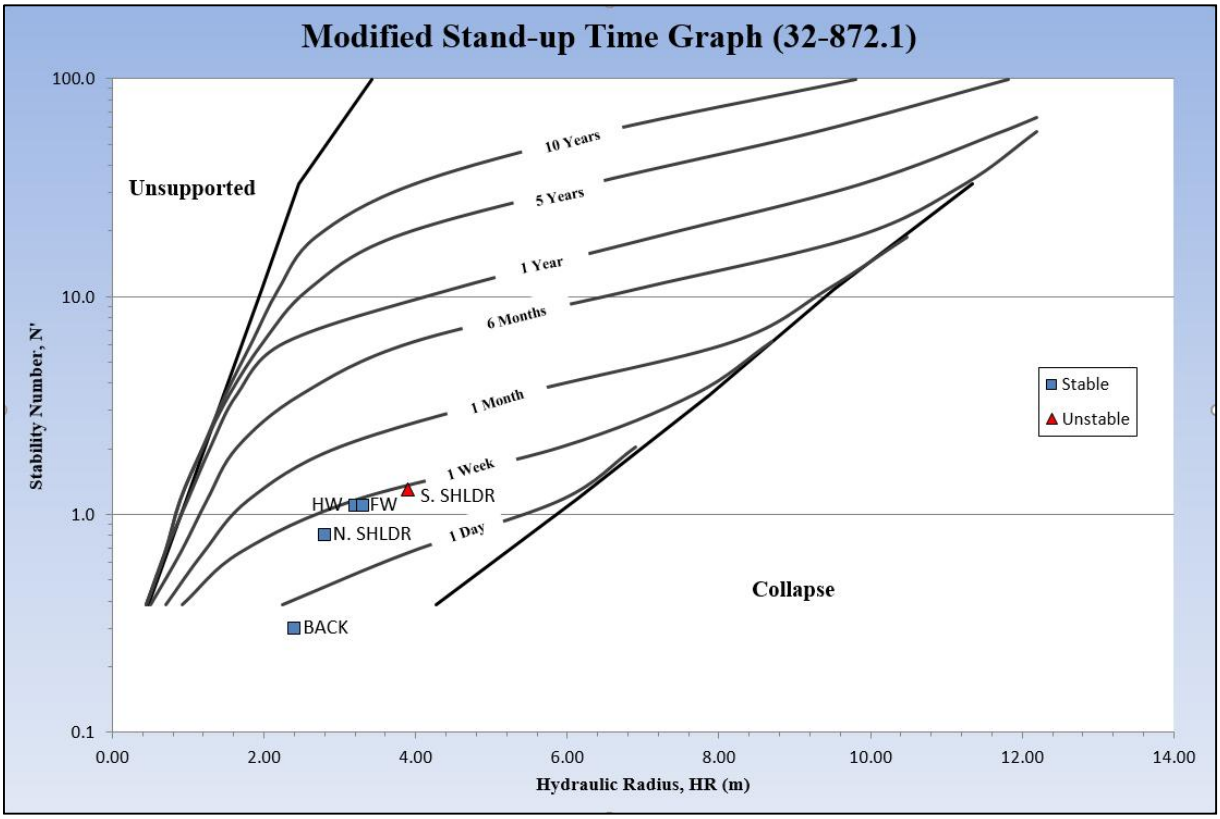

Figure 5.8 Modified stand-up time graph: 32-872.1

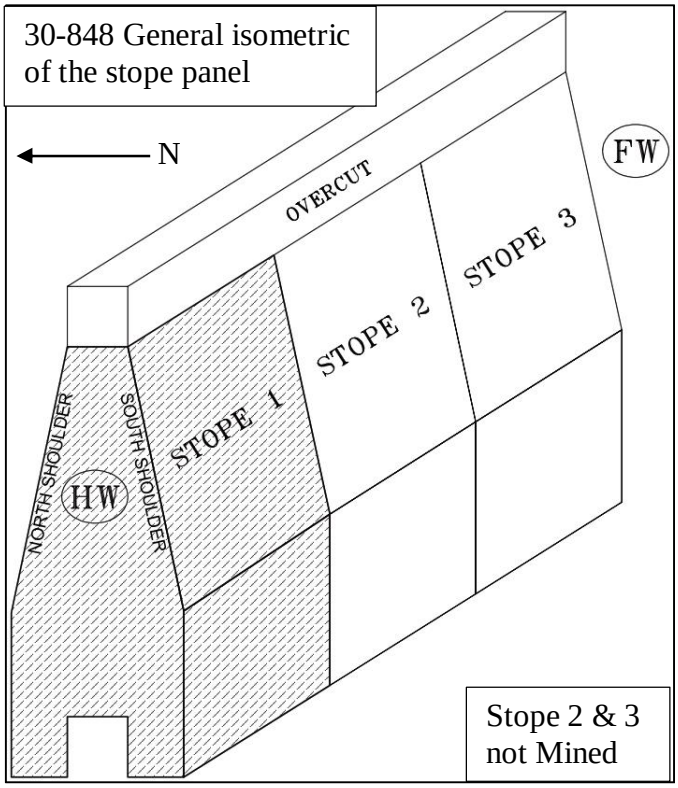

Figure 5.9 Isometric of standard stope panel at Birchtree Mine showing the location of the 32-872.1 stope in relation to other stopes in the panel

5.1.4 Case History 33-840.1

For the 33-840.1 Stope, a total of three blast were taken. The first blast letter was issued on August 15, 2010 and blast 3 was issued on August 22nd, 2010. After the final stope blast, all stope surfaces appeared to be stable. There were no signs of potential slough up to this point. As ore was removed from the block, the south shoulder and footwall of the block began to slough, eventually going above the back of the drill room (overcut) (Figure 5.10). Mucking of the block was stopped on August 29th, 2010. A small amount of cemented rock fill was placed in the block, but due to continuing slough, filling was stopped and the remaining void was allowed to choke itself off and fill with the sloughed material. Table 5.4 summarizes the rock classification data and Figure 5.11 shows a plot of the predicted stand-up times for the 33-840.1 stope.

Table 5.4 Rock classification data for stope 33-840.1

33-840.1	N. Shoulder	S. Shoulder	Hanging Wall	Footwall	Back
Critical Joint Orientation (°)	71	61	71	59	59
Maximum Induced Stress (MPa)	60	62	58	57	103
Unconfined Compressive Strength (MPa)	67	67	67	67	67
Q'	9.1	9.1	9.1	9.1	9.1
A Factor	0.1	0.1	0.1	0.1	0.1
B Factor	0.3	0.2	0.2	0.2	0.8
C Factor	6.2	6.5	8	8	2
N' Stability Number	1.7	1.2	1.5	1.5	1.5
Hydraulic Radius (m)	3.1	3.2	3.7	4.3	2.9
Peridotite Concentration (%)	27	43	28	41	-
Surface Condition	Stable	Unstable	Stable	Unstable	Stable
Exposure Time	> 1 day	< 1 day	> 1 day	> 1 day	> 1 day

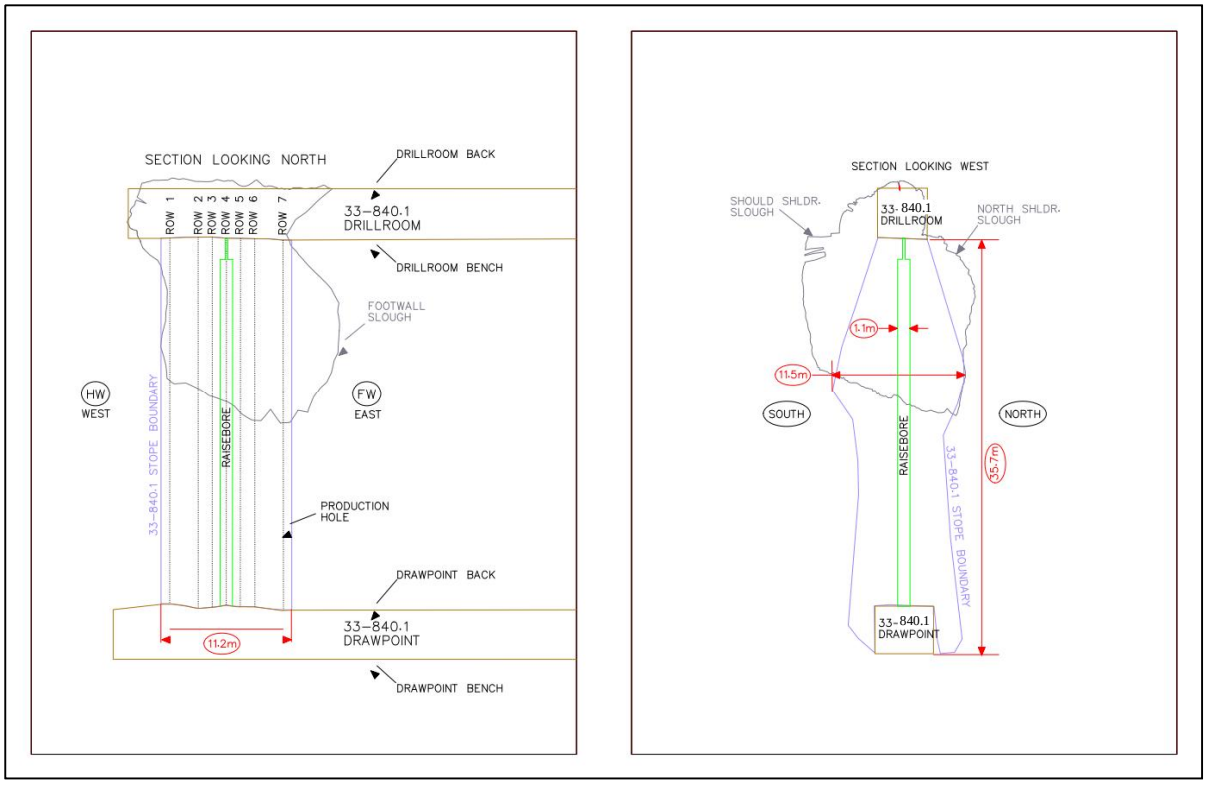

Figure 5.10 Longsection and cross-section of the 33-840.1 stope

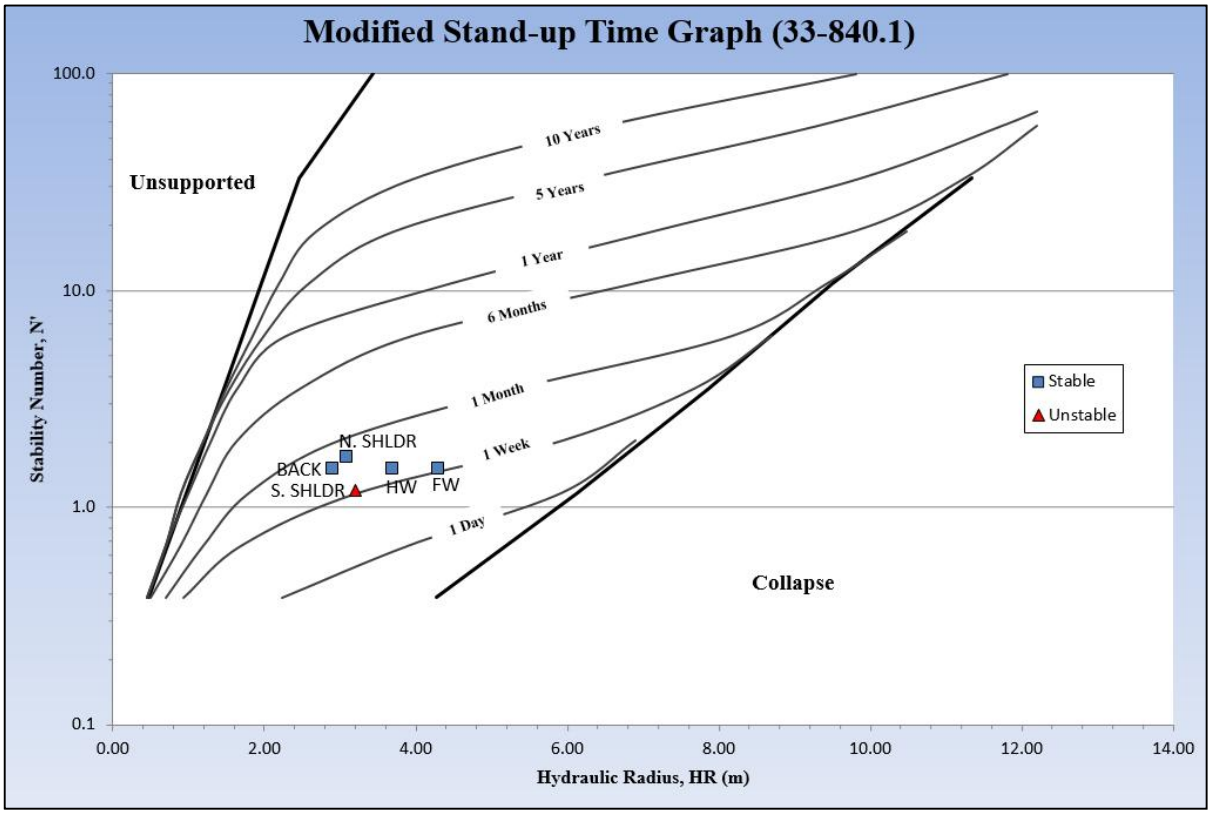

Figure 5.11 Modified Stand-up Time Graph: 33-840.1

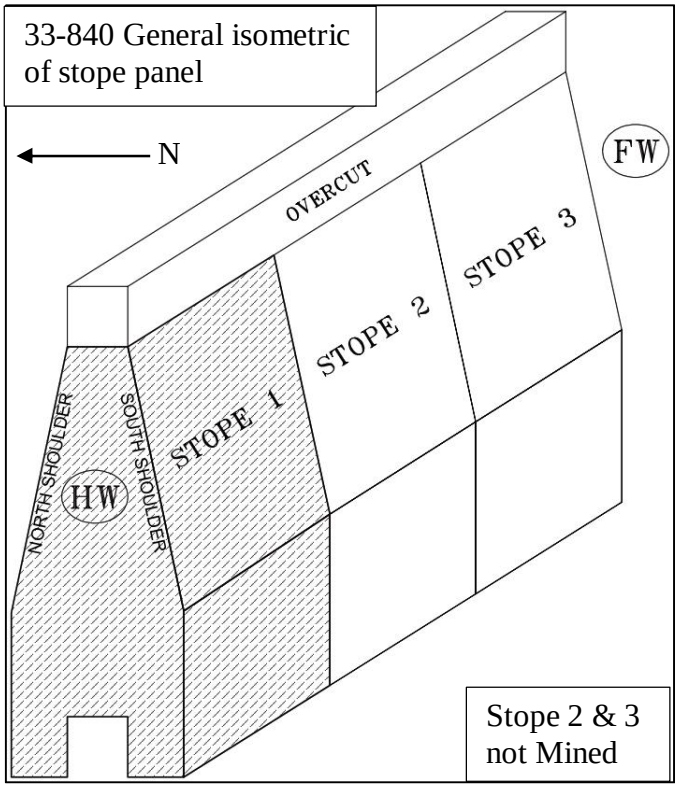

Figure 5.12 Isometric of standard stope panel at Birchtree Mine showing the location of the 33-840.1 stope in relation to other stopes in the panel

5.1.5 Case History 33-848.1

For the 33-848.1 Stope, a total of three blast were taken. The first blast was issued on March 17th, 2010, with the final blast issued on the 21st. No issues were encountered while blasting this stope, however, when extracting the ore after blast 3, the footwall began to slough (Figure 5.13). The block was never completely emptied due to the sloughing and the remaining void was filled with cemented rock fill. The last ore mucked from the block was on March 26th, 2010. A summary of the rock classification and a plot of the predicted stand-up times for the 33-848.1 stope is shown in Table 5.5 and Figure 5.14 respectively. Figure 5.15 is an isometric sketch showing the relative location of the stope in the mining panel.

Table 5.5 Rock classification data for stope 33-848.1

33-848.1	N. Shoulder	S. Shoulder	Hanging Wall	Footwall	Back
Critical Joint Orientation (°)	71	61	71	59	59
Maximum Induced Stress (MPa)	75	52	75	93	125
Unconfined Compressive Strength (MPa)	67	67	67	67	67
Q'	9.5	9.5	9.5	9.5	9.5
A Factor	0.1	0.1	0.1	0.1	0.1
B Factor	0.2	0.2	0.2	0.2	0.8
C Factor	5.2	6.5	8	8	2
N' Stability Number	1.0	1.2	1.5	1.5	1.5
Hydraulic Radius (m)	2.6	2.7	2.7	3.4	2.5
Peridotite Concentration (%)	61	66	33	51	-
Surface Condition	Stable	Stable	Stable	Unstable	Stable
Exposure Time	> 1 day	> 1 day	> 1 day	< 1 day	> 1 day

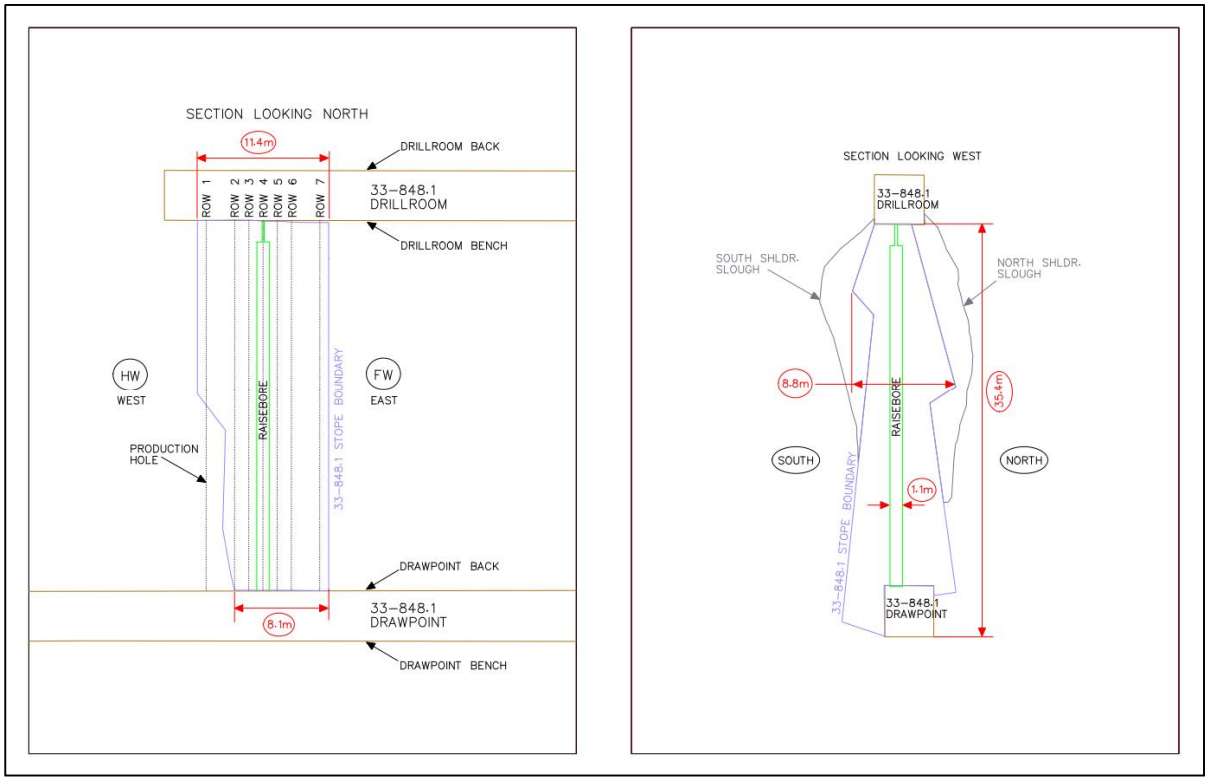

Figure 5.13 Longsection and cross-section of the 33-848.1 stope

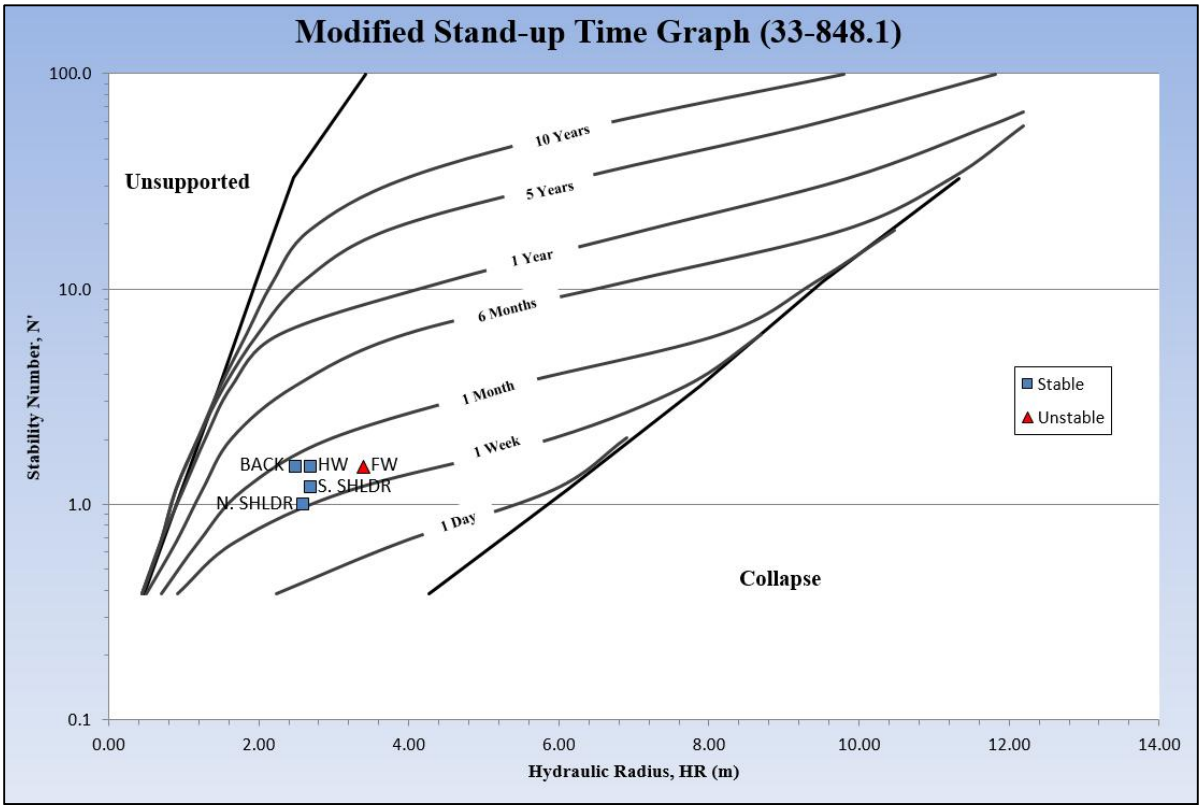

Figure 5.14 Modified Stand-up Time Graph: 33-848.1

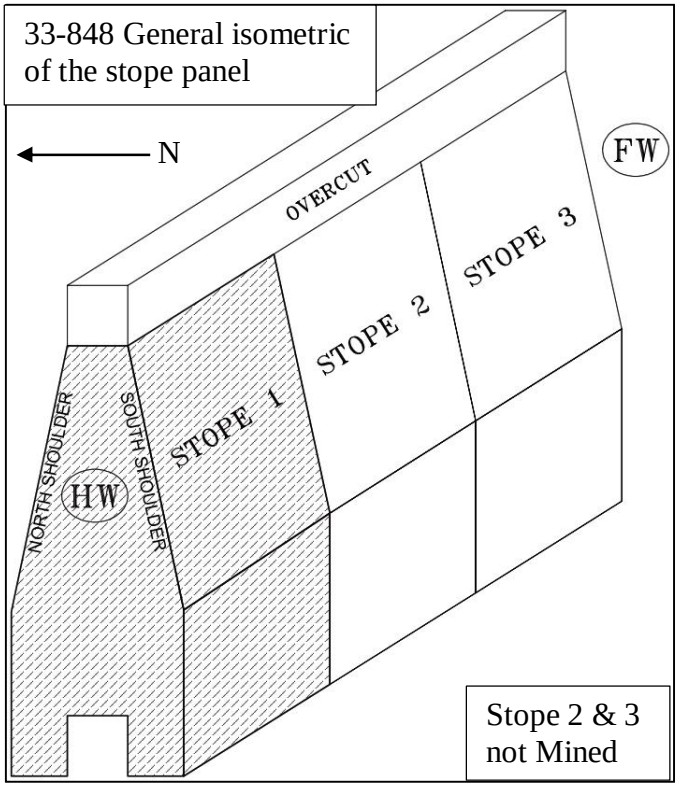

Figure 5.15 Isometric of standard stope panel at Birchtree Mine showing the location of the 33-848.1 stope in relation to other stopes in the panel

5.1.6 Case History 33-848.2

The 33-848.2 block was classified as an unstable case history. There were a total of three blasts that were taken from this block. The first blast was issued on April 30th, 2010 and the final blast was issued on June 20th, 2010. After the first blast, there was a minor instability that did not cause concern. After blast 2 was taken, the temporary back for the remaining drill room floor sloughed along rows 7 and 8, exposing an opening in the bench. After it was safe to continue mining, the remaining drill room floor was taken on the 20th of June and the stope was mucked until July 5th. The block was never completely emptied and the remaining void was filled with cemented rock fill. A summary of rock classification values for the stope surfaces are presented in Table 5.6 and a plot of the predicted stand-up times are shown in Figure 5.17. Peridotite concentration along the hanging wall was not collected as it was the second stope in the panel (i.e. 33-848.1 was mined out in front of it). A pillar was left between the 33-848.1 stope and the hanging wall of the 33-848.2 stope (Figure 5.16). Figure 5.18 is an isometric sketch showing the relative location of the stope in the mining panel.

Table 5.6 Rock classification data for stope 33-848.2

33-848.2	N. Shoulder	S. Shoulder	Hanging Wall	Footwall	Back
Critical Joint Orientation (°)	71	61	71	59	59
Maximum Induced Stress (MPa)	51	53	0	94	127
Unconfined Compressive Strength (MPa)	67	67	67	67	67
Q'	6.5	6.5	6.5	6.5	6.5
A Factor	0.1	0.1	1	0.1	0.1
B Factor	0.3	0.2	0.2	0.2	0.8
C Factor	6	6.9	8	8	2
N' Stability Number	1.2	0.9	10.4	1.0	1.0
Hydraulic Radius (m)	3.8	3.6	3.1	2.8	3.0
Peridotite Concentration (%)	55	70	N/A	28	-
Surface Condition	Stable	Stable	Stable	Stable	Unstable
Exposure Time	> 1 day	> 1 day	> 1 day	> 1 day	< 1 day

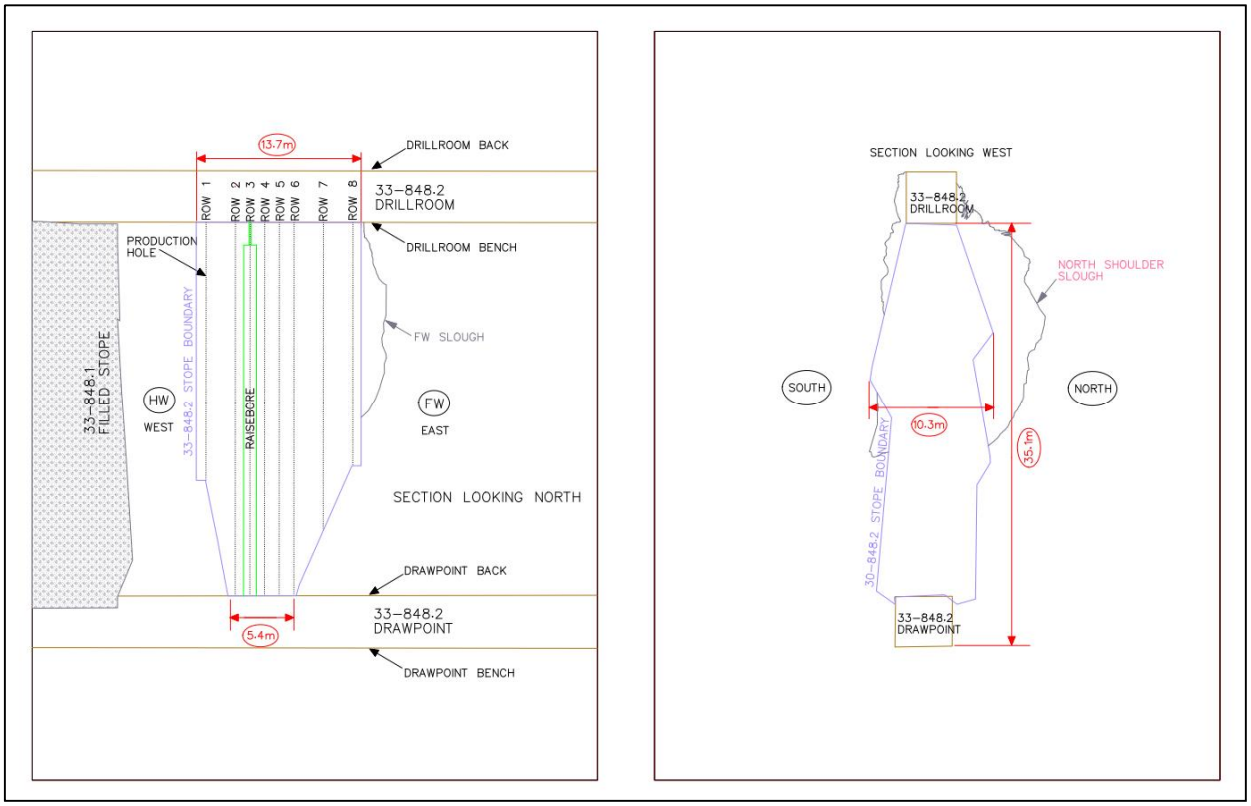

Figure 5.16 Longsection and cross-section for the 33-848.2 stope

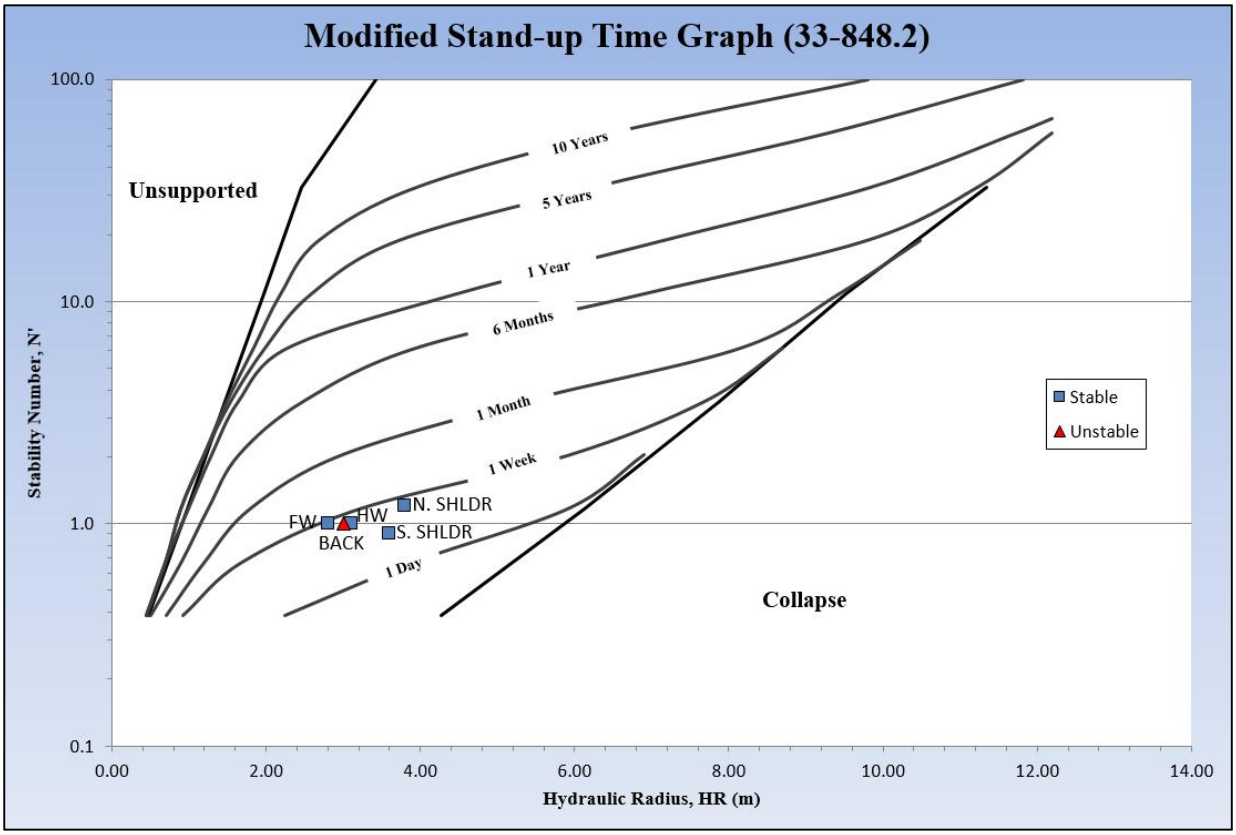

Figure 5.17 Modified Stand-up Time Graph: 33-848.2

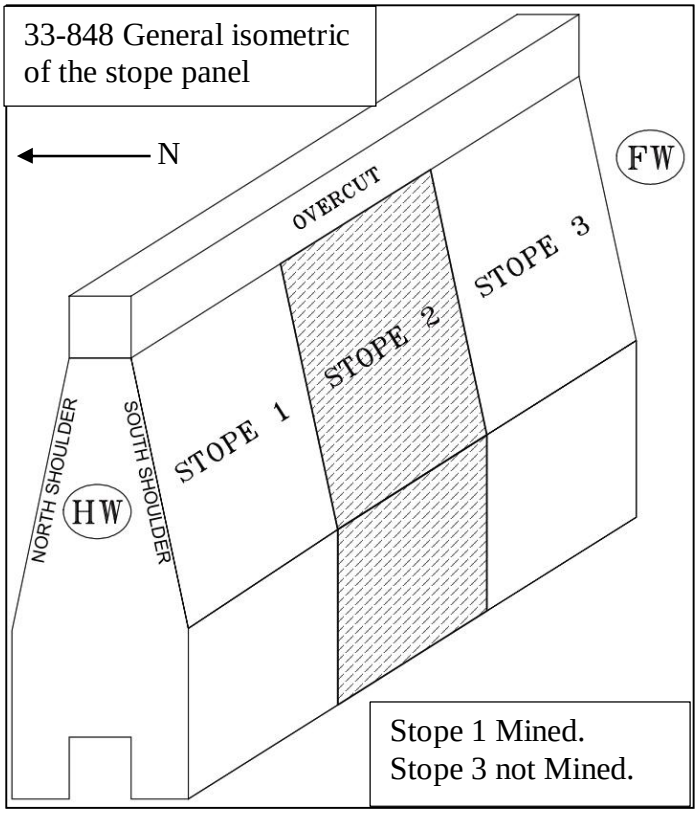

Figure 5.18 Isometric of standard stope panel at Birchtree Mine showing the location of the 33-848.2 stope in relation to other stopes in the panel

5.1.7 Case History 33-936.2

The 33-936.2 stope was classified as an unstable case history. The instability occurred in the back of the drawpoint before any stopes were taken in the 936 panel (Figure 5.19). Due to the instability in the back, the first stope (936.1) could not be mined, as such, the 936.2 stope was then scheduled to be taken. This stope was laid out to encompass the void created by the instability in the back of the drawpoint that experienced the sloughing. No other issues were encountered once the 936.2 stope began blasting. A total of 2 blasts were taken with the first and last blasts being conducted on April 20th and 25th, 2010 respectively. The block was emptied on May 5th and was completely filled with cemented rock fill on May 21st. A summary of the rock classification data and a plot of the predicted stand-up times are shown in Table 5.7 and Figure 5.20 respectively. Figure 5.21 is an isometric sketch showing the relative location of the stope in the mining panel.

Table 5.7 Rock classification data for stope 33-936.2

33-936.2	N. Shoulder	S. Shoulder	Hanging Wall	Footwall	Back
Critical Joint Orientation (°)	70	63	59	59	10
Maximum Induced Stress (MPa)	92	123	35	35	87
Unconfined Compressive Strength (MPa)	67	67	67	67	67
Q'	12.9	12.9	12.9	12.9	12.9
A Factor	0.1	0.1	0.1	0.1	0.1
B Factor	0.25	0.23	0.2	0.2	0.2
C Factor	6	5.8	5.9	5.9	2
N' Stability Number	1.9	1.7	1.5	1.5	0.5
Hydraulic Radius (m)	4.4	3.7	3.3	2.8	3.2
Peridotite Concentration (%)	-	-	-	-	-
Surface Condition	Stable	Stable	Stable	Stable	Unstable
Exposure Time	> 1 day	> 1 day	> 1 day	> 1 day	< 1 day

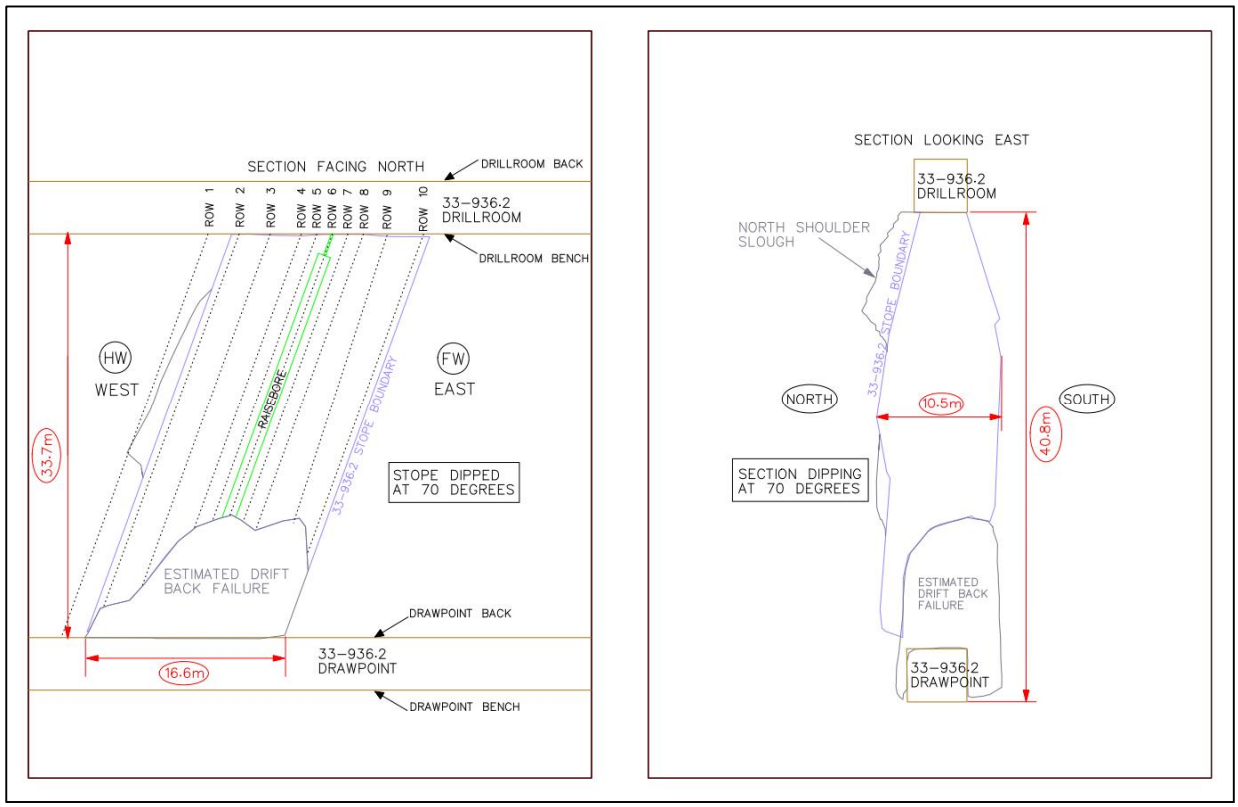

Figure 5.19 Longsection and cross-section of the 33-936.2 stope

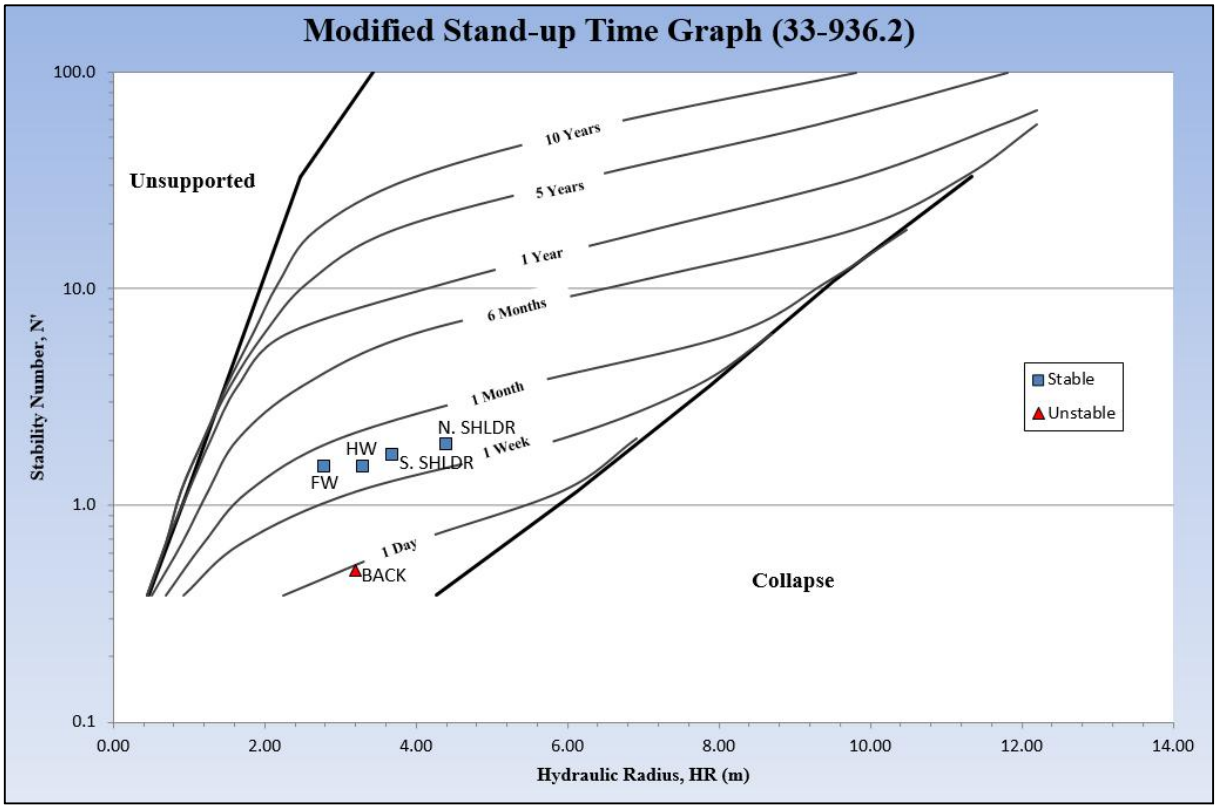

Figure 5.20 Modified Stand-up Time Graph: 33-936.2

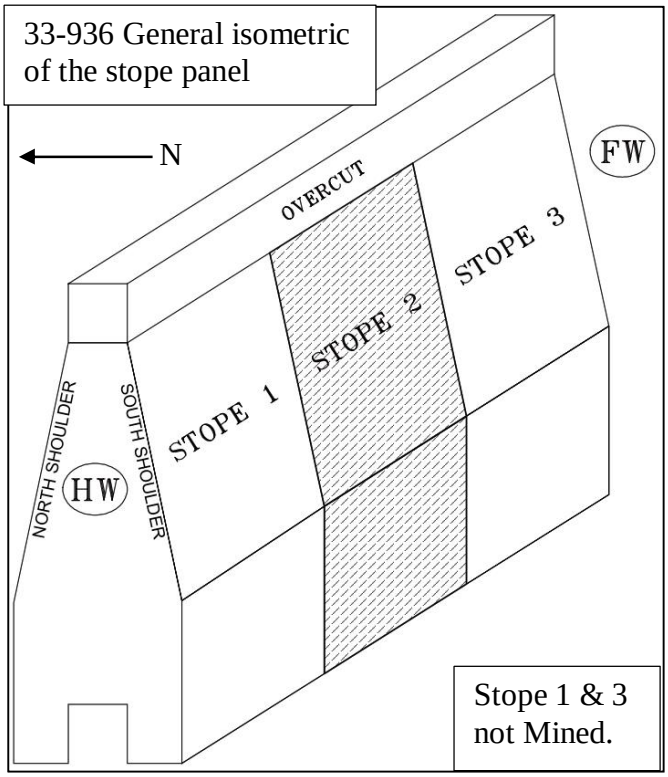

Figure 5.21 Isometric of standard stope panel at Birchtree Mine showing the location of the 33-936.2 stope in relation to other stopes in the panel

5.1.8 Case History 33-916.2

The 33-916.2 stope was considered unstable. Three blasts were taken in this stope and it was completely mucked out before sloughing of the north shoulder occurred (Figure 5.22). The first blast letter was issued on September 7th, 2010 and the final blast letter was issued on September 15th. The last of the ore was removed from the stope on September 21st and the stope was filled with cemented rock fill. Rock classification data is presented in Table 5.8. A plot of predicted stand-up times for the 33-916.2 stope is shown in Figure 5.23. Figure 5.24 is an isometric sketch showing the relative location of the stope in the mining panel.

Table 5.8 Rock classification data for stope 33-916.2

33-916.2	N. Shoulder	S. Shoulder	Hanging Wall	Footwall	Back
Critical Joint Orientation (°)	71	61	71	59	59
Maximum Induced Stress (MPa)	200	152	0	35	138
Unconfined Compressive Strength (MPa)	67	67	67	67	67
Q'	4.8	4.8	4.8	4.8	4.8
A Factor	0.1	0.1	1.0	0.1	0.1
B Factor	0.3	0.2	0.2	0.2	0.8
C Factor	6.0	5.8	8.0	8.0	2.0
N' Stability Number	0.9	0.6	7.6	0.8	0.8
Hydraulic Radius (m)	3.3	3.2	3.4	3.5	3.2
Peridotite Concentration (%)	-	-	-	-	-
Surface Condition	Unstable	Stable	Stable	Stable	Stable
Exposure Time	< 6 days	> 6 days	> 6 days	> 6 days	> 6 days

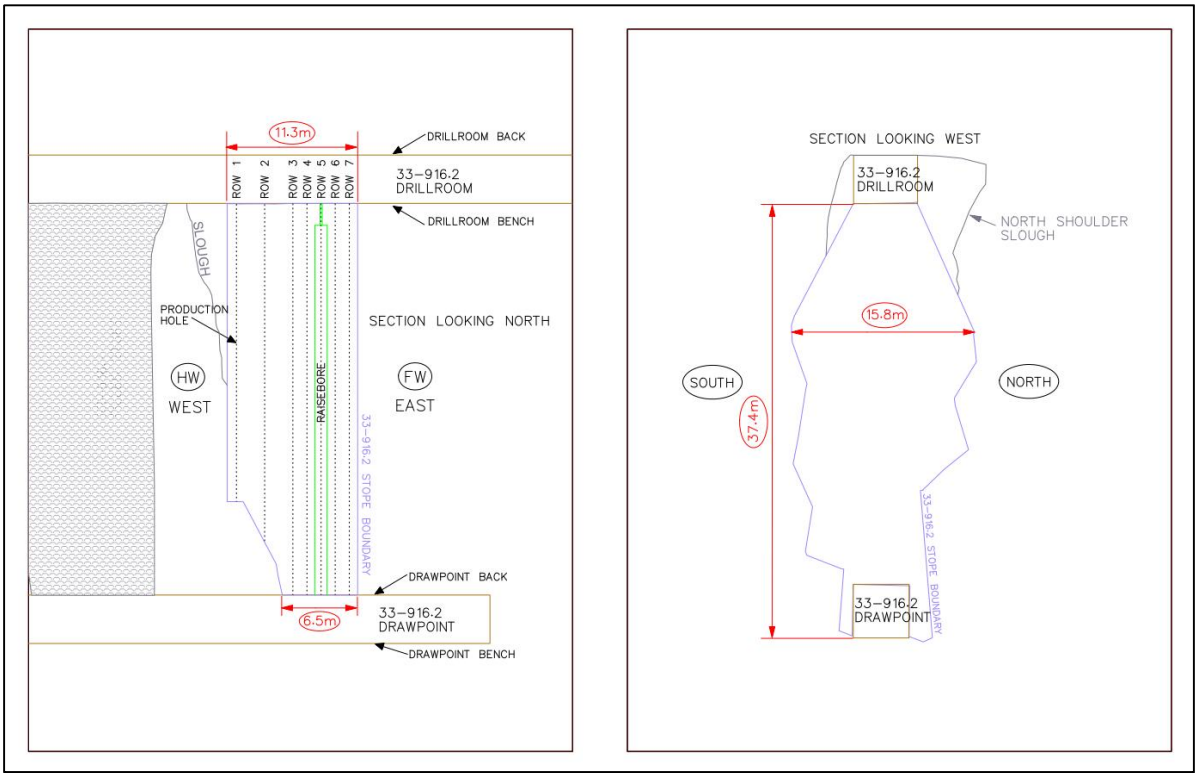

Figure 5.22 Longsection and cross-section of the 33-916.2 stope

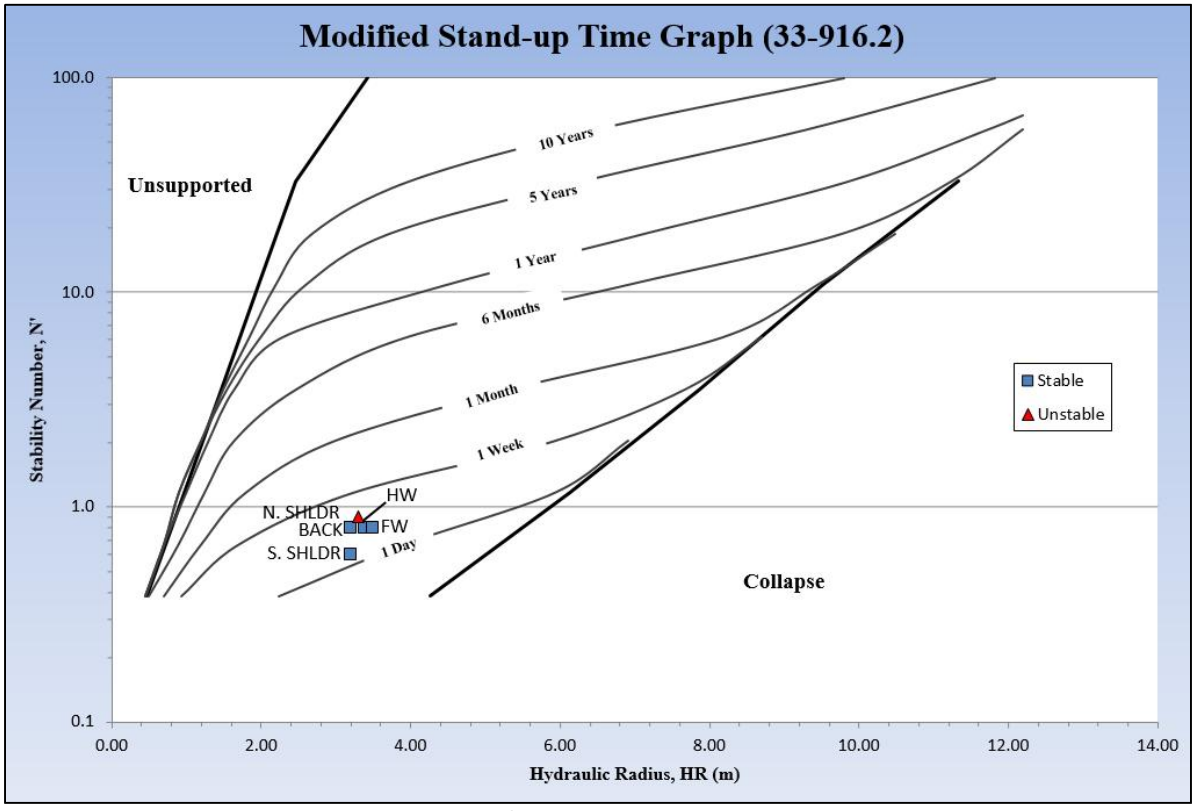

Figure 5.23 Modified Stand-up Time Graph: 33-916.2

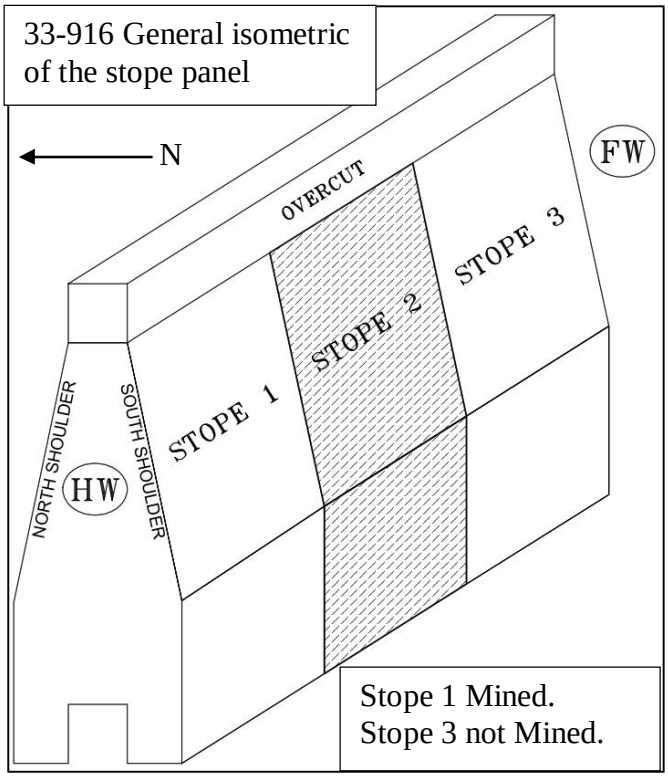

Figure 5.24 Isometric of standard stope panel at Birchtree Mine showing the location of the 33-916.2 stope in relation to other stopes in the panel

5.2 Successful Case Histories

5.2.1 Case History 32-928.1

For the 32-928.1 case history, a total of 3 blasts were successfully taken. The first blast letter was issued on May 7th, 2010 with the final blast letter issued on May 13th, 2010. The block was completely emptied by May 16th, 2010 and filling began on the 23rd of the same month, ending on the 29th. This block was blasted and completely filled in less than one month. A longsection and cross-section is shown in Figure 5.25. A summary of the rock classification data and a plot of the predicted stand-up times for the 32-928.1 stope are shown in Table 5.9 and Figure 5.25 respectively. Figure 5.27 is an isometric sketch showing the relative location of the stope in the mining panel.

Table 5.9 Rock classification data for the 32-928.1 stope

32-928.1	N. Shoulder	S. Shoulder	Hanging Wall	Footwall	Back
Critical Joint Orientation (°)	81	75	81	81	20
Maximum Induced Stress (MPa)	75	79	68	68	79
Unconfined Compressive Strength (MPa)	67	67	67	67	67
Q'	9.0	9.0	9.0	9.0	9.0
A Factor	0.1	0.1	0.1	0.1	0.1
B Factor	0.25	0.3	0.3	0.2	0.2
C Factor	6.5	6.4	7.2	7.2	2.0
N' Stability Number	1.5	1.7	1.9	1.3	0.4
Hydraulic Radius (m)	3.2	2.8	2.1	3.5	2.5
Peridotite Concentration (%)	2.0	14	4.0	22	-
Surface Condition	Stable	Stable	Stable	Stable	Stable
Exposure Time	> 16 days	> 16 days	> 16 days	> 16 days	> 16 days

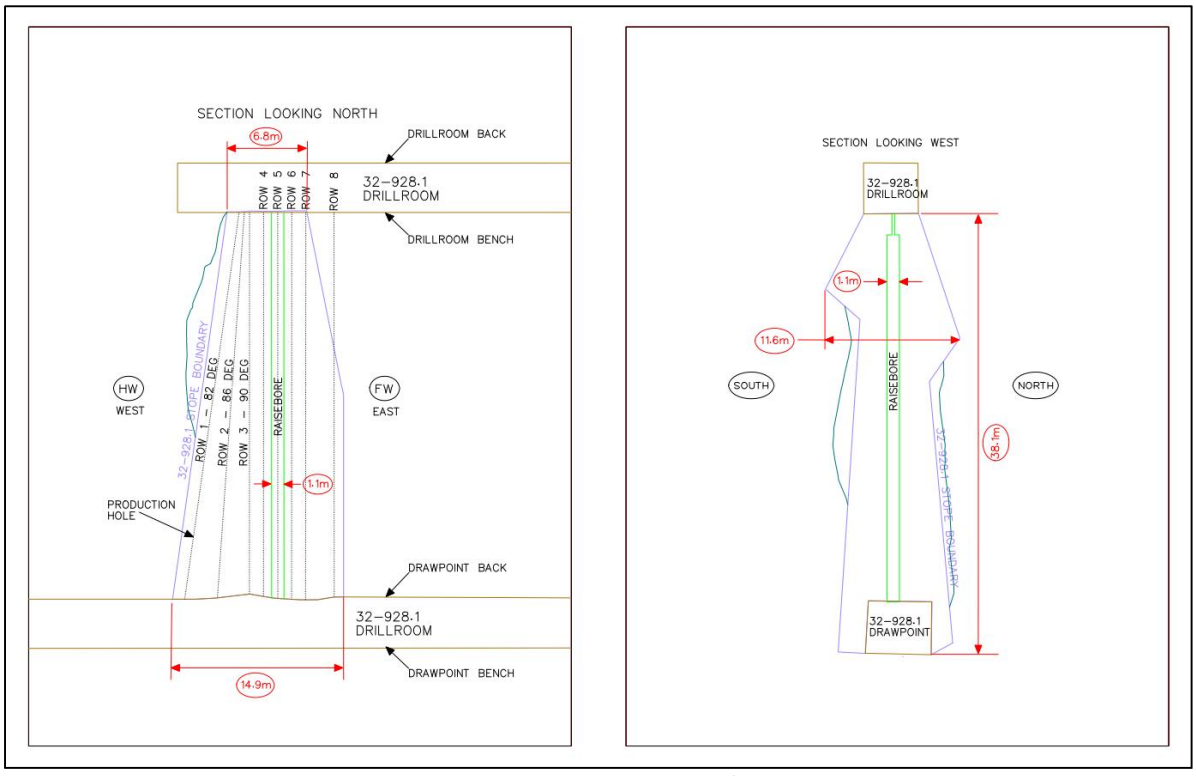

Figure 5.25 Longsection and cross-section of the 32-928.1 stope

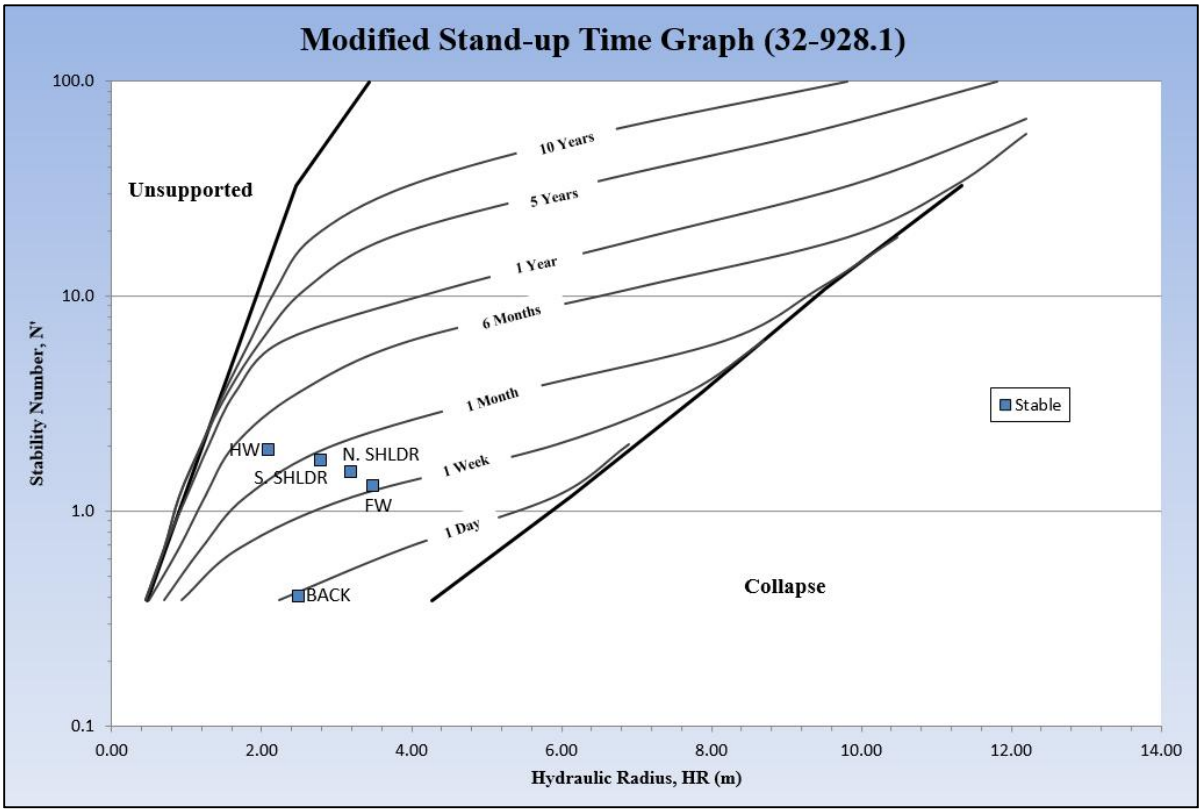

Figure 5.26 Modified Stand-up Time Graph: 32-928.1

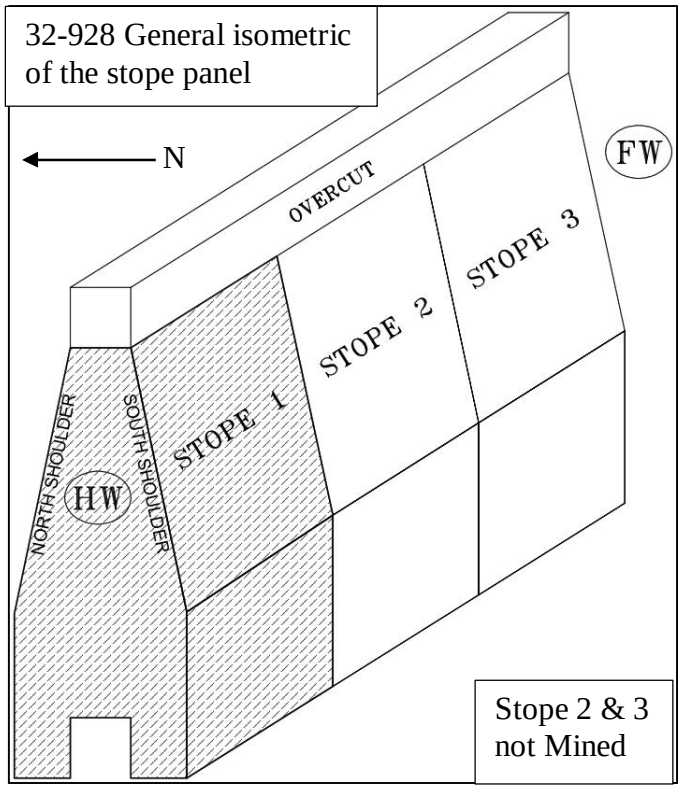

Figure 5.27 Isometric of standard stope panel at Birchtree Mine showing the location of the 32-928.1 stope in relation to other stopes in the panel

5.2.2 Case History 33-916.3

The 33-916.3 Stope was classified as a stable case history. No major sloughing was recorded. A total of three blasts were taken for this block, with the first and last blast letter being issued on November 4th and 8th, 2010 respectively. The last of the ore was removed from the stope on November 11th and the block was filled with uncemented rock. A longsection and cross-section of the stope is shown in Figure 5.28. Rock classification data is summarized in Table 5.10 and a plot of the predicted stand-up times are shown in Figure 5.29. Figure 5.30 is an isometric sketch showing the relative location of the stope in the mining panel.

Table 5.10 Rock classification data for the 33-916.3 stope

33-916.3	N. Shoulder	S. Shoulder	Hanging Wall	Footwall	Back
Critical Joint Orientation (°)	81	75	75	81	22
Maximum Induced Stress (MPa)	125	100	0	45	125
Unconfined Compressive Strength (MPa)	67	67	-	67	67
Q'	7.0	7.0	-	7.0	7.0
A Factor	0.1	0.1	-	0.1	0.1
B Factor	0.2	0.2	-	0.3	0.3
C Factor	4.5	5.3	-	8.0	2.0
N' Stability Number	0.6	0.7	-	1.6	0.4
Hydraulic Radius (m)	2.9	2.3	3.6	4.1	3.0
Peridotite Concentration (%)	33.0	39	55.0	8.0	-
Surface Condition	Stable	Stable	Stable	Stable	Stable
Exposure Time	> 10 days	> 10 days	> 10 days	> 10 days	> 10 days

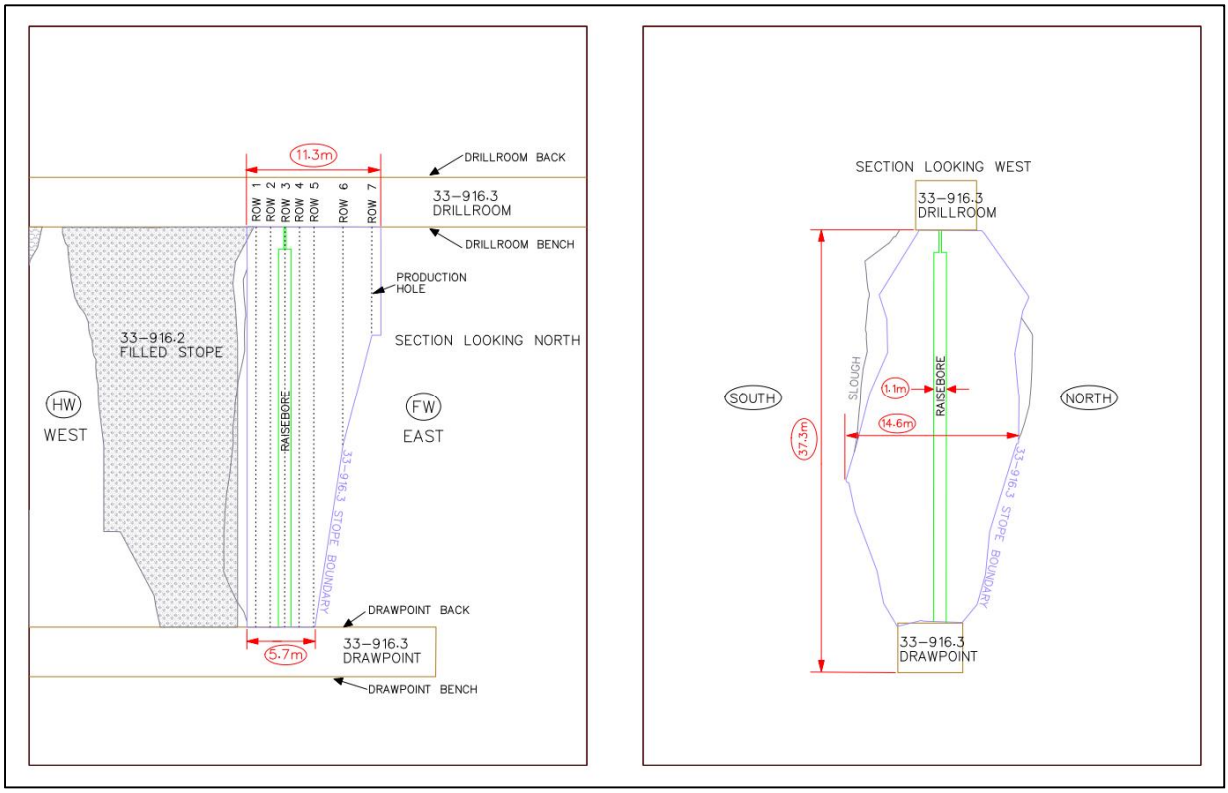

Figure 5.28 Longsection and cross-section of the 33-916.3 Stope

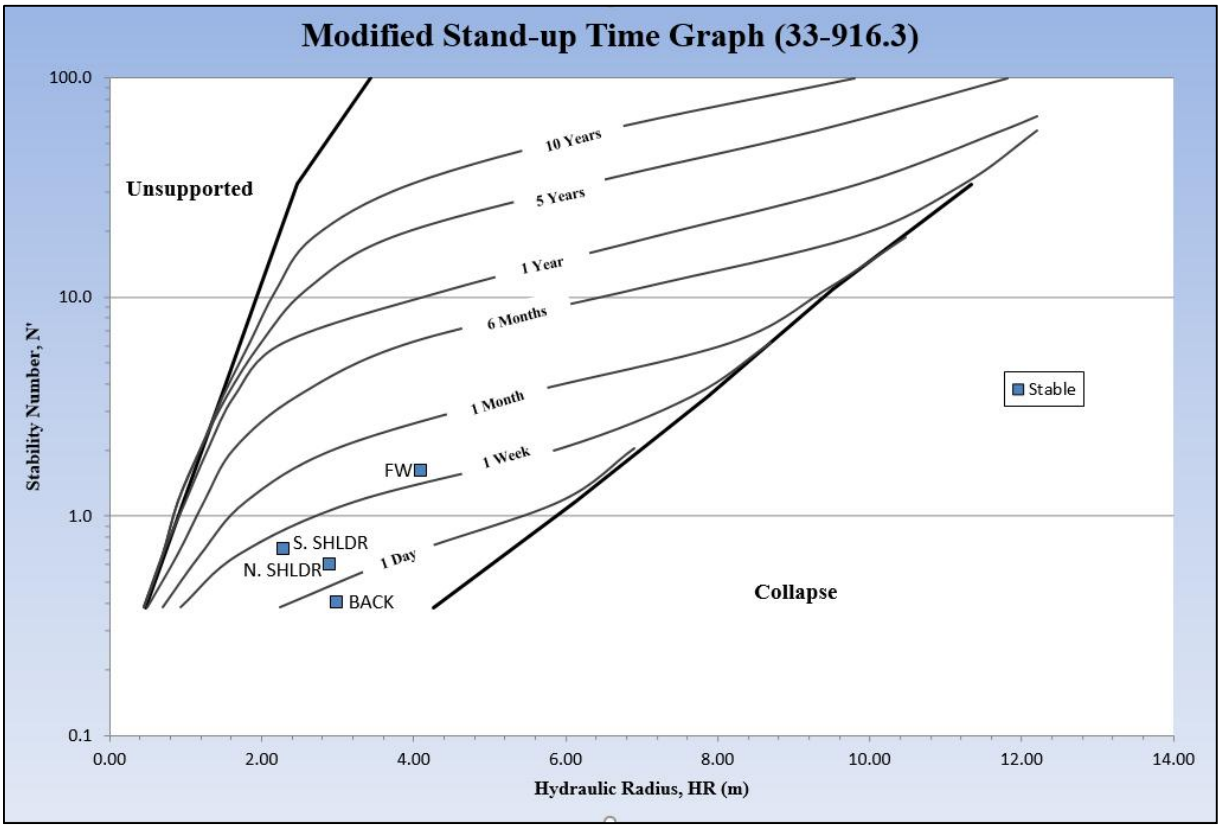

Figure 5.29 Modified Stand-up Time Graph: 33-916.3

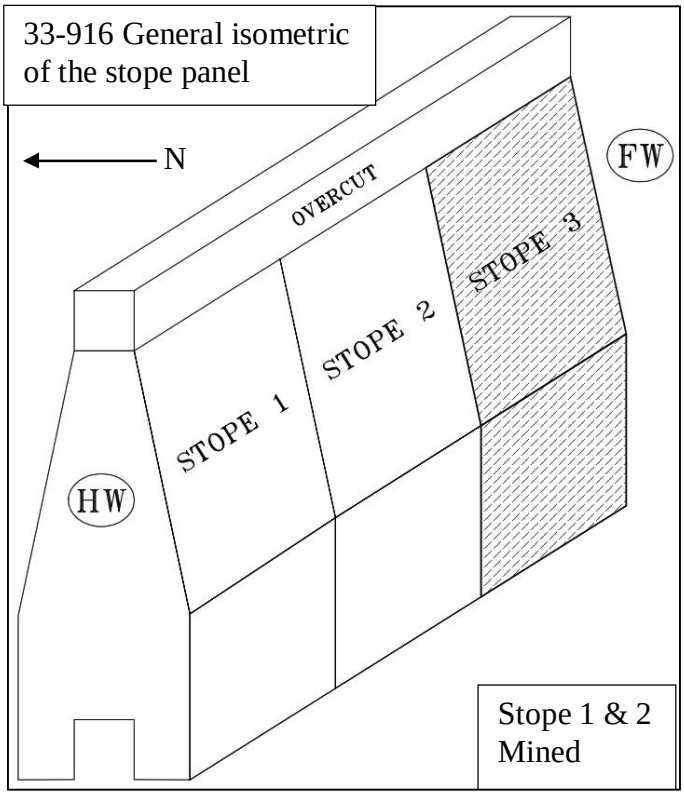

Figure 5.30 Isometric of standard stope panel at Birchtree Mine showing the location of the 33-916.3 stope in relation to other stopes in the panel

CHAPTER 6
ANALYSIS

6.1 Birchtree Case Histories

Case histories from the Birchtree Mine were gathered to see how well actual stand-up times compared to predicted stand-up times based on the newly developed Modified Stand-up Time (MST) Graph. A total of ten case histories were collected. Each case history provided five data points, one for each exposed surface. The total number of data points for stable and unstable surfaces is 43 and 8 respectively. It should be noted that a stope could contain both unstable and stable surfaces. If only one surface experienced instability, all other surfaces were considered to be stable. Figure 6.1 and 6.2 show the stable and unstable case histories plotted on the MST Graph.

Figures 6.1 and 6.2 show that the majority of the data points are concentrated in the one day to one month predicted stand-up time range. For the stable case histories only 6 of the 43 data points plot above a one month predicted stand-up time, and for the unstable cases, all data points plot below approximately two weeks. The small range in which the data is concentrated reflects conditions observed at the Birchtree Mine, as most stopes remain fully exposed for relatively short periods of time. Filling usually begins immediately or shortly after all recoverable ore has been removed from the stope, to help limit potential instabilities.

To better classify the Birchtree data, a plot showing the relationship between predicted and actual stand-up times for stable case histories is shown in Figure 6.3. The following comparisons were made:

i. Actual recorded stand-up time is less than or equal to the predicted stand-up time (predicted stability and remained stable) and;

ii. Actual recorded stand-up time is greater than predicted stand-up time (remained stable but predicted instability).

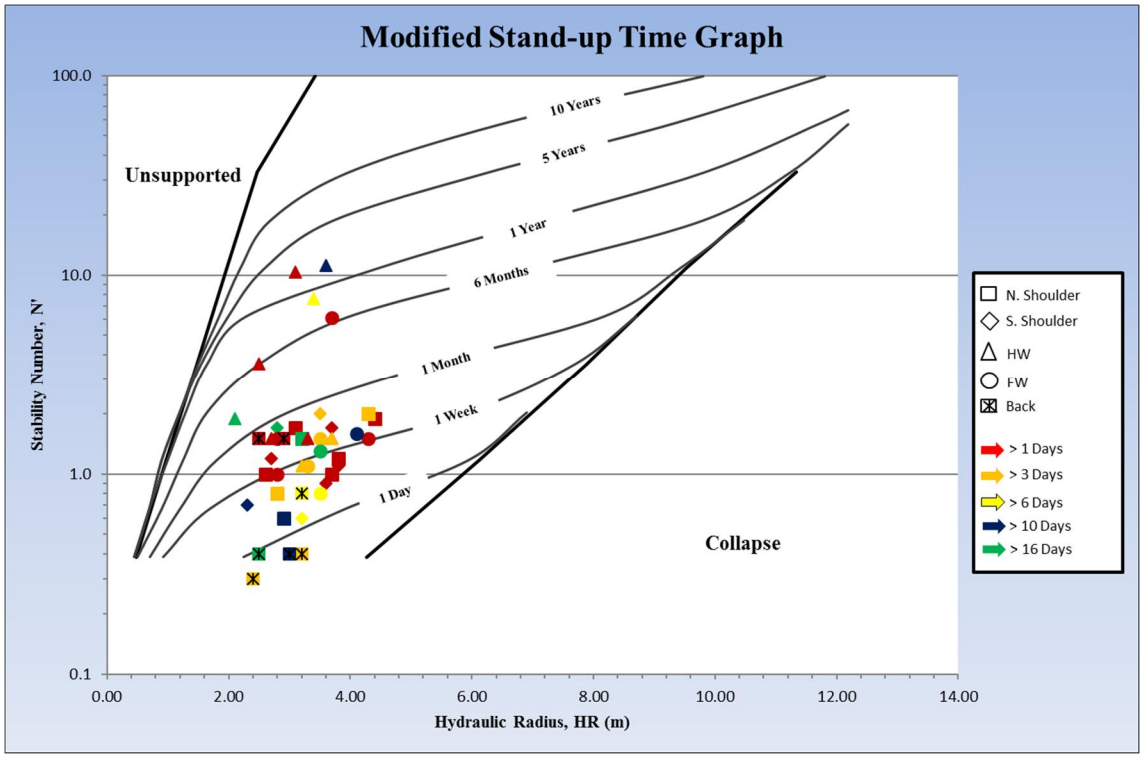

Figure 6.1 Birchtree 43 stable case histories

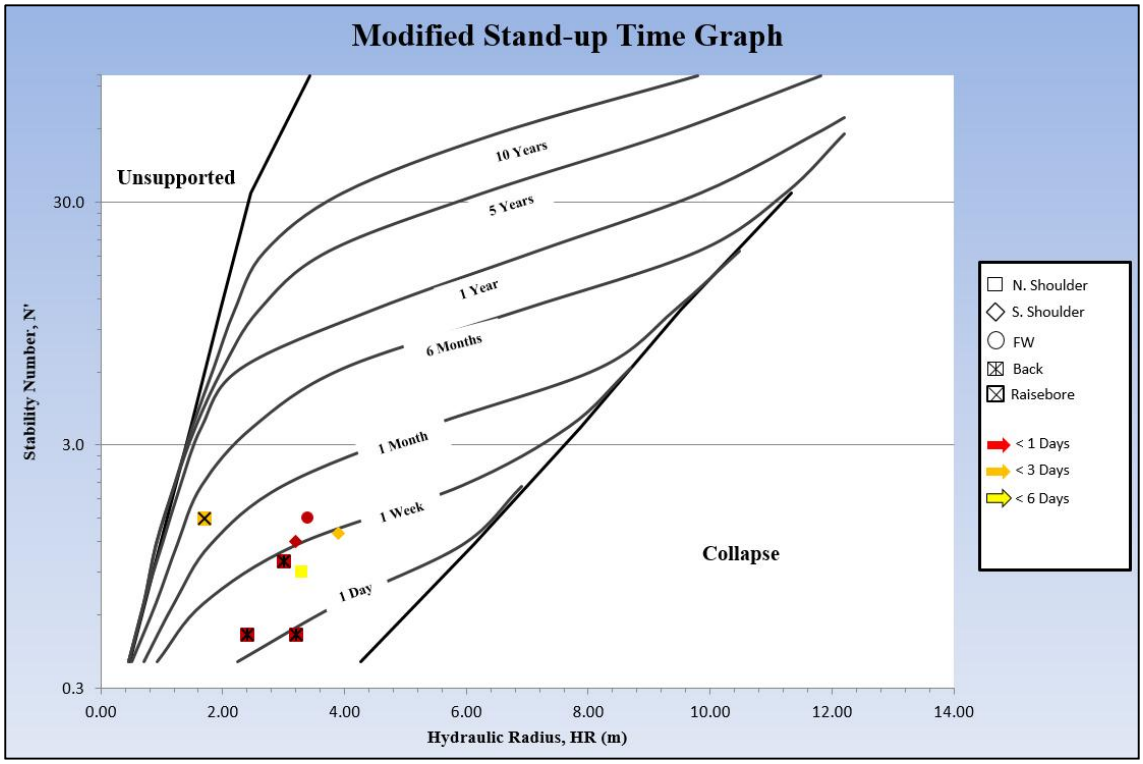

Figure 6.2 Birchtree 8 unstable case histories

Figure 6.3, shows the stand-up time for the case histories that did not experience instability and were exposed for less time than the predicted stand-up time (grey dots). These case histories do not support or disagree with the MST Graph. The case histories that were stable longer than the predicted stand-up time (red squares) disagree with the MST Graph. Table 6.11 shows the predicted and recorded stope stability for these cases. These comparisons show that 23 percent of case histories disagreed with the MST Graph and predicted less stand-up time than was achieved (Figure 6.3). The unstable case histories plotted in Figure 6.2 also show all unstable cases plotted with a predicted stability of 2 weeks or less. This figure suggests that any case histories that plot below the two-week line on the Modified Stand-up Time Graph have a higher probability of instability; however, this may be misleading, as only 21% of the data points that plotted below the two-week line were considered unstable.

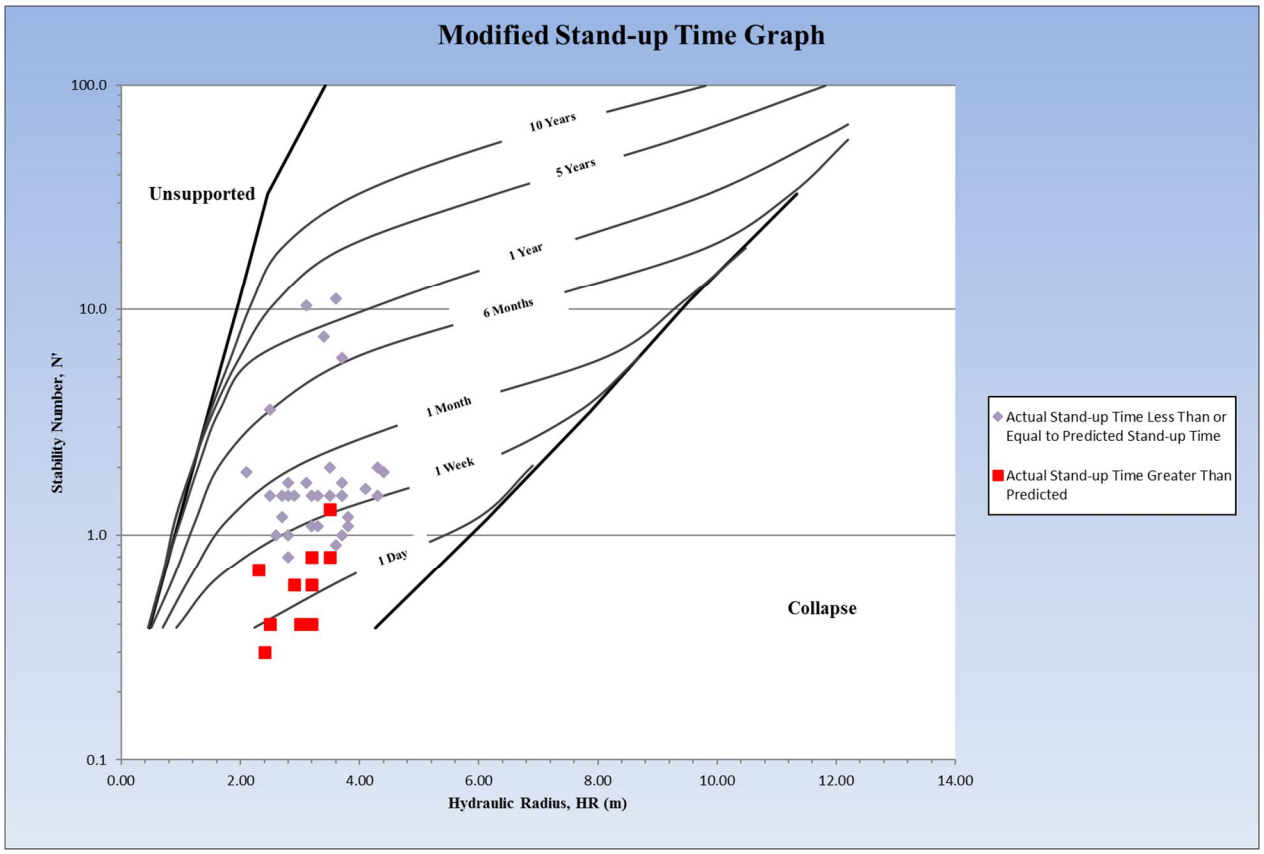

Figure 6.3 Actual stand-up times vs. predicted stand-up times for stable case histories

Table 6.1 Summary of stope surface information for actual and predicted stand-up times (Peridotite = PRDT)

Stope	Surface	N'	HR	Actual Time (days)	Predicted Time (days)	Error (days)	Max Stress (MPa)	% PRDT
29-864.1	Back	0.5	2.4	< 1 day	2	+1	89	N/A
	N. Shoulder	1	3.7	> 1 day	4	-	85	69.22
	S. Shoulder	1.1	3.8	> 1 day	5	-	85	59
	HW	3.6	2.5	> 1 day	180	-	84	-
	FW	6.1	3.7	> 1 day	195	-	84	-
30-848.1	Back	0.4	3.2	> 3 days	0	-3	100	-
	N. Shoulder	2	4.3	> 3 days	17	-	92	-
	S. Shoulder	2	3.5	> 3 days	21	-	98	-
	HW	1.5	3.7	> 3 days	10	-	92	-
	FW	1.5	3.5	> 3 days	12	-	92	-
	Raisebore	1.5	1.7	< 3 days	90	+87	98	-
32-872.1	Back	0.3	2.4	> 3 days	0	-3	100	-
	N. Shoulder	0.8	2.8	> 3 days	5	-	91	40.09
	S. Shoulder	1.3	3.9	< 3 days	6	+3	91	68.13
	HW	1.1	3.2	> 3 days	7	-	91	56.18
	FW	1.1	3.3	> 3 days	6	-	91	65.8
32-928.1	Back	0.4	2.5	> 16 days	0	-16	79	-
	N. Shoulder	1.5	3.2	> 16 days	16	0	75	0
	S. Shoulder	1.7	2.8	> 16 days	26	-	79	0
	HW	1.9	2.1	> 16 days	105	-	68	3
	FW	1.3	3.5	> 16 days	7	-	68	21
33-840.1	Back	1.5	2.9	> 1 day	19	-	100	-
	N. Shoulder	1.7	3.1	> 1 day	21	-	91	27
	S. Shoulder	1.2	3.2	< 1 day	7	+6	91	37
	HW	1.5	3.7	> 1 day	12	-	91	27
	FW	1.5	4.3	> 1 day	7	-	91	41
33-848.1	Back	1.5	2.5	> 1 day	25	-	125	-
	N. Shoulder	1	2.6	> 1 day	7	-	125	58
	S. Shoulder	1.2	2.7	> 1 day	12	-	130	66
	HW	1.5	2.7	> 1 day	21	-	120	54
	FW	1.5	3.4	< 1 day	14	+13	125	52
33-848.2	Back	1	3	< 1 day	6	+5	165	62
	N. Shoulder	1.2	3.8	> 1 day	6	-	92	70
	S. Shoulder	0.9	3.6	> 1 day	4	-	83	55
	HW	10.4	3.1	> 1 day	1095	-	0	51
	FW	1	2.8	> 1 day	7	-	148	54
33-916.2	Back	0.8	3.2	> 6 days	4	-	150	-
	N. Shoulder	0.9	3.3	< 6 days	4	-2	270	55
	S. Shoulder	0.6	3.2	> 6 days	2	-	190	50
	HW	7.6	3.4	> 6 days	330	-	0	55
	FW	0.8	3.5	> 6 days	3	-	40	46
33-916.3	Back	0.4	3	> 10 days	0	-10	125	-
	N. Shoulder	0.6	2.9	> 10 days	2	-8	125	38
	S. Shoulder	0.7	2.3	> 10 days	5	-5	100	39
	HW	11.2	3.6	> 10 days	910	-	0	55
	FW	1.6	4.1	> 10 days	10	0	45	21
33-936.2	Back	0.5	3.2	< 1 day	1	0	115	13
	N. Shoulder	1.9	4.4	> 1 day	14	-	120	9
	S. Shoulder	1.7	3.7	> 1 day	16	-	160	7
	HW	1.5	3.3	> 1 day	14	-	70	4
	FW	1.5	2.8	> 1 day	21	-	40	24

6.2 Actual vs. Predictied Stand-up Times

Figure 6.4 is a graph of actual stand-up times of Birchtree case histories vs. predicted stand-up times. As part of the graph, a 1:1 line has been drawn showing the line at which actual stand-up times would be equal to the predicted stand-up times. Figure 6.4 shows all the stable data points. All data points above the prediction line represent surfaces where predicted stand-up times were longer than actual stand-up times. All data points below the prediction line, represent surfaces where predicted stand-up times were less than actual stand-up times. It should be noted that the majority of the data points represent surfaces from stopes where at least one surface experienced insability. As noted previously, once a single surface experienced instability, all other surfaces were considered stable, as the influence of the unstable surface on those remaining, could not be predicted. As such, actual stand-up times may have been greater than what is reflected in the Figure 6.4.

Figure 6.5 is a graph of actual stand-up times vs. predicted stand-up times for unstable case histories at the Birchtree Mine. Data points above the prediction line represent surfaces that experienced instability before predicted. Data points below the prediction line represent surfaces where predicted stand-up times were less than actual stand-up times. The raisebore instability cannot be seen in Figure 6.5 as the predicted stand-up time was 90 days, which is well outside the maximum value of the x and y axis. This case history plots well above the prediction line. A summary of the data used in Sections 6.1 and 6.2 is shown in Table 6.1.

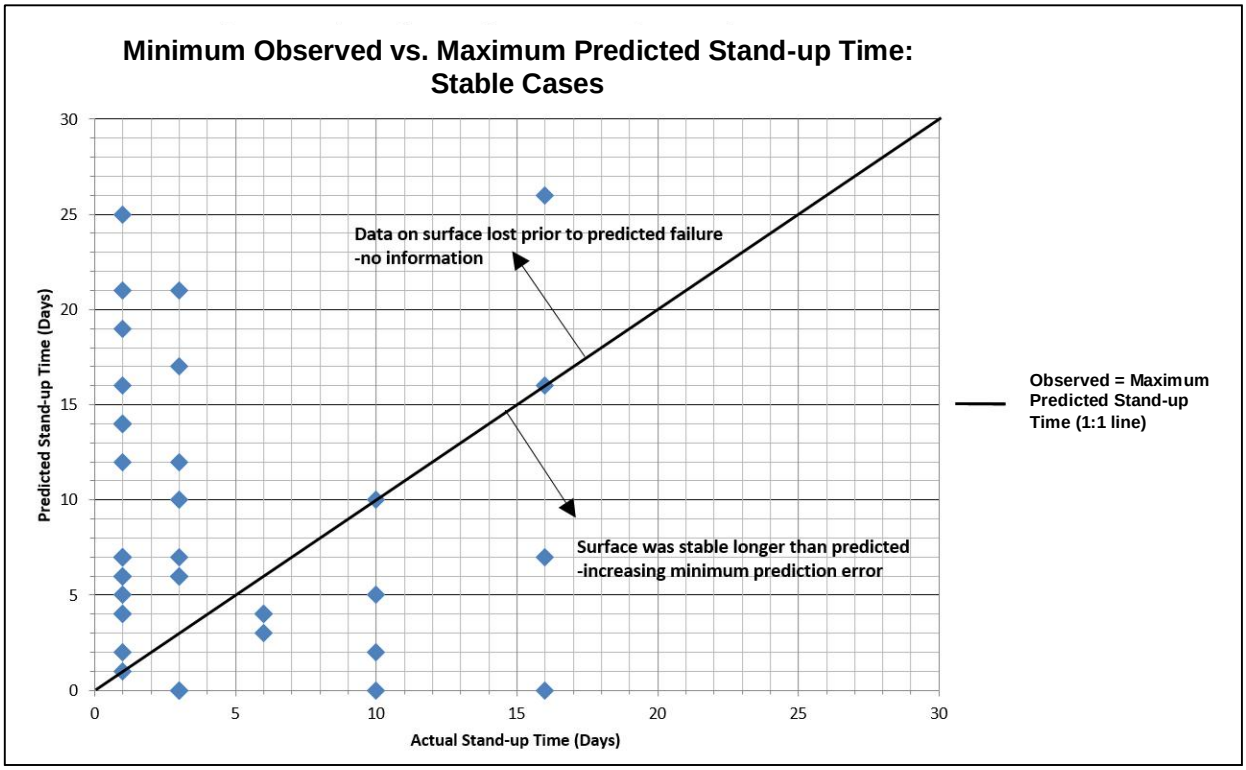

Figure 6.4 Minimum Observed vs. Maximum Predicted Stand-up Time for Stable Case Histories

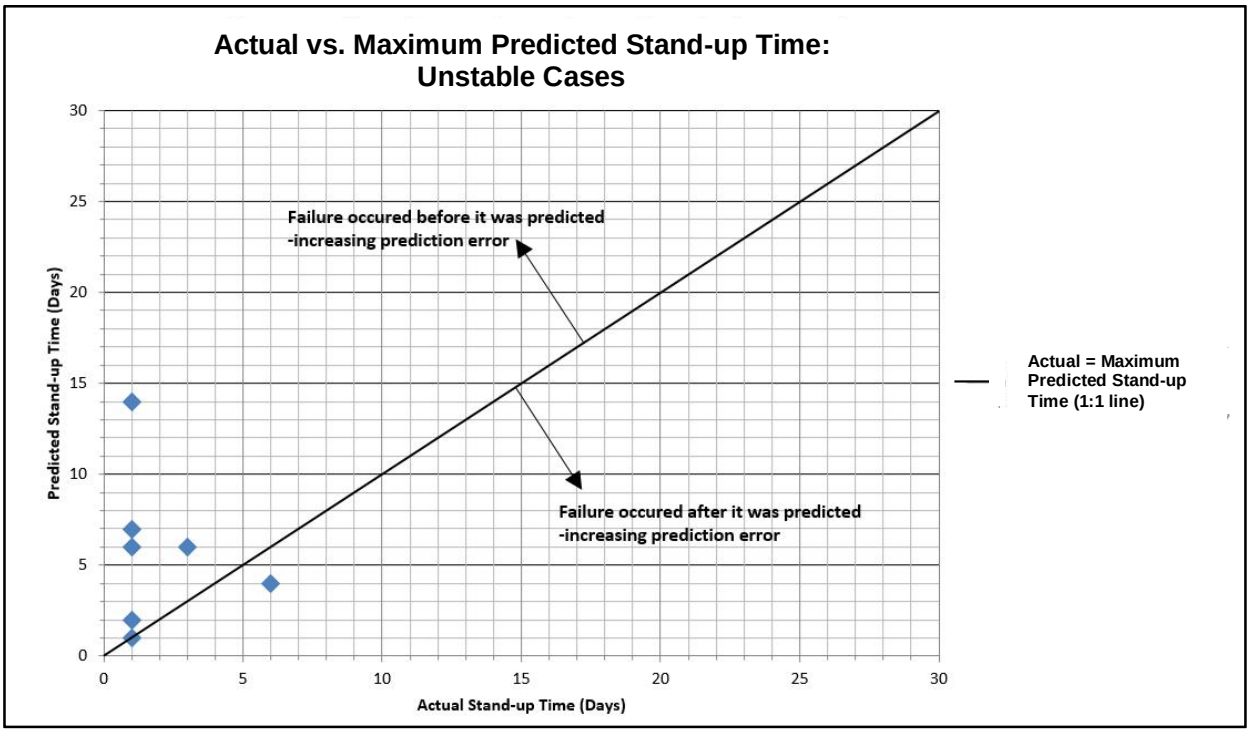

Figure 6.5 Actual vs. Maximum Predicted Stand-up Time for Unstable Case Histories

6.3 Birchtree Data vs. Bieniawski Data

Figure 6.6 includes data from both Birchtree case histories and Bieniawski's (1989) RMR Stand-up Time Graph. Not all data was included. Data was limited to Bieniawski's case histories, with stand-up times of 2 weeks or less, and the unstable surfaces from the Birchtree case histories. Only unstable surfaces from Birchtree were included as these surfaces were observed until instability occurred. Stand-up time for stable surfaces is at least the surface exposure time, but could be much longer as these surfaces could only be observed until the stope was backfilled. Bieniawski's data was limited to stand-up times of 2 weeks or less, as all unstable Birchtree case histories occurred within that time frame. Figure 6.6 shows how Birchtree case histories compare to Bieniawski's data (1989). As shown in this graph, the predicted stand-up times for the unstable case histories fit very well when compared to Bieniawski's data (Bieniawski, 1989).

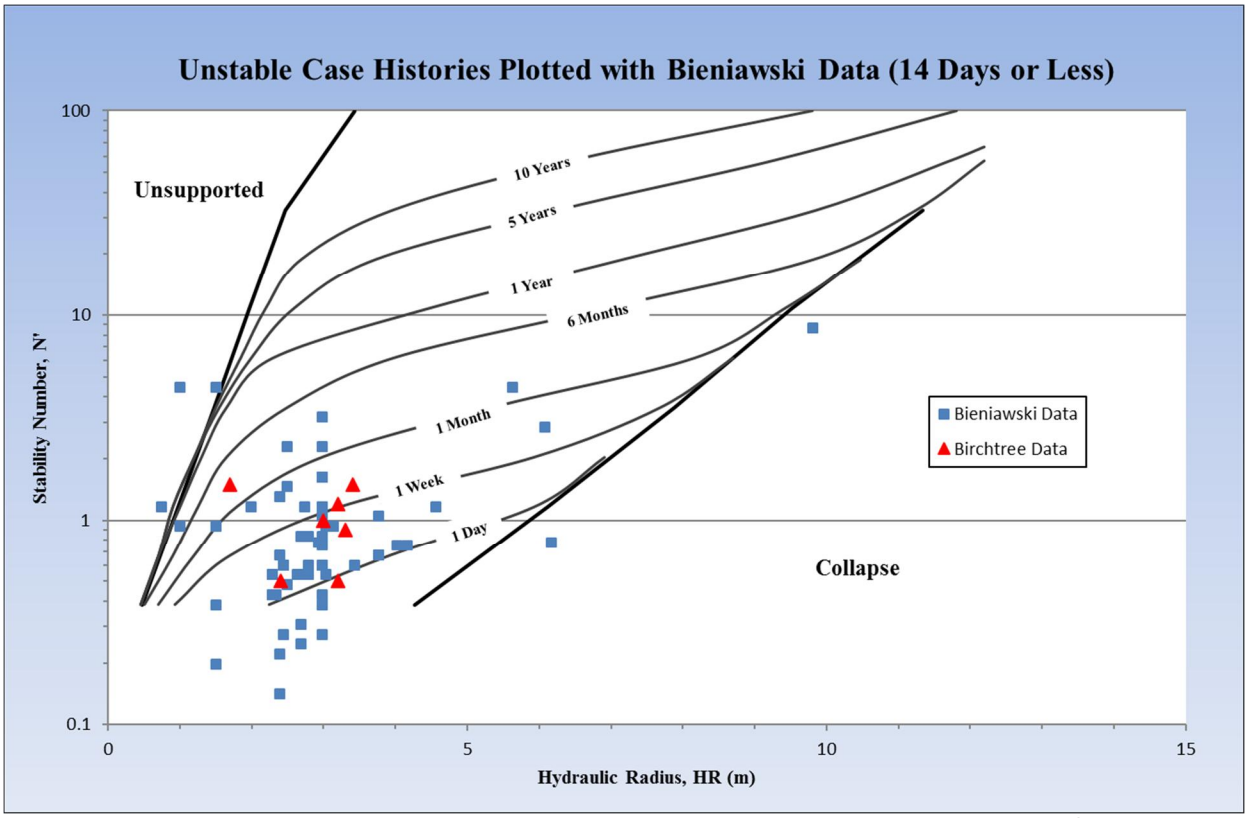

Figure 6.6 Unstable Birchtree Case Histories plotted with Bieniawski data points with stand-up times of 2 weeks or less

6.4 Time Factor Analysis

The MST Graph only considers the final geometry of an opening surface. The graph works by assessing three general factors which are felt to influence the stand-up time for an opening surface:

- Rock mass conditions, joint orientation, surface orientation, and stress (Stability Number N')
- Opening geometry as expressed by hydraulic radius.
- Exposure time

For assessing drifts and tunnels, this approach is valid since the total tunnel span is usually exposed by a single blast. In mining where large stopes are excavated, an individual excavation surface will often be exposed by a series of blasts. The exposure time for a sequentially exposed surface is not straight forward. To account for the incremental exposure of an opening surface by a series of blasts, an overall stand-up time was developed, which is a weighted average based on hydraulic radius and exposure time. This method incorporates the use of the MST graph for each blast geometry. For this method, each blast's hydraulic radius and stability number is plotted on the MST graph to obtain a predicted stand-up time. For each step, the actual exposure time is divided by the predicted time to failure, which can be expressed as a percentage of the time to failure. These incremental failure percentages are added to obtain a total percent time to failure, producing a time factor. For example, if the hydraulic radius of sequential blasts are 2.2, 4.7, and 15 metres, with a modified stability number of 3.0, the corresponding predicted stand-up times for each geometry would be 180, 30, and 7 days respectively. With corresponding exposures times of 10, 8, and 3 days respectively, the Time Factor would be as follows:

$$\text{Time Factor} = \frac{\text{Actual Stand-up Time}_{HR1}}{\text{Predicted Stand-up Time}_{HR1}} + \frac{\text{Actual Stand-up Time}_{HR2}}{\text{Predicted Stand-up Time}_{HR2}} + \frac{\text{Actual Stand-up Time}_{HR2}}{\text{Predicted Stand-up Time}_{HR3}} \quad \text{.....(6.1)}$$

$$\text{Time Factor} = \frac{10\ \text{days}}{180\ \text{days}} + \frac{8\ \text{days}}{30\ \text{days}} + \frac{3\ \text{days}}{7\ \text{days}}$$

$$= 0.75$$

This approach suggests the surface is three quarters of the way to failure for the current predicted stand-up time of 7 days. This means that it should be stable for an additional 1.75 days at the final stope geometry (Equation 6.2).

$$\text{Remaining Stability} = (1 - 0.75)\ x\ 7\ days \quad \text{.....(6.2)}$$

$$= 1.75$$

Many factors contribute to the stability of an opening, and the time that an opening will remain stable. The next section discusses some of the factors not considered in this approach, such as exceptionally high stress levels and other factors that may have a significant effect on stand-up time.

6.5 Other Factors that may Affect Stability

Peridotite is one of the common rock types found at the Birchtree Mine. It is an ultramafic rock that tends to have stability issues when mining occurs within or near this rock type. As part of the analysis, peridotite concentration was compared to various rock properties and conditions, to try and identify a correlation between the amount of peridotite present and the stability of open stopes. Section 4.4.2 gives a detailed description of how peridotite concentrations were determined. The analysis included the following:

i. Peridotite concentration vs. stable and unstable surfaces
ii. Peridotite concentration vs. RQD

6.5.1. Peridotite Concentration vs. Stable and Unstable Surfaces

To better understand how peridotite affects stability, peridotite concentration was estimated for the HW, FW, South Shoulder, and North Shoulder for various stopes where data was available. Figure 6.7 shows the actual vs. predicted stand-up times for stable surfaces', with each surfaces' associated peridotite concentration. Not all surfaces had available data to determine peridotite concentrations.

In Figure 6.7, it would be expected that any data that plots below the 1:1 line would have decreasing peridotite concentrations (zone 2), and above the 1:1 (zone 1), would have an increasing peridotite concentration. From Figure 6.7, there is no trend showing peridotite concentration decreasing for points further below the 1:1 line. An average peridotite concentration in this area for six case histories is 42%.

Figure 6.8 shows the actual vs. predicted stand-up time for the unstable case histories with each surfaces' associated peridotite concentration. This graph contains very few data points, and only four of those have associated peridotite concentrations. A lot of the unstable surfaces were associated with the backs and temporary backs of the open stopes, which do not have data available to determine peridotite concentrations. It should be noted that some of the data is not visible in Figures 6.7 and 6.8, as the predicted stand-up times were significantly larger than those currently displayed. This would have made the data very difficult to observe in both of these figures. These data points and their associated peridotite concentrations can be found in Table 6.1.

Figure 6.8 shows the unstable case histories, where higher peridotite concentrations would be expected. An average value, for the three case histories, is 52%. Where lower peridotite is expected (zone 2), the concentration of the only case history is 55%. In summary:

- Stable cases, Figure 6.7, Zone 2 – case histories stable longer than expected, low peridotite expected, 42% average peridotite concentration (6 case histories).
- Unstable cases, Figure 6.8, Zone 1 – Predicted stability longer than actual, high peridotite concentration expected, 52% average peridotite concentration (3 case histories).
- Unstable cases, Figure 6.8, Zone 2 – Predicted stability less than actual, low peridotite concentration expected, 55% average peridotite concentration (1 case history).

Figure 6.9 shows the prediction error for stand-up time versus the peridotite concentration. The raisebore instability was not included on this graph since it appeared to be an outlier with a prediction error of 87 days. This graph shows a tendency of stope instability prior to the predicted failure with increasing peridotite concentration; however, there is significant scatter in the peridotite concentrations and limited data.

To try and get additional data on peridotite, overbreak and underbreak data from blast holes were investigated for stopes outside the database of stopes for this study. Unfortunately, no trends were observed.

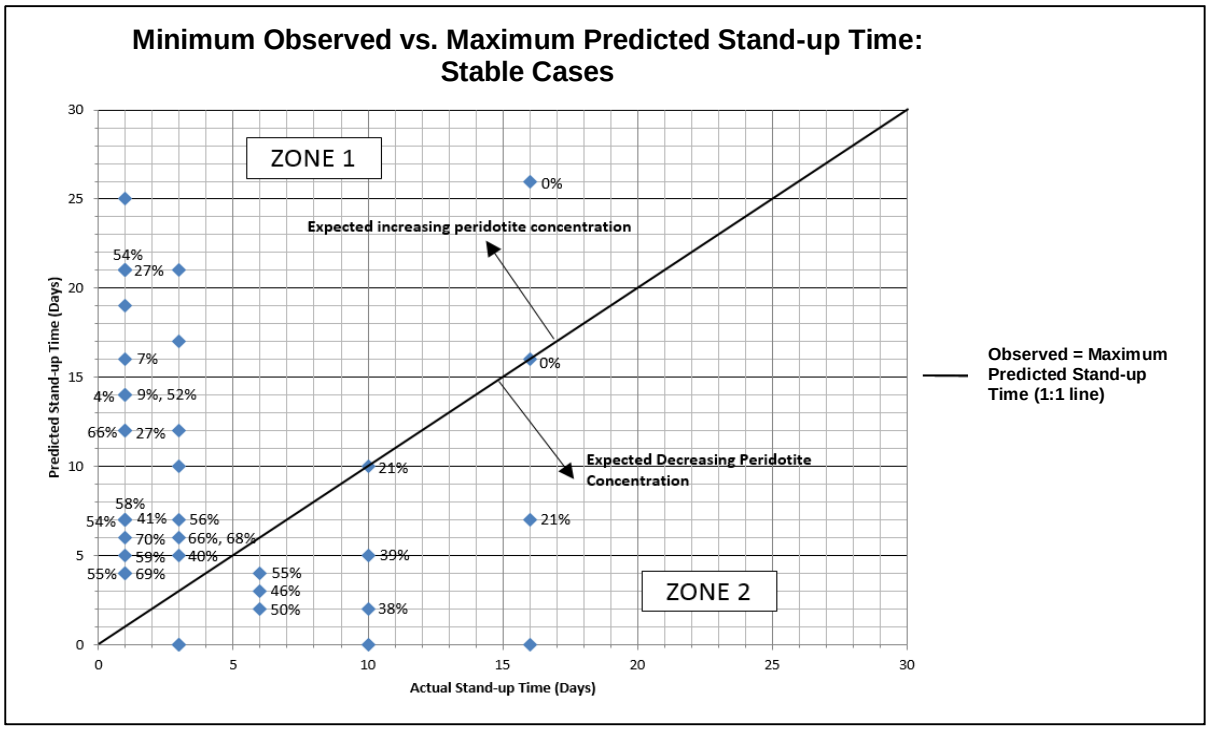

Figure 6.7 Peridotite concentration vs. stable surfaces

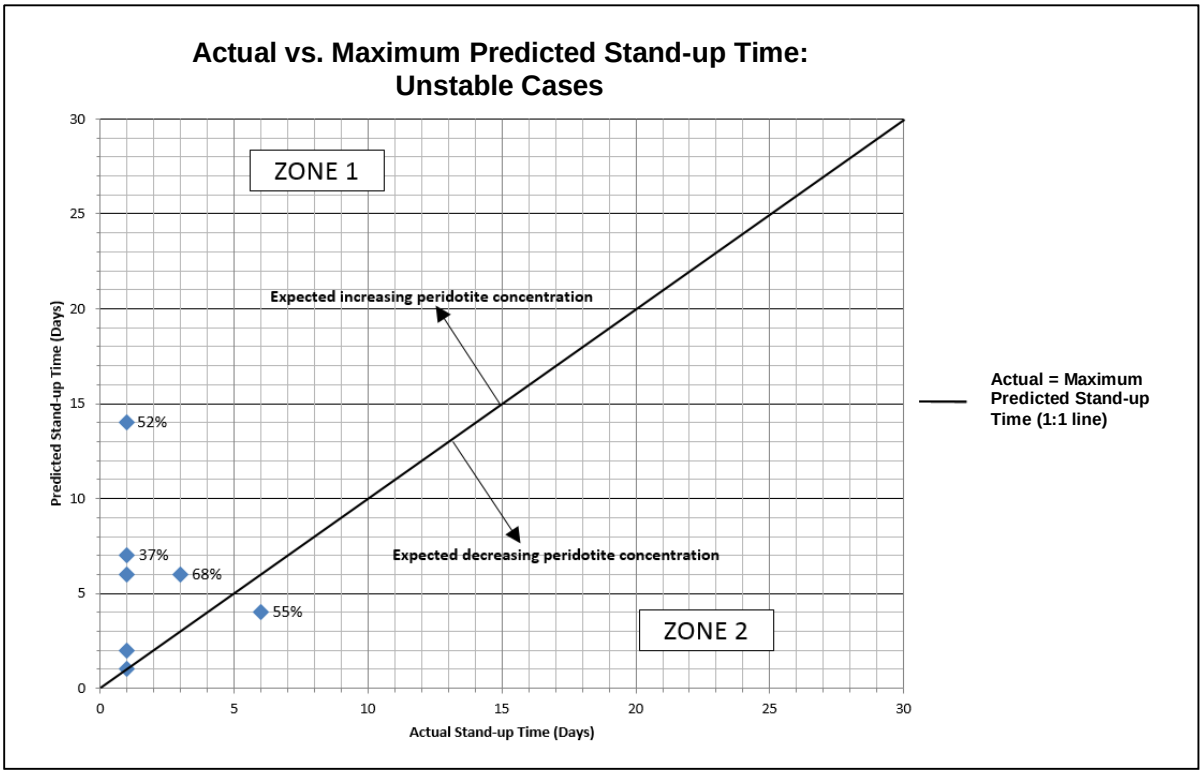

Figure 6.8 Peridotite concentration vs. unstable surfaces

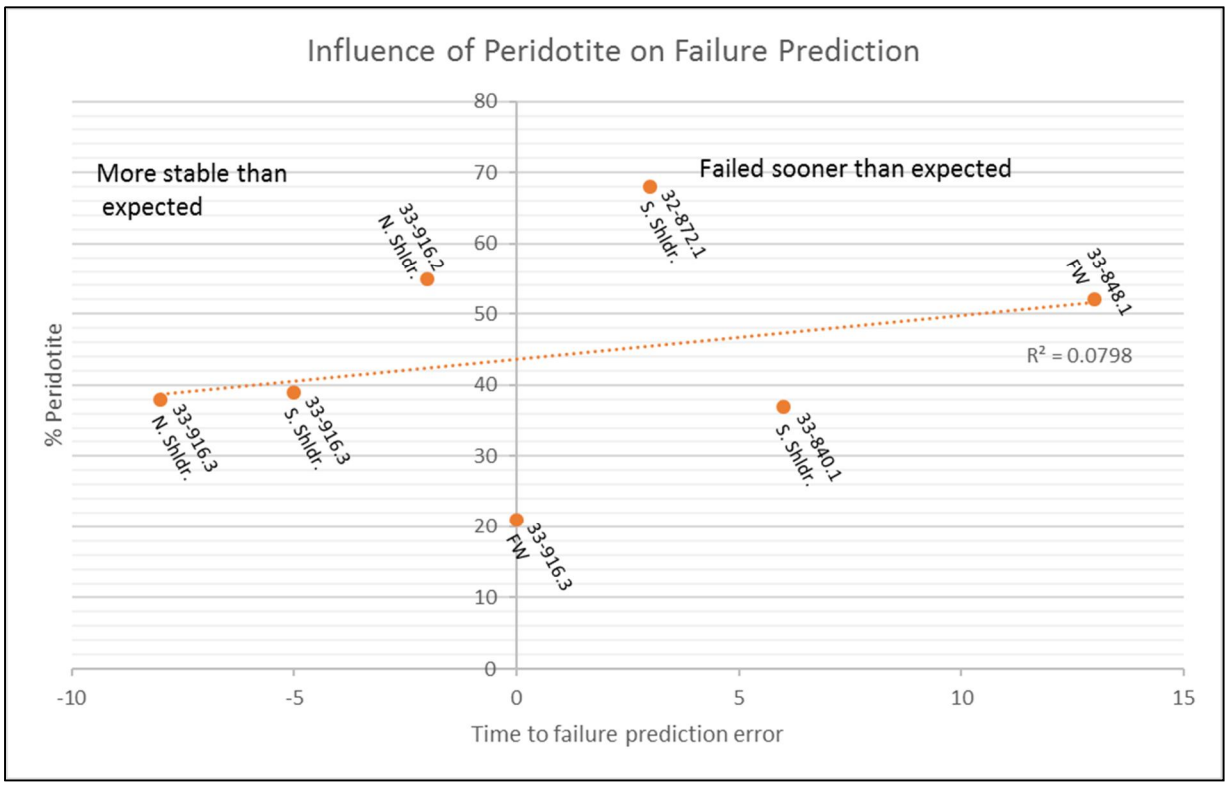

Figure 6.9 Influence of peridotite on time to failure prediction (Note: the raisebore failure has not been included; prediction error was 87 days)

6.5.2 Peridotite Concentration vs. RQD

From the previous two sections, it appears that the concentration of peridotite has little effect on the time to failure. Another possible reason why the presence of peridotite may appear to create issues for stability is if a higher peridotite concentration corresponds to a lower RQD. In order to test this possibility, peridotite concentrations were compared to RQD for various diamond drill holes.

For this analysis, a total of 11 stope case histories were used. Each stope contains 2 to 16 diamond drill holes, with an average of 5. It should be noted that the diamond drill holes may not fully define the entire stope as they pass through at various dips and locations. This also means that the portion of the diamond drill hole passing through each stope will vary in length.

RQD was recorded for the peridotite and for all other rock types in each stope. The assumption was that if peridotite effected RQD, it should be apparent in a stope by stope assessment. Figure 6.10 shows that the RQD values for peridotite range from 25 to 75%. The average RQD for peridotite for these case histories is 59. The RQD values for the non-peridotite rocks range from 38 to 64. The average RQD value for non-peridotite rock types for these case histories is 52. As instabilities are observed more often in peridotite than other rock types (Southern, 2017), ideally the RQD values would be less than those found in the non-peridotite rock types. For drill holes assessed, this is not the case. For the majority of the case histories presented in Figure 6.10, the RQD values for peridotite are actually higher than the non-peridotite rock types. Only three of the eleven (27 percent) non-peridotite case histories had RQD values higher than their peridotite counterparts. From these 11 stopes, there is no indication that RQD plays a role in the instabilities observed in peridotite.

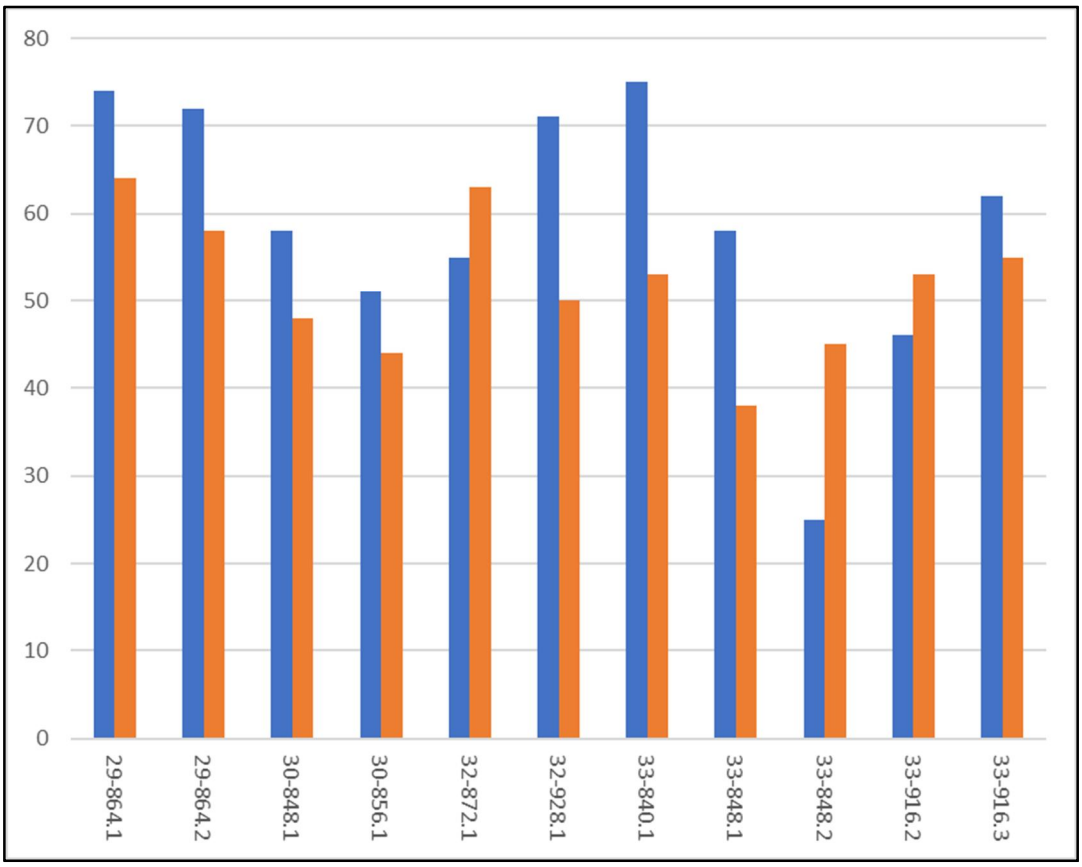

Figure 6.10 RQD comparison for peridotite and combined RQD of remaining rock types

6.5.3 Stress Effects on Time to Failure

Stress is assessed in the MST graph with the A factor used in the Modified Stability Graph (Potvin, 1988) shown in Figure 6.11. For the Birchtree case histories, the unconfined compressive strength of the rock is 67 MPa and the induced stress for all but three of the case histories is over 40 MPa (Table 6.1). This results in an A factor of 0.1, which is the maximum influence possible for high stress. This does not allow for any differentiation between the magnitude of high stress experienced by the case history stope surfaces. To determine if the prediction error for the case histories was influenced by the stresses present, a graph of induced stress versus the stand-up time prediction error is shown in Figure 6.11. This graph shows a tendency of stope failure prior to the predicted failure with increasing induced stress; however, there is significant scatter in the results and limited data.

As was stated previously in Section 2.3.2, most of case histories from the Yves Potvin's thesis (Potvin, 1988), had an A value of 1.0, indicated low stress conditions. Most of the data presented in this thesis was for case histories with high stress conditions, or A values of 0.1. This difference can likely be attributed to the differences in the HR radius of the case histories for each data set. The majority of the data in Potvin's thesis (1988) was for open stopes with larger hydraulic radii than those for the Birchtree case histories. Larger openings will push stress further away from the openings surface, creating larger zones of relaxation, and lower stresses. Smaller openings will tend to experience stresses closer to the opening's surface, and thus undergo higher stress concentrations.

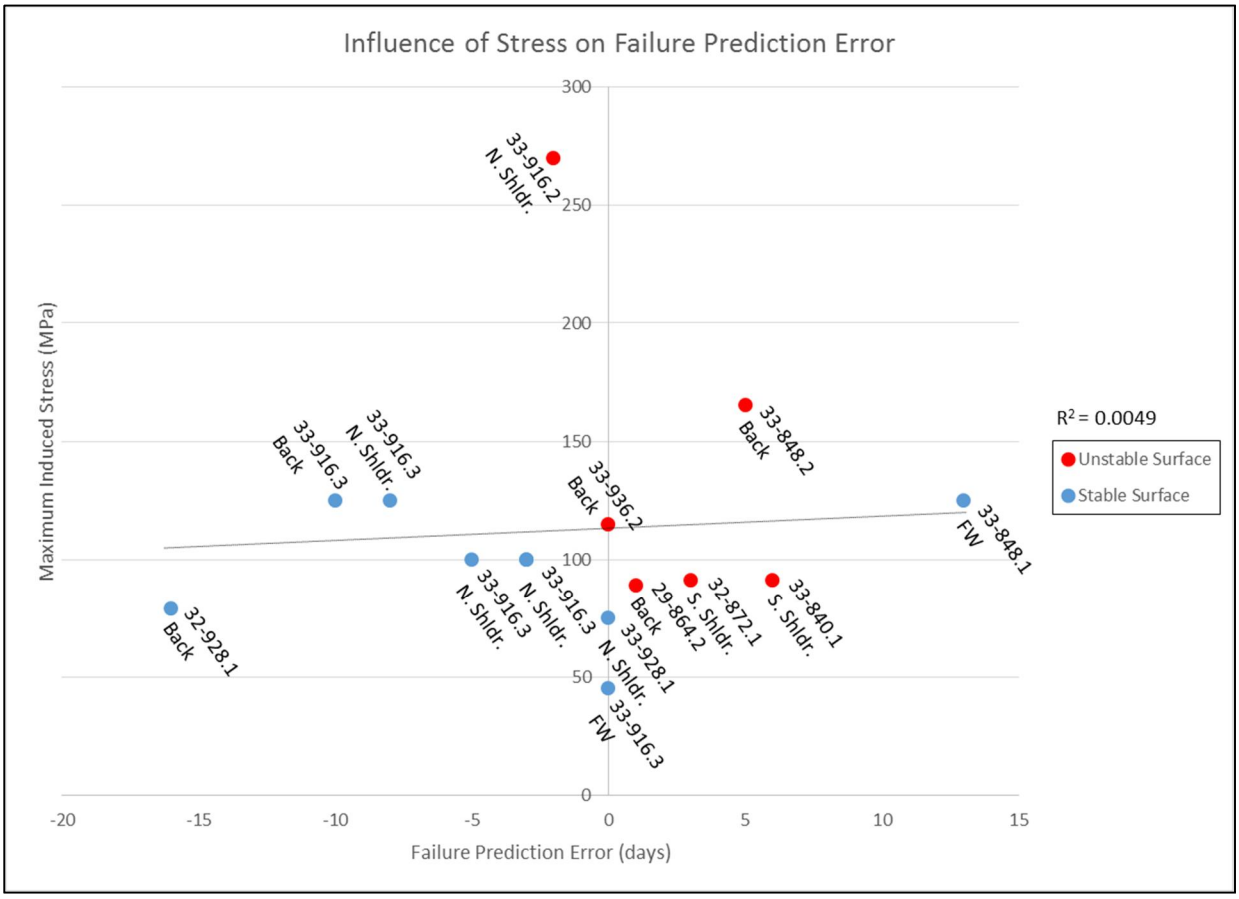

Figure 6.11 Influence of stress on time to failure prediction (Note: the raisebore failure has not been included; prediction error was 87 days)

CHAPTER 7
CONCLUSIONS

The main goal of this research has been to assess the influence of exposure time on open stopes at Birchtree Mine. Quantifying the effect of exposure time on stope stability will enable the engineer to alter stope designs to avoid time dependant instability.

To initiate this research, a technique for assessing exposure time, primarily from civil engineering applications for tunnel roof design, was investigated. The RMR Stand-up Time Graph for tunnelling (Bieniawski, 1989) formed the basis of a new methodology to assess the effect of time on open stope stability for mining. The Modified Stand-up Time Graph (MST) was the result of incorporating assessment factors more commonly used in modern mine design to Bieniawski's data base for stand-up time. As part of the development of the MST Graph, Bieniawski's original stand-up time graph was analyzed to determine the accuracy of the time lines incorporated into the method.

7.1 Modified Stability Graph and Bieniawski

As discussed in Section 3.3, the Modified Stand-up Time graph was developed to incorporate standards more commonly used in the mining industry. This involved the conversion of multiple variables to produce equivalent N' values from RMR and hydraulic radius values from span. The Bieniawski data base consisted primarily of case histories from a shallow depth, usually in sedimentary rock. Due to the predominance of civil structures and coal mining cases from the Eastern United States, near horizontal bedding was assumed. The case histories all investigated roof stability which was also assumed to correspond to sub-horizontal roofs. This, coupled with established conversions between RMR and Q classification values, allowed approximations to be made, which allowed estimation of the N' value for the stability graph design method (as discussed in Section 3.1.2). Since the hydraulic radius of a long tunnel is approximately equal to one half the tunnel span, this parameter was easily estimated. The Modified Stand-up Time Graph was developed using the format of the Stability Graph design method, coupled with the data and

interpretation approach of Bieniawski's Stand-up Time Graph.

In Section 3.3, the MST Graph was compared to the commonly used Modified Stability Graph by overlaying the two graphs on one another (Figure 3.20). The Modified Stability Graph has a built in assessment for stand-up time and this is highlighted in Figure 3.20. If you consider a hydraulic radius of 10, this corresponds to a stand-up time of 6 months to 1 year. If you consider a hydraulic radius of 4, this corresponds to a stand-up time of 1 day to 1 month. The difference in stand-up times is a function of the time it will take to mine out a stope. A smaller stope with a hydraulic radius of 4, will take less time to mine than a larger stope with a hydraulic radius of 10.

As another means of testing the validity of the proposed empirical design method, data from Bieniawski's RMR Stand-up Time Graph was plotted on the MST Graph. From Figures 3.7 to 3.12, it can be seen that the data for stand-up times of less than one month is rather scattered. This is not surprising as the time periods within this interval are relatively small, and small variations are easily observed. For stand-up times of one month to one year, the data appears to fit these lines very well. Small variations in data will no longer be apparent as the time intervals are becoming much larger (i.e. instead of tracking stand-up time in days, it is now being plotted in intervals of weeks and months). For time intervals greater than one year, the available data is very limited. It is likely that these stand-up times were inferred based on the data from the previous time intervals and the limited data available for stand-up times greater than one year. Any data for stand-up times greater than one year will generally be limited, as most open stopes will not remain open for this period of time. Mines generally do not like to leave these voids open for extended periods of time, as this will drastically increase the risk of a failure occurring, creating issues for safety and production.

To further assess the effectiveness of the MST graph, ten case histories from Birchtree open stopes were assessed. Each case history included the assessment of five, or in one instance, six, stope surfaces. As part of each case history, opening geometry, estimated stress conditions, rock mechanical properties, and geological factors that could affect stability were determined. To assess the accuracy of the MST Graph, the case history data was used to predict stand-up time. These predicted times were compared to the actual stand-up times of the case histories to determine the difference between predicted and actual stand-up times.

From Figures 6.1 and 6.2, it could be seen that most of the case history data was concentrated in a small time interval of one month or less. This is generally because Birchtree Mine has various restrictions on stope sizes that limit the range of hydraulic radius values. This is also due to stope conditions at the Birchtree Mine, as stopes are generally not left open for long periods, due to previously observed stope stability issues. It was also observed that the stand-up times for the unstable case histories were generally predicted to experience some form of instability within two weeks or less. This again reflects actual observations from unstable case histories. The majority of failures that occur at Birchtree generally happen within a short period of time after stope blasting.

Assessing any one factor for stope design, such as exposure or stand-up time, is challenging because there are many highly variable factors influencing stability in the field. This may account for some of the observed discrepancy between predicted and actual stope surface stand-up times. Some of these variables, such as post mining stress, the orientation of structure, and rock mass classification, were quantified and assessed in the MST design method, though often with limited reliability. Other variables, such as blasting, blast hole deviation, and pre-mining stress are usually not measured and are not assessed with current design methods.

Differences between the MST graph and the RMR Stand-up Time Graph may be a result of converting RMR to N'. To convert RMR, Equation 3.2 was used to calculate Q', as this data was not available in the original data set for the RMR Stand-up Time Graph. Since the Q' data was not available, this was the best means for calculating this value at the time.

7.2 Other Factors Influencing Stability

Peridotite was assessed as part of this study to determine if there was a link between peridotite and stability as reported at the Birchtree Mine (Section 6.4). As part of the assessment, peridotite was compared to RQD, overbreak/underbreak, and stable/unstable surfaces. From these analyses, no trend was observed that linked peridotite to stability. High stress, in excess of the stress levels that are differentiated using the stability graph design techniques, were encountered at the Birchtree Mine. High stress levels were compared to the observed error in stand-up time predicted using the MST graph, however, no trends were observed.

7.3 Future Work

To further develop the MST Graph for use in underground applications, more case histories need to be gathered and tested with the proposed method. The current data set is relatively small and lacks some detailed data, particularly information concerning joint conditions from scan lines. Ideally, each case history included on the MST Graph would have its own scan line for that particular stope, to reduce the number of assumptions required for analysis. This would require significant time and resources, but could be conducted over an extended period of time, and added to the MST Graph as the data becomes available. Once a larger data set is available, it would be possible to make adjustments to the MST graph to better represent mine specific conditions. Further data would allow for more refinement to the time intervals included on the MST Graph.

Outside of the current scope of the project, other factors such as blast damage, undercutting, and geological influences also need to be accounted for as they can have a significant impact on stability. These factors were briefly discussed, but not incorporated into the MST Graph. Ideally, these factors could be incorporated in the MST design graph to improve the predictability of the design method. Each of these factors could be a study on their own, and once again, would require significant resources to complete. There have been numerous research projects conducted at various mine sites pertaining to these particular subjects, but very few, if any, studies exist that account for the combined effects of these factors.

7.4 Summary

As part of the research, a new approach has been developed to assess stand-up time for open stopes. There is currently no reliable approach for predicting time to failure for mine stopes and this method provides mine engineers with a valuable planning tool. This approach incorporates the N' and HR variables, which are commonly used in the current mining industry. It is hoped that other factors influencing stability will be added to this design method. As this technique is applied by industry, it is expected that added case histories will improve the accuracy and reliability of this design method.

REFERENCES

Andrieux, P., & Simser, B. (2001). Ground-Stability-Based Mine Design Guidelines at the Brunswick Mine. In W. A. Hustrulid, & R. L. Bullock, Underground Mining Methods: Engineering Fundamentals and International Case Studies (pp. 207-214). Littleton, Colorado: Society for Mining, Metallurgy, and Exploration, Inc.

Barton, N. R., & Bandis, S. C. (1982). Effects of block size on the shear behaviour of jointed rock. 23rd U.S. symposium on rock mechanics, (pp. 739-760). Berkeley.

Barton, N. R., & Choubey, V. (1977). The shear strength of rock joints in theory and practice. In Rock Mechanics (pp. 1-54).

Barton, N. R., Lien, R., & Lunde, J. (1974). Engineering classification of rock masses for the design of tunnel support. In Rock Mechanics (pp. 189-239).

Bieniawski. (1984). Rock Mechanics Design in Mining and Tunnelling. Rotterdam: Balkema.

Bieniawski, Z. T. (1976). Rock mass classification in rock engineering. In Z. T. Bieniawski (Ed.), In Exploration for rock engineering, proc. of the symp. 1 (pp. 97-106). Cape Town: Balkema.

Bieniawski, Z. T. (1989). Engineering rock mass classifications. New York: Wiley.

Birchtree Mine. (2002-2010). Birchtree Mine Scanline Binder. Retrieved from Birchtree Mine, Thompson, Manitoba.

Birchtree Mine. (2010). Major Faults Located in the Birchtree Mine. Thompson, Manitoba, Canada: Vale Canada.

Birchtree Mine. (2010). Material Properties Table for Birchtree Mine. Thompson, Manitoba, Canada: Vale Canada.

Capes, G.W. (2006). Open stope hanging wall design based on general and detailed data collection in rock masses with unfavourable hanging wall conditions (Ph.D. Thesis). University of Saskatchewan, Saskatoon, Canada.

Clark, L. M., & Pakalnis, R. C. (1997). An empirical approach for estimating unplanned dilution from open stope hangingwalls and footwalls. 99th CIM annual general meeting. Vancouver: Canadian Institute of Mining, Metallurgy and Petroleum.

Deere, D. U. (1963). Technical Description of Rock Cores for Engineering Purposes. In Rock Mechanics and Engineering Geology Vol. 1 No. 1 (pp. 16-22).

Digital Globe. (2017, April 4). Google Maps. https://www.google.ca/maps/place/Thompson,+MB/@55.7259041,-97.8507261,8843m/data=!3m1!1e3!4m5!3m4!1s0x525fc66cc346c559:0xd1985426b2df902d!8m2!3d55.7449251!4d-97.8508715. Retrieved April 4, 2017

Eckstrand, O. R., & Hulbert, L. J. (2007). Magmatic Nickel-Copper-Platinum Group Element Deposits. Mineral Deposits of Canada: A Synthesis of Major Deposit Types, District Metallogeny, the Evolution of Geological Provinces, and Exploration Methods, 205-222. Geological Association of Canada, Special Publication No. 5.

Exadaktylos, G. E., & Stavropoulou, M. C. (2002). A closed-form elastic solution for stresses and displacements around tunnels. International Journal of Rock Mechanics and Mining Sciences, 905-916.

Folmer, D. (1992). Analysis of the Blocks Program and Empirical Rockmass Classification Systems Used at INCO Thompson. Thompson: INCO.

Goodman, R. E. (1989). Common Laboratory Strength Tests. In R. E. Goodman, Introduction to Rock Mechanics Second Edition (p. 61). John Wiley & Sons.

Goodman, R. E. (1989). Openings in Competent Rock. In R. E. Goodman, Introduction to Rock Mechanics Second Edition (pp. 225-232). Berkeley, California: John Wiley and Sons.

Hoek, E., & Brown, E. T. (1980). Underground Excavations in Rock. London: Institution of Mining and Metallurgy.

Hoek, Evert and E.T. Brown (1980). Empirical strength criterion for rock masses. Journal of Geotechnical Engineering Div., ASCE **106** (pp. 1013-1035).

Hoek, E., & Brown, E. T. (1988). The Hoek-Brown failure criterion - a 1988 update. In J. H. Curran (Ed.), Proceedings of the 15th Canadian Rock Mechanics Symposium (pp. 31-38). Toronto: Civil Engineering Department, University of Toronto.

Hoek, E., & Brown, E. T. (1990). Stresses Around Underground Openings. In E. Hoek, & E. T. Brown, Underground Excavations in Rock (pp. 87-131). Abingdon, Oxon: Taylor & Francis.

Hutchinson, D. J., & Diederichs, M. S. (1996). Cablebolting in underground mines. Richmond, BC: BiTech Publishers Ltd.

Kirsch, G. (1898). Die theorie der Elastizitat und die bedurfnisse der festigkeitslehre. Zeit Ver Deut Ing J, 797-807.

Lang, B. (1994). Span design for entry type excavations (M.Sc. Thesis). University of British Columbia, Vancouver, Canada.

Laubscher, D.H. Geomechanics Classification of Jointed Rock Masses: Mining Applications. *Transactions of the Institute for Mining and Metallurgy,* vol. 86, 1977, pp. A1-A8.

Lauffer, H. (1958). Gebirgsklassifizierung fur den Stollenbau. In Geologie und Bauwesen Vol. 24 (pp. 46-51).

Li, L., Ouellet, S., & Aubertin, M. (2009). An improved definition of rock quality designation, RQDc. In M. Diederichs, & G. Grasselli (Ed.), Proceedings of the 3rd CANUS Rock Mechanics Symposium (pp. 1-10). Toronto: ROCKENG09.

McDowell, G. M., Stewart, R., & Monteiro, R. N. (2007). In-mine Exploration and Delineation Using an Integrated Approach. In B. Milkereit (Ed.), Proceedings of Exploration 07: Fifth Decennial International Conference on Mineral Exploration, (pp. 571-589).

Milne, D. (1997). Underground Design and Deformation Based on Surface Geometry (Ph.D. Thesis). University of British Columbia, Vancouver, Canada

Milne, D., Hadjigeorgiou, J. and Pakalnis, R., (1998). Rock mass characterization for underground hard rock mines. *Tunnelling and Underground Space Technology*, Oct. 1998, vol. 13, no 4, pp. 383-391.

Milne, D. (2016). Personal communication. (M.Violot, Interviewer).

Nickson, S. D. (1992). Cable support guidelines for underground hard rock mine operations (M.Sc. Thesis). University of British Columbia, Vancouver, Canada.

Pakalnis, R. T. (1986). Empirical Stope Design at the Ruttan Mine, Sherritt Gordon Mines LTD (Ph.D. Thesis). University of British Columbia, Vancouver, Canada.

Palmstrom, A. (1982). The volumetric joint count- a useful and simple measure of the degree of rock jointing. Proc. 4th Congress. Int. Assn. Engineering Geology, (pp. 221-228). Delhi.

Potvin, Y. (1988). Empirical open stope design in Canada (Ph.D. Thesis). University of British Columbia, Vancouver, Canada.

Rafigul, I., & Shinjo, R. (2009). Numerical simulation of stress distributions and displacements around an entry roadway with igneous intrusion and poitnetial sources of seam gas emission of the Barapukuria coal mine, NW Bangladesh. International Journal of Coal Geology, 249-262.

Southern, J. (2011). Birchtree Mine 2011 84 Orebody Block Model Report. Thompson, Manitoba: Vale Manitoba Operations.

Southern, J. (2017, January 13). Birchtree 84 Complex Geology. (M.Violot, Interviewer)

Suorineni, F. T. (2010). The stability graph after three decades in use: Experiences and the way forward. International Journal of Mining, Reclamation and Environment, Vol. 24, No. 4, 307-339.

Vale Canada. (2016, March 17). Birchtree Mine Longitudinal. Retrived from Birchtree Mine, Thompson, Manitoba.

Wang, J. (2004). Influence of Stress, Undercutting, Blasting and Time on Open Stope Stability and Dilution (Ph.D. Thesis). University of Saskatchewan, Saskatoon, Canada.

APPENDIX A
SCANLINE DATA

Location: 2950 South Ext (2007).

Applied to the following stopes:

- 30-848.1

Table A.1 Scanline data used for the 30-848.1 Stope (After Birchtree Scanline Binder, 2010)

Rock Type	Structure Type	Distance (m)	Dip Direction (^{O})	Dip (^{O})	Strike (^{O})	J_r	J_a
IF	JNT	0.03	312	29	222	1.00	0.75
IF	JNT	0.03	112	9	22	1.00	0.75
IF	JNT	0.6	32	79	302	1.00	0.75
IF	JNT	0.9	172	58	82	1.00	0.75
IF	JNT	1.2	182	36	92	1.00	0.75
IF	JNT	1.2	332	65	242	1.50	0.75
IF	JNT	1.5	312	27	222	1.50	4.00
IF	JNT	2.1	282	81	192	1.00	20.00
IF	JNT	3.0	12	74	282	1.50	10.00
IF	JNT	3.2	72	76	342	1.00	10.00
IF	JNT	3.7	177	49	87	1.50	0.75
IF	JNT	3.9	242	79	152	1.00	10.00
IF	JNT	7.3	322	40	232	1.50	1.00
IF	JNT	6.1	122	9	32	1.00	4.00
IF	JNT	8.6	297	84	207	1.00	0.75
IF	JNT	9.9	292	3	202	1.00	0.75
IF	JNT	12.5	329	28	239	1.00	0.75
IF	JNT	13.1	192	62	102	1.00	10.00
IF	JNT	13.7	327	40	237	1.00	0.75
IF	JNT	14.0	168	46	78	1.50	10.00
IF	JNT	15.6	297	81	207	1.00	4.00
IF	JNT	16.5	112	15	22	1.00	0.75

Location: 3200 928

Applied to the following stopes:

- 30-848.1, 32-872.1, 32-928.1, 33-916.2, 33-916.3

Table A.2 Scanline data used for the 30-848.1, 32-872.1, 32-928.1, 33-916.2, and 33-916.3 Stope (After Birchtree Scanline Binder, 2010)

Rock Type	Structure Type	Distance (m)	Dip Direction (^{O})	Dip (^{O})	Strike (^{O})	J_r	J_a
SCH	JNT		105	37	15	1.50	0.75
SCH	JNT	2.7	44	88	314	1.00	4.00
SCH	JNT	4.0	20	20	290	1.50	4.00
SCH	JNT	6.1	10	88	280	1.50	10.00
SCH	JNT	6.7	165	86	75	1.00	10.00
SCH	JNT	9.1	140	65	50	1.50	20.00
SCH	JNT	11.1	150	58	60	1.00	4.00
SCH	JNT	12.2	130	81	40	1.50	10.00
SCH	JNT	12.8	315	82	225	1.50	0.75
SCH	JNT	14.6	265	88	175	1.00	0.75
SCH	JNT	15.8	130	65	40	1.00	0.75
SCH	JNT	17.7	315	67	225	1.50	20.00
SCH	JNT	18.0	151	56	61	1.50	0.75
SCH	JNT	18.6	128	80	38	1.00	4.00
SCH	JNT	19.2	260	86	170	1.00	4.00
SCH	JNT	19.2	130	75	40	1.50	0.75
SCH	JNT	19.8	313	85	223	1.50	4.00
SCH	JNT	20.7	10	82	280	1.00	10.00
SCH	JNT	21.6	40	20	310	1.50	0.75
SCH	JNT	22.3	100	30	10	1.50	0.75
SCH	JNT	22.9	120	75	30	1.50	4.00

Location: 3325 South

Applies to the following stopes:

- 33-840.1, 33-848.1, 33-848.2, 33-936.2

Table A.3 Scanline data used for the 33-840.1, 33-848.1, 33-848.2, and 33-936.2 Stopes (After Birchtree Scanline Binder, 2010)

Rock Type	Structure Type	Distance (m)	Dip Direction (^{O})	Dip (^{O})	Strike (^{O})	J_r	J_a
AMPT	JT	0.3	37	62	307	1.50	4.00
AMPT	JT	0.5	152	60	62	1.50	4.00
AMPT	JT	0.7	152	68	62	1.50	4.00
AMPT	JT	1.1	267	75	177	1.50	4.00
AMPT	JT	1.2	269	75	179	1.50	10.00
SCH	FOTN	1.5	297	72	207	1.50	10.00
SCH	FOTN	1.8	287	70	197	1.00	4.00
AMPT	JT	1.8	57	65	327	1.00	4.00
SCH	FOTN	2.1	287	72	197	1.50	4.00
SCH	FOTN	2.4	277	60	187	1.50	4.00
AMPT	JT	4.0	57	35	327	1.00	4.00
SCH	FOTN	4.3	277	60	187	1.50	4.00
AMPT	JT	4.4	22	70	292	1.50	4.00
AMPT	JT	4.6	22	70	292	1.50	1.00
AMPT	JT	4.9	22	70	292	1.50	4.00
AMPT	JT	5.2	22	70	292	1.50	1.00
AMPT	JT	5.5	262	60	172	1.50	4.00
AMPT	JT	5.9	147	60	57	1.50	4.00
AMPT	JT	6.1	147	60	57	1.50	4.00
AMPT	JT	6.4	47	65	317	1.50	4.00
AMPT	JT	7.0	77	30	347	1.00	4.00
AMPT	JT	7.6	77	30	347	1.00	4.00
AMPT	JT	7.9	77	30	347	1.00	4.00
AMPT	JT	8.4	37	80	307	1.00	4.00
SCH	FOTN	10.4	257	30	167	1.50	1.00
SCH	FOTN	11.0	257	30	167	1.50	1.00
SCH	FOTN	11.3	257	30	167	1.50	1.00
SCH	JT	11.8	177	60	87	1.50	4.00
SCH	JT	12.3	147	70	57	2.25	10.00
SCH	FOTN	12.8	277	45	187	1.50	1.00
SCH	FOTN	13.1	277	45	187	1.50	1.00
SCH	FOTN	13.7	277	45	187	1.50	1.00
SCH	JT	13.8	162	55	72	1.50	4.00
SCH	JT	14.9	277	50	187	1.00	4.00
SCH	FOTN	15.2	62	40	332	2.25	1.00
SCH	FOTN	17.1	267	60	177	2.25	1.00
SCH	FOTN	17.2	267	60	177	2.25	1.00
SCH	FOTN	18.3	267	60	177	2.25	1.00
SCH	FOTN	18.4	267	60	177	2.25	1.00

Location: 3325 South

Applies to the following stope:

- 33-840.1, 33-848.1, 33-848.2

Table A.4 Scanline data for the 33-840.1, 33-848.1, and 33-848.2 Stopes (After Birchtree Scanline Binder, 2010)

Rock Type	Structure Type	Distance (m)	Dip Direction	Dip (^{O})	Strike (^{O})	J_r	J_a
SCH	JNT	0.6	157	59	67	1.00	4.00
SCH	JNT	1.2	207	82	117	1.00	4.00
SCH	JNT	1.8	302	31	212	1.00	4.00
SCH	JNT	1.8	132	26	42	1.00	4.00
SCH	JNT	3.4	152	20	62	1.00	4.00
SCH	JNT	4.6	202	86	112	1.50	4.00
SCH	JNT	6.1	17	81	287	1.00	10.00
SCH	JNT	6.1	112	25	22	1.00	10.00
SCH	JNT	6.7	112	34	22	1.00	4.00
SCH	JNT	6.7	162	75	72	1.50	4.00
SCH	JNT	6.7	302	2	212	1.00	10.00
SCH	JNT	9.1	192	84	102	1.00	4.00
SCH	JNT	10.7	122	69	32	1.00	20.00
SCH	JNT	11.0	157	16	67	1.00	10.00
SCH	JNT	11.6	142	79	52	1.00	4.00
SCH	JNT	14.6	112	75	22	1.00	20.00
SCH	JNT	14.6	172	20	82	1.00	20.00
SCH	JNT	15.2	282	54	192	1.00	1.00
SCH	JNT	15.2	252	79	162	1.50	4.00

Location: 3325 10070

Applies to the following stopes:

- 33-936.2

Table A.4 Scanline data used for the 33-936.2 Stope (After Birchtree Scanline Binder, 2010)

Rock Type	Structure Type	Distance (ft)	Distance (m)	Dip Direction	Dip (^{O})	Strike (^{O})	J_r	J_a
SCH	FOL	1.5	0.5	56	70	326	3.00	0.75
SCH	FOL	9.2	2.8	286	85	196	3.00	0.75
SCH	SHR	11.0	3.4	181	85	91	3.00	10.00
SCH	FOL	15.0	4.6	16	80	286	3.00	10.00
SCH	FOL	17.0	5.2	236	85	146	3.00	10.00
SCH	JNT	19.0	5.8	111	90	21	3.00	1.00
SCH	SHR	27.0	8.2	276	80	186	3.00	20.00
SCH	SHR	31.0	9.4	276	80	186	3.00	1.00
SCH	JNT	20.0	6.1	356	10	266	1.50	1.00
SCH	JNT	30.0	9.1	356	10	266	1.50	1.00
SCH	JNT	32.0	9.8	16	10	286	1.50	1.00
SCH	FOL	33.0	10.1	256	80	166	3.00	1.00
SCH	FOL	37.0	11.3	256	85	166	3.00	0.75
SCH	FOL	41.3	12.6	271	90	181	2.00	0.75
SCH	JNT	54.0	16.5	21	80	291	3.00	0.75
SCH	JNT	54.0	16.5	16	10	286	1.50	0.75
SCH	JNT	54.0	16.5	346	76	256	2.00	1.00
SCH	JNT	72.0	21.9	216	78	126	3.00	1.00
SCH	FOL	76.0	23.2	246	80	156	3.00	0.75
SCH	JNT	80.0	24.4	356	10	266	1.50	1.00
SCH	JNT	81.0	24.7	356	10	266	1.50	1.00
SCH	FOL	82.0	25.0	236	75	146	3.00	0.75
SCH	JNT	84.0	25.6	96	35	6	2.25	1.00
SCH	JNT	85.0	25.9	306	50	216	3.00	1.00
SCH	JNT	89.0	27.1	206	85	116	3.00	1.00
SCH	FOL	91.0	27.7	236	75	146	3.00	0.75

APPENDIX B
MAP3D OUTPUTS

Open Stope: 29-864.1 Blast 1

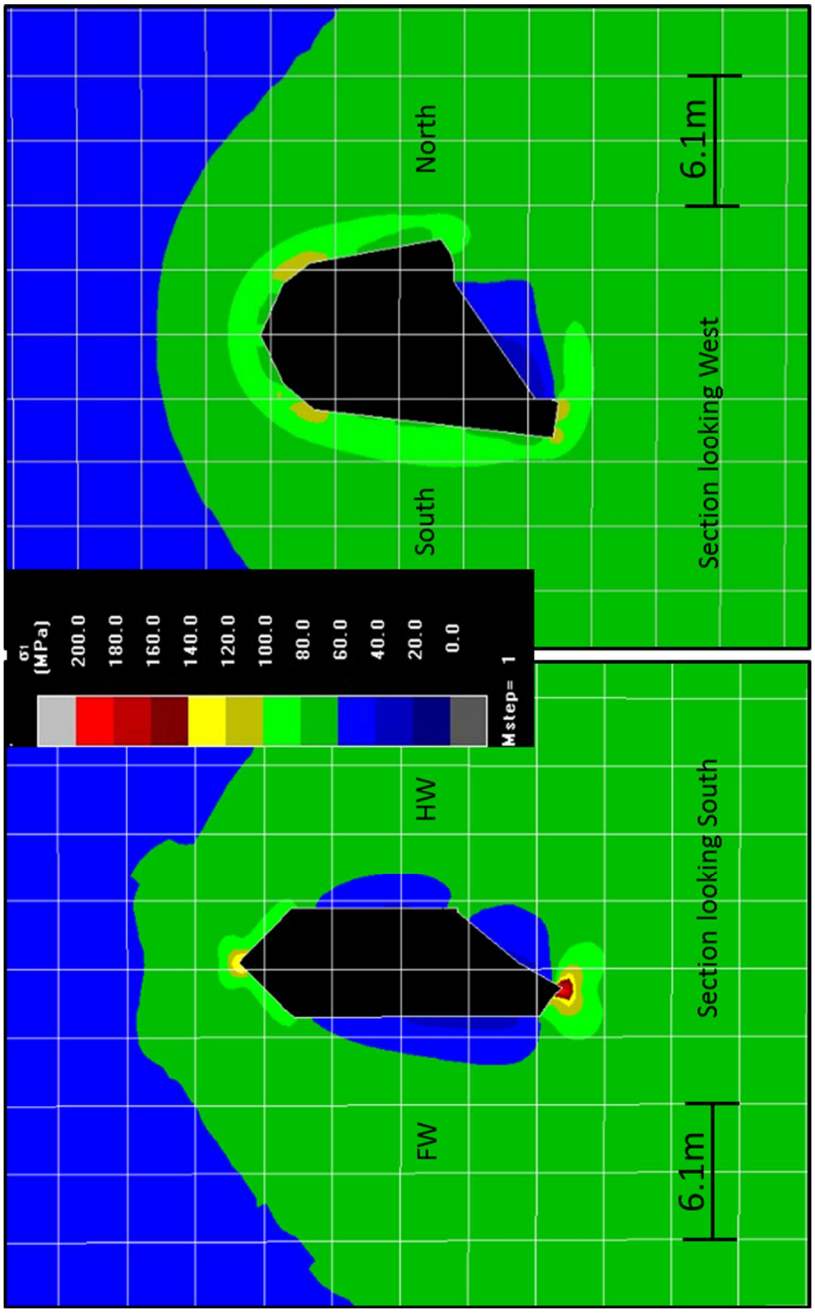

Figure B.1 Map3D output for the 29-864.1 Stope (Blast 1)

Open Stope: 29-864.1 Full Stope

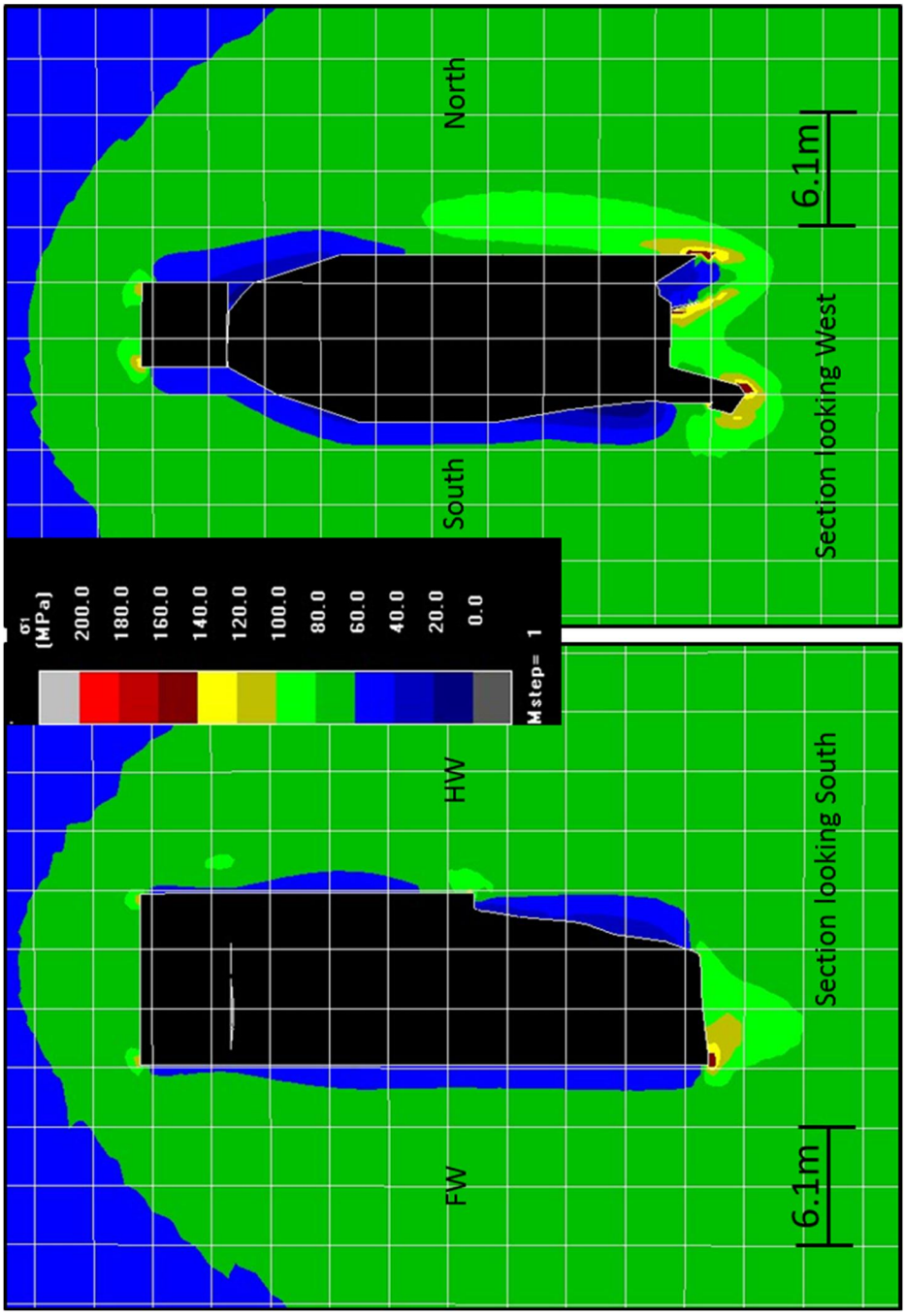

Figure B.2 Map3D output for the 29-864.1 Stope (Full Stope)

Open Stope: 30-848.1

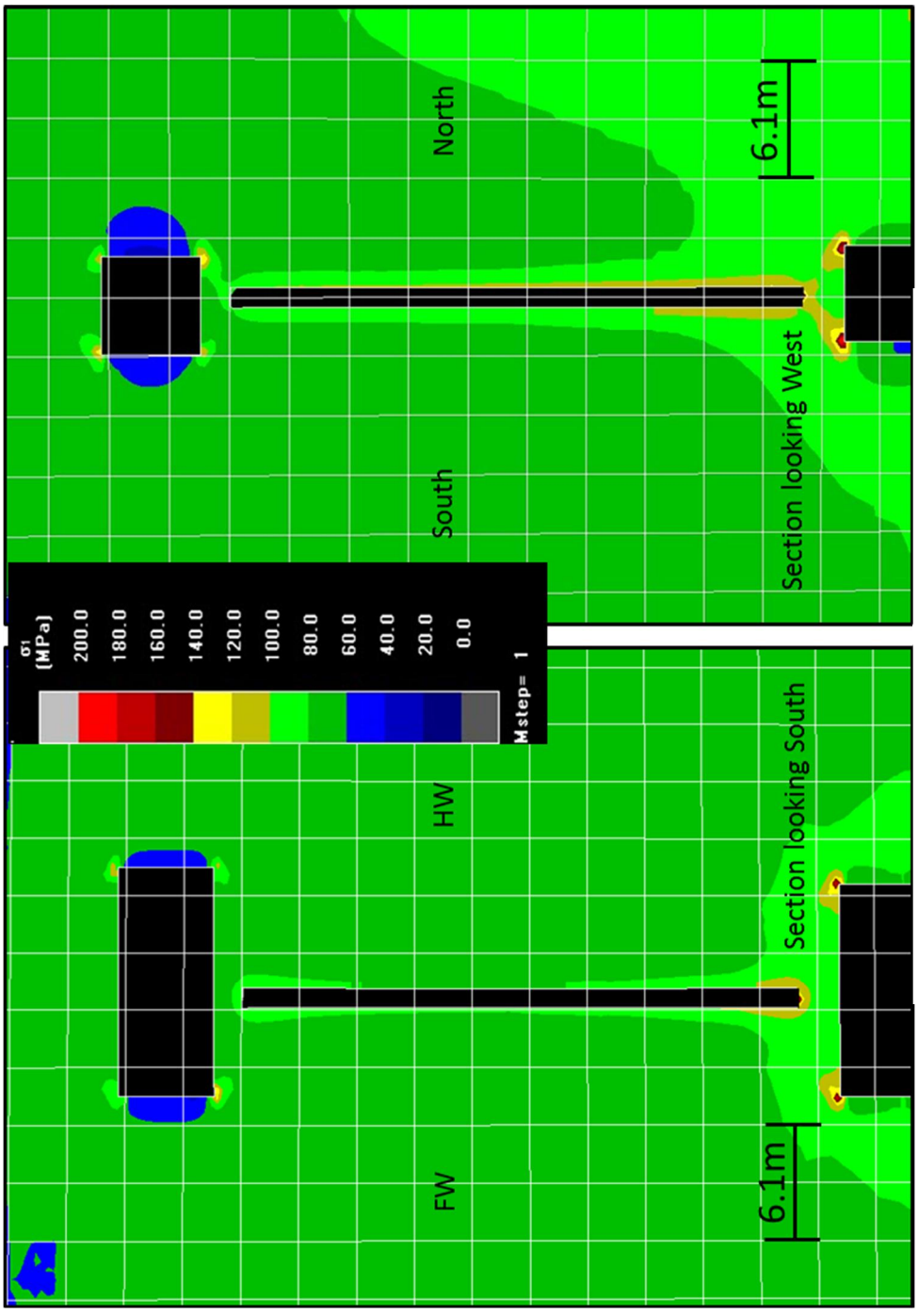

Figure B.3 Map3D output for the 30-848.1 Stope (Raisebore)

Open Stope: 30-848.1 Full Stope

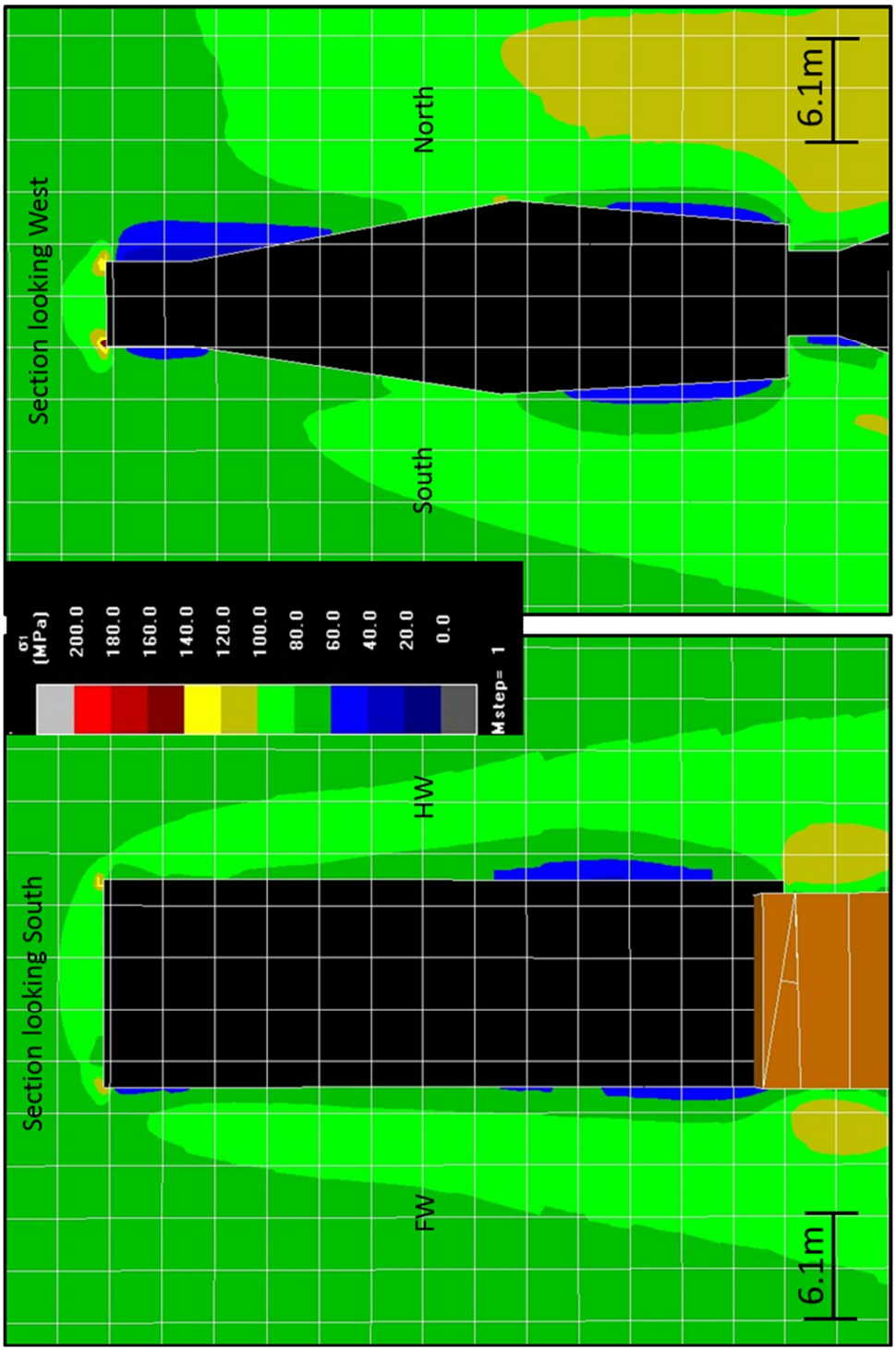

Figure B.4 Map3D output for the 30-848.1 Stope (Full Stope)

Open Stope: 32-872.1

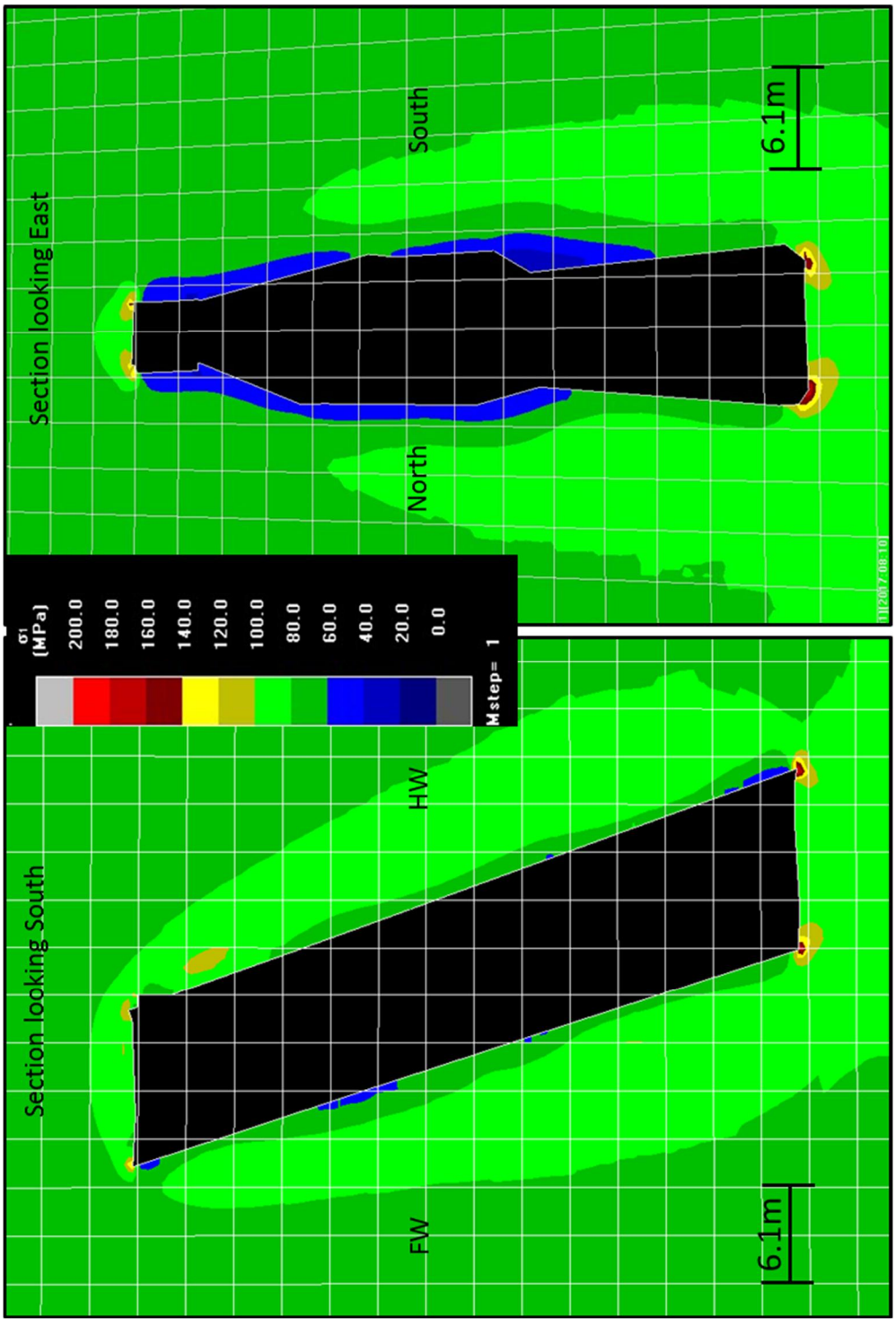

Figure B.5 Map3D output for the 32-872.1 Stope

Open Stope: 32-928.1

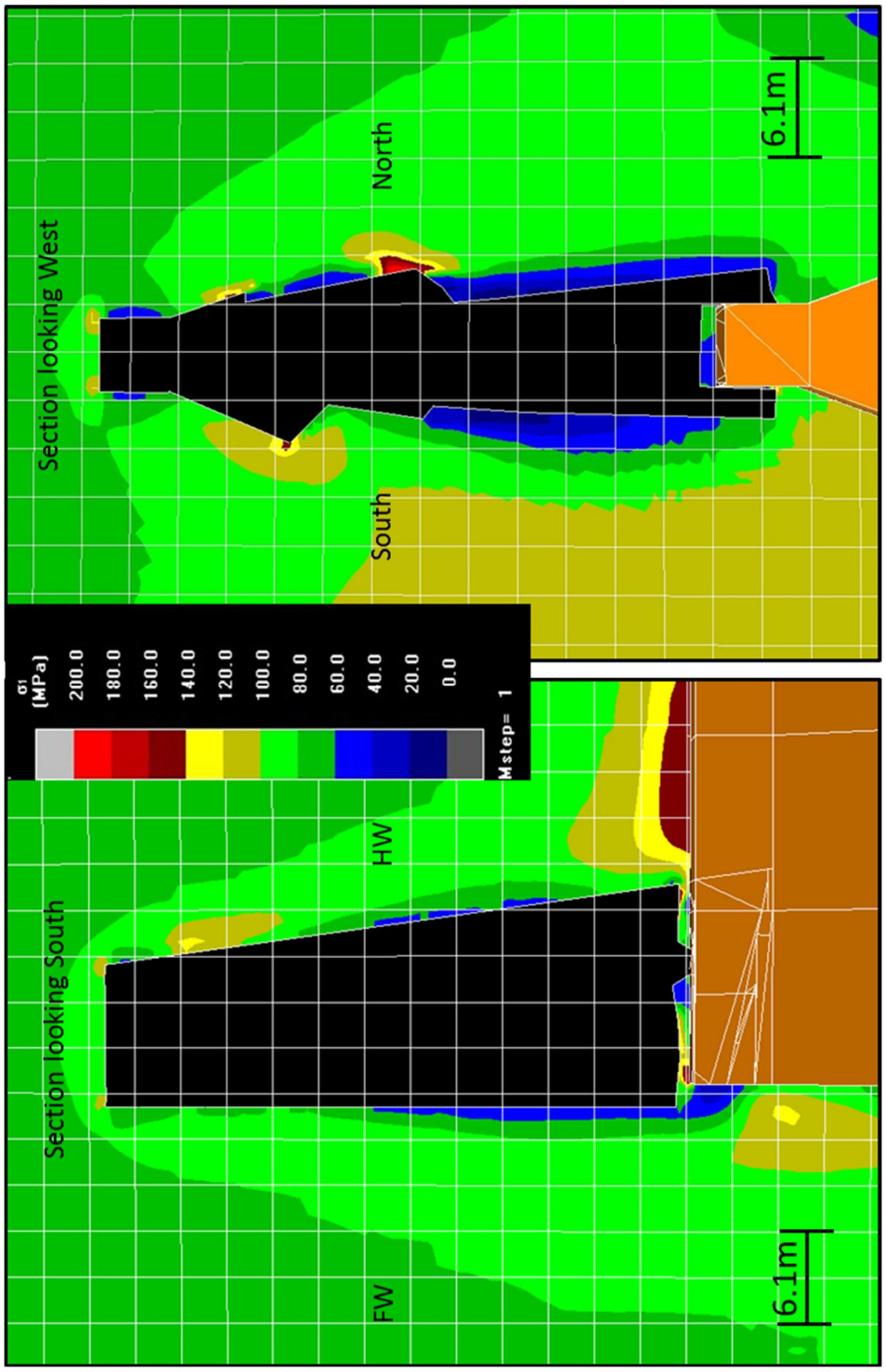

Figure B.6 Map3D output for the 32-928.1 Stope

Open Stope: 33-840.1

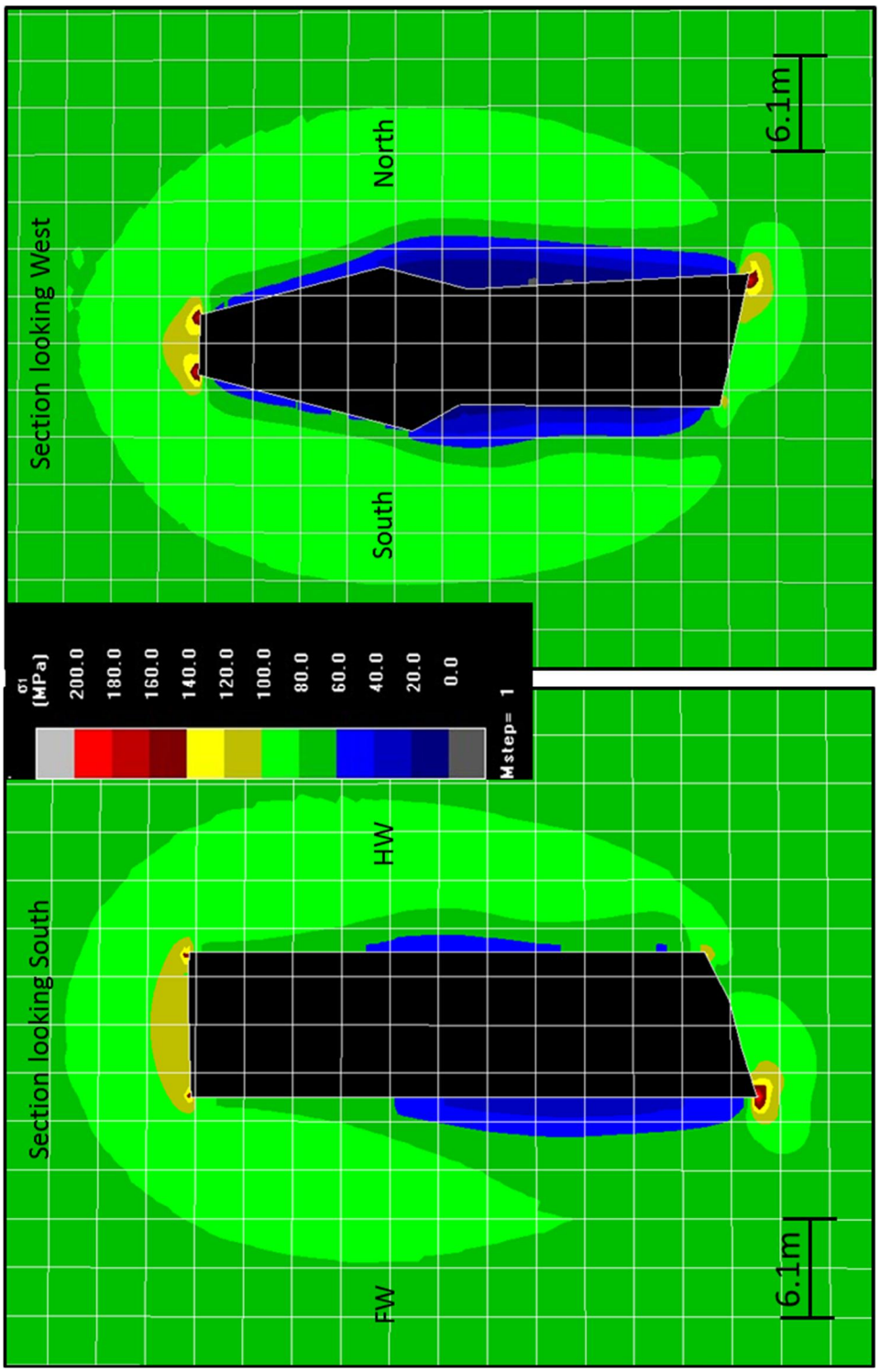

Figure B.7 Map3D output for the 33-840.1 Stope

Open Stope: 33-848.1

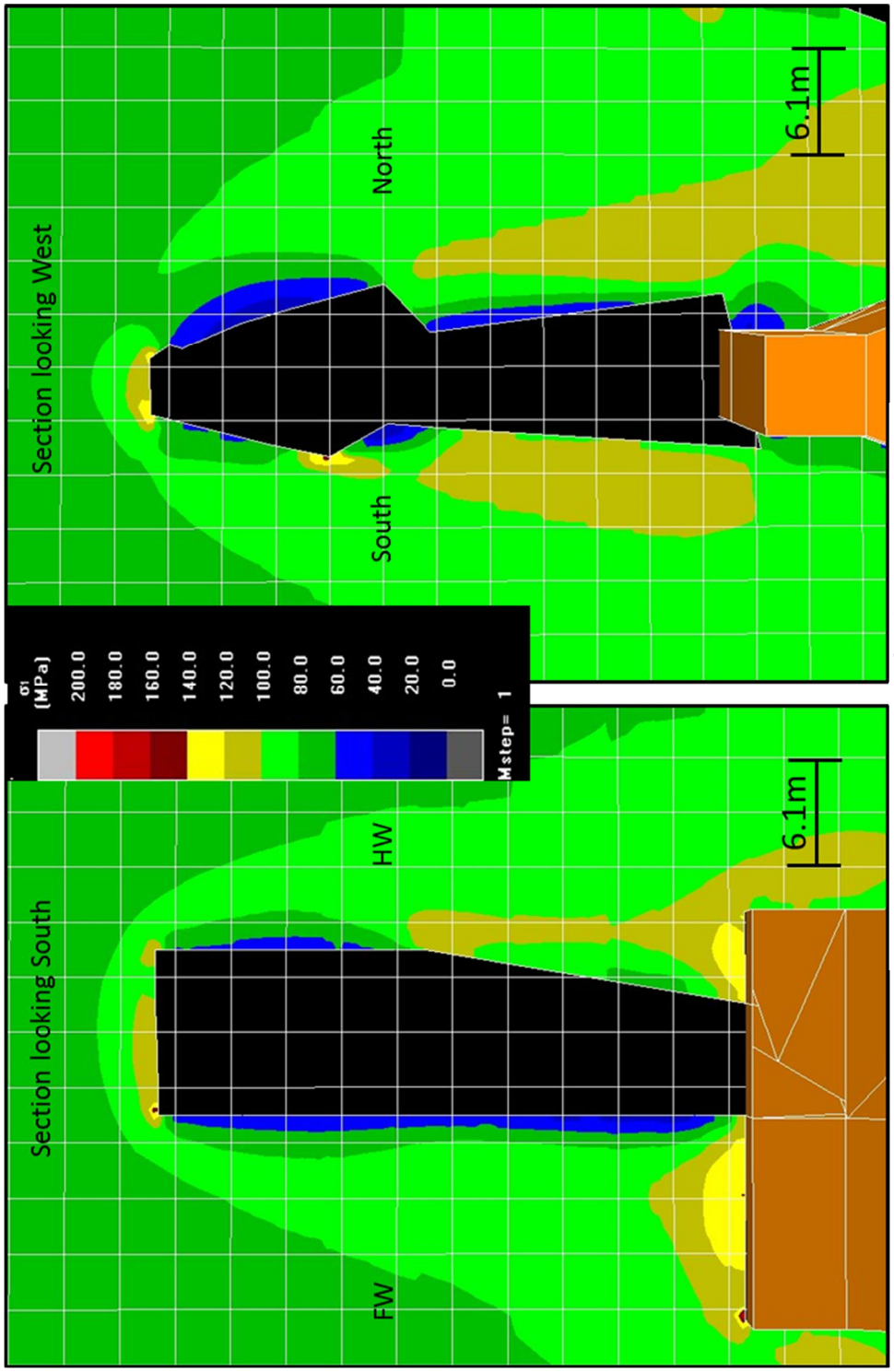

Figure B.8 Map3D output for the 33-848.1 Stope

Open Stope: 33-848.2

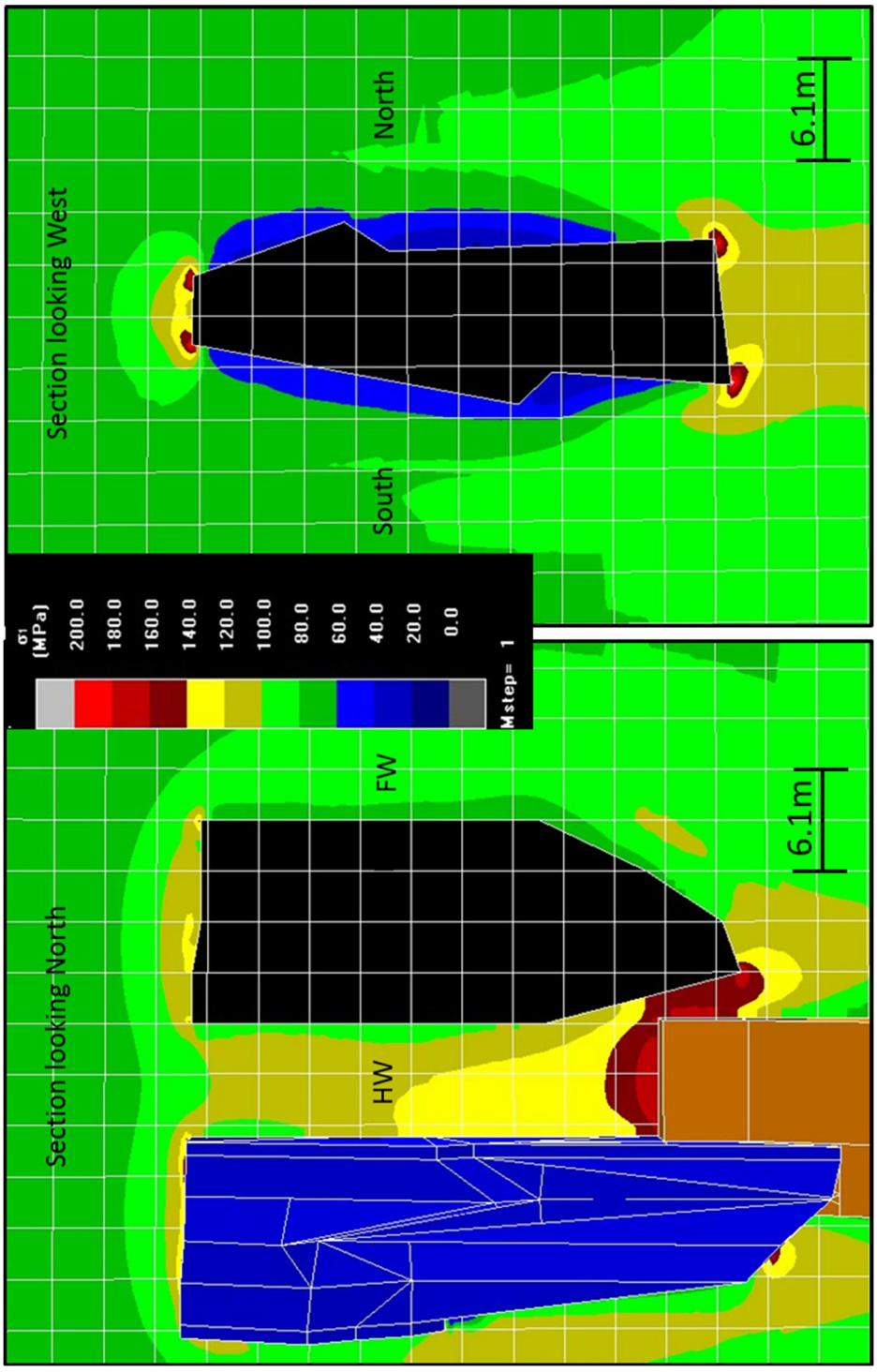

Figure B.9 Map3D output for the 33-848.2 Stope

Open Stope: 33-916.2

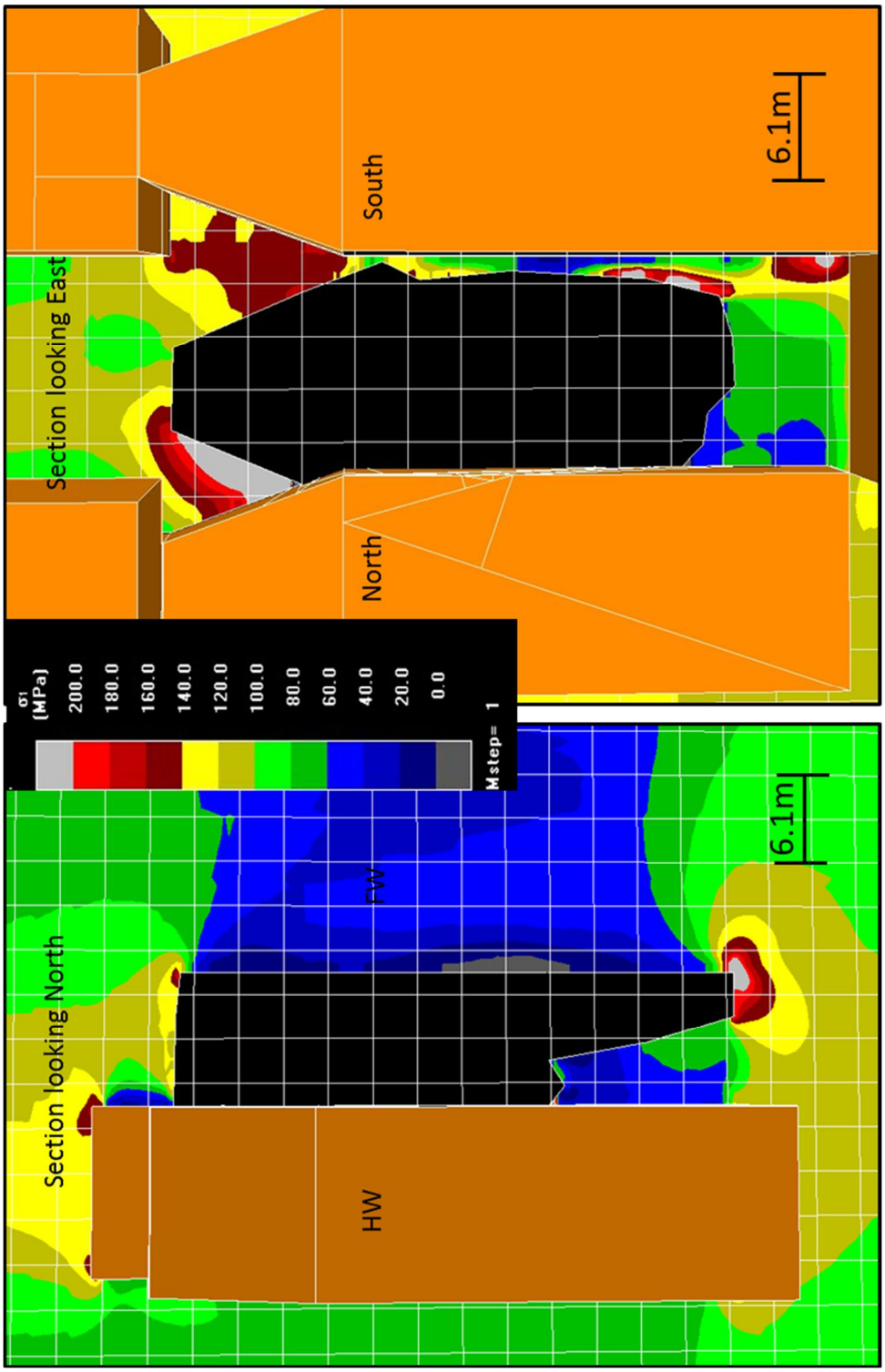

Figure B.10 Map3D output for the 33-916.2 Stope

Open Stope: 33-916.3

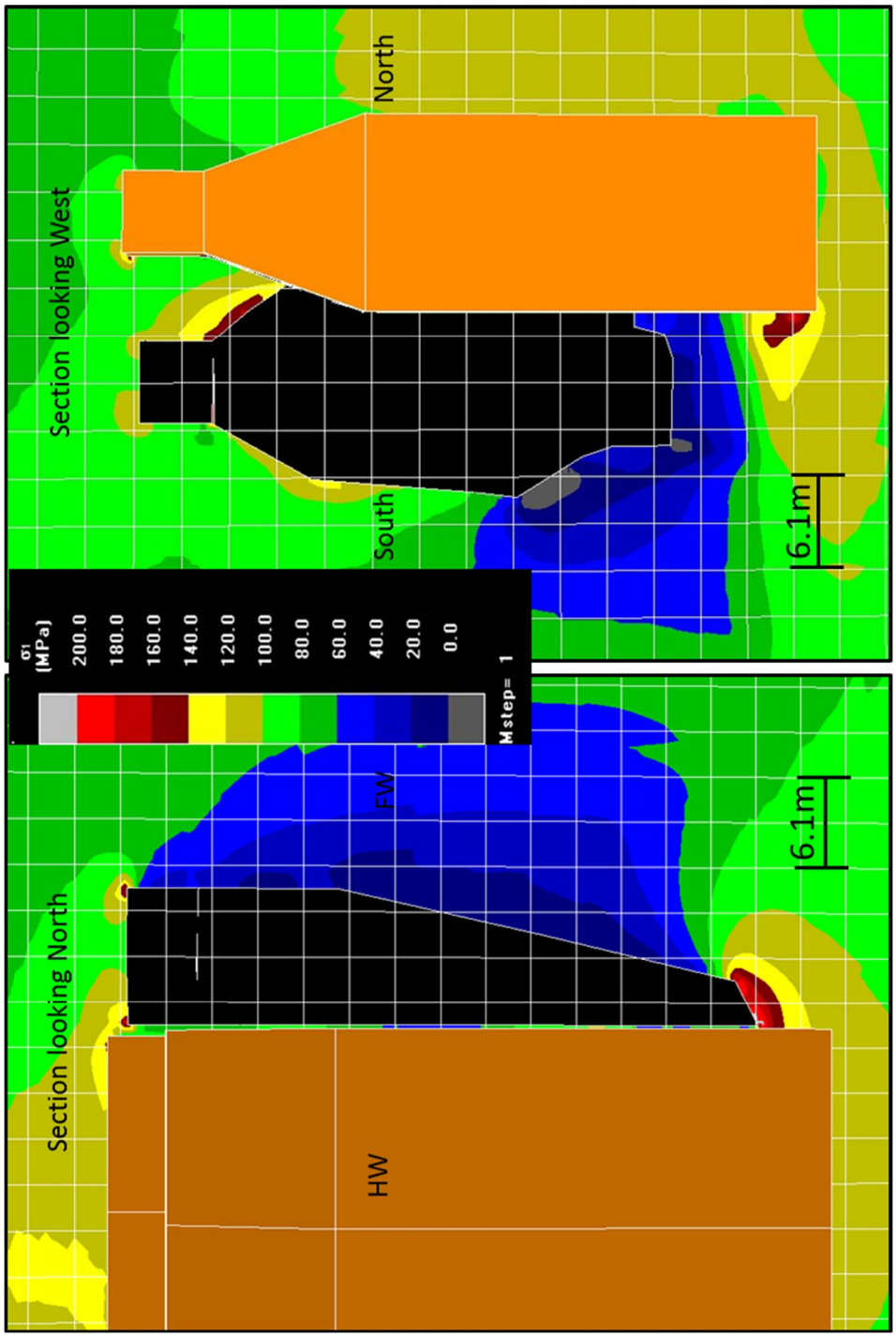

Figure B.11 Map3D output for the 33-916.3 Stope

Open Stope: 33-936.2 Undercut

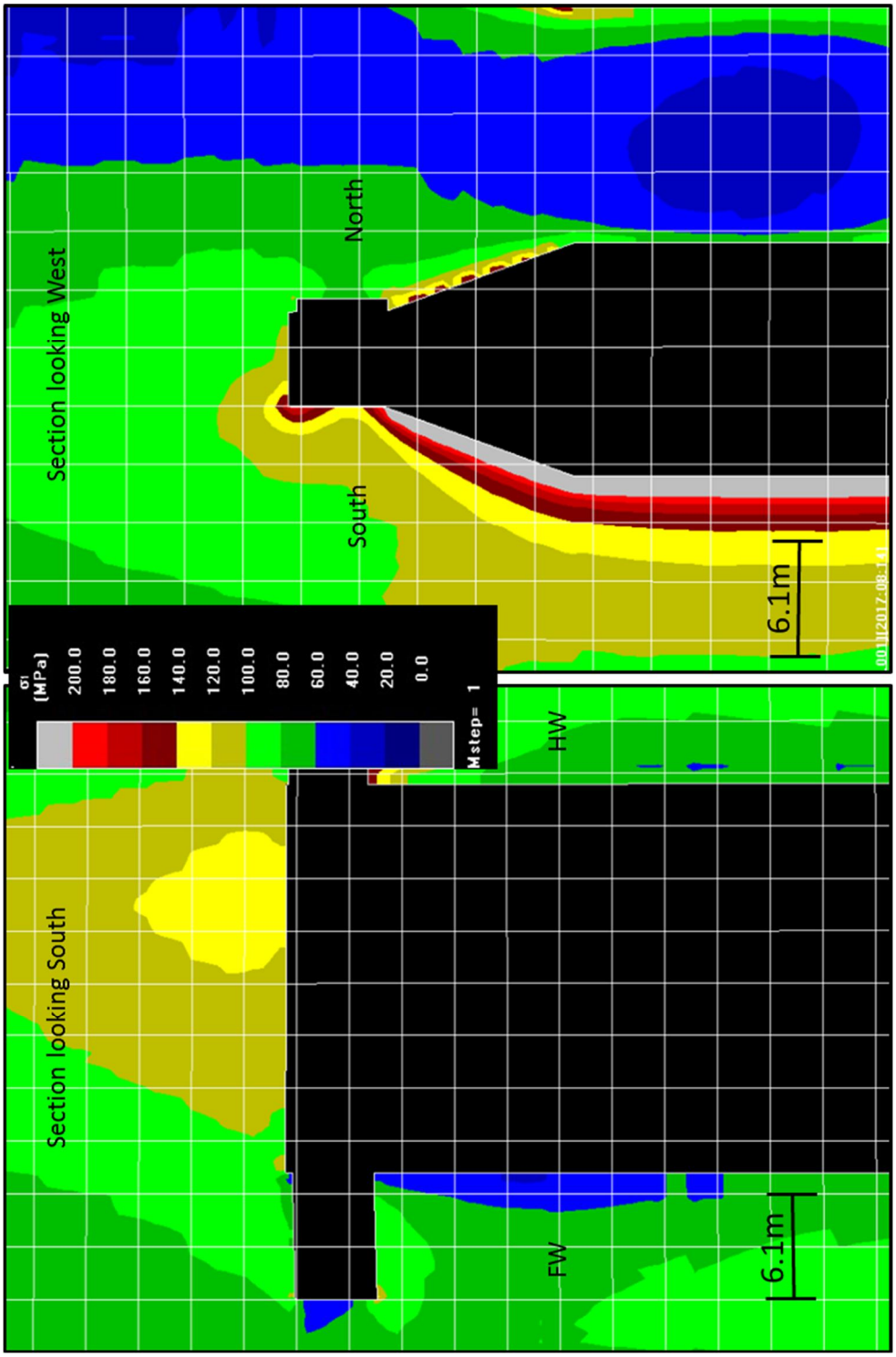

Figure B.12 Map3D output for the 33-936.2 Stope (Undercut)

Open Stope: 33-936.2 Full Stope

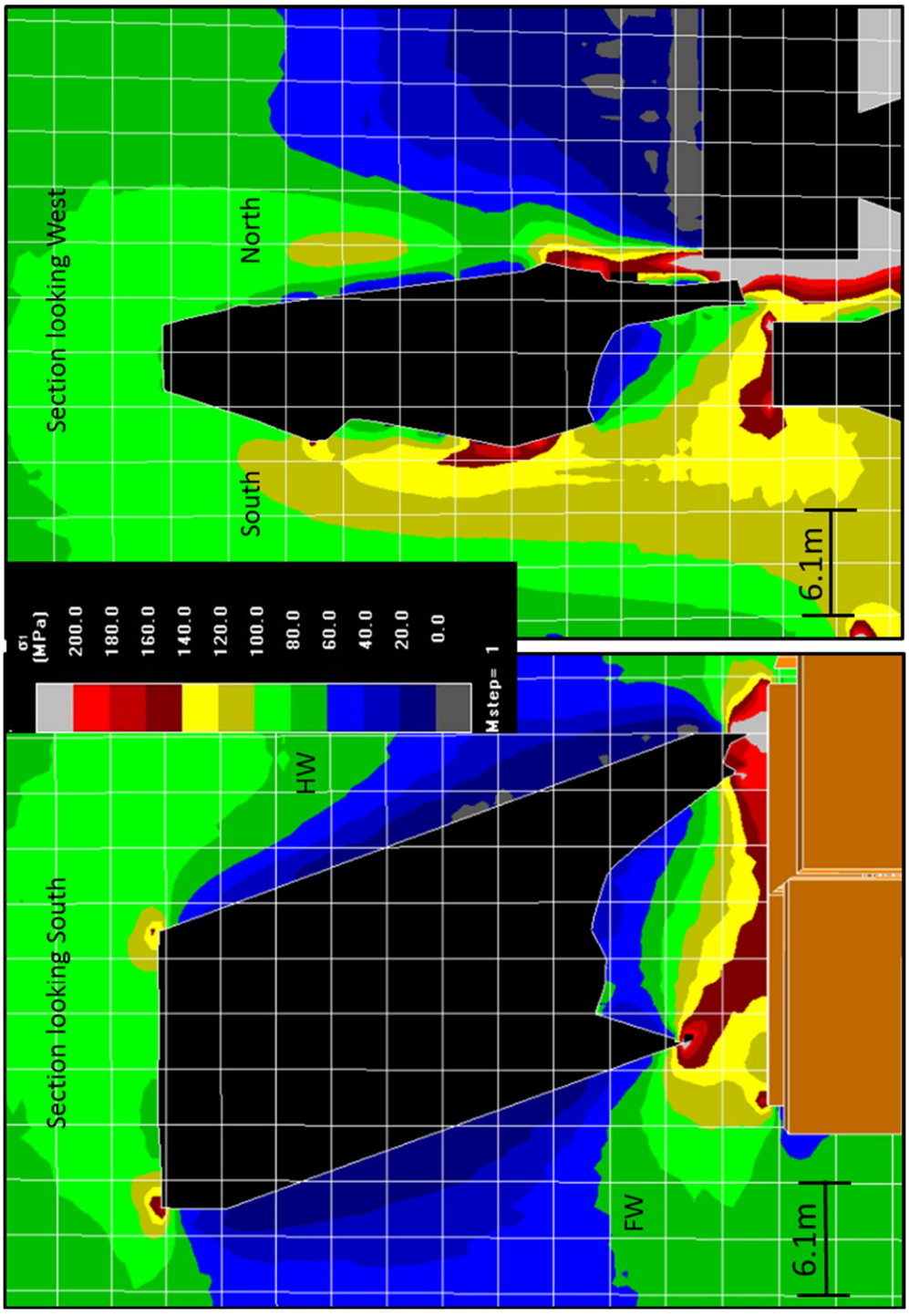

Figure B.13 Map3D output for the 33-936.2 Stope (Full Stope)

APPENDIX C
ROCK MASS CLASSIFICATION DATA FOR CASE HISTORIES

Table C.1 29-864.1 Rock Mass Classification Data

29-864.1	N. Shoulder	S. Shoulder	Hanging Wall	Footwall	Back
Critical Joint Orientation (^{o})	45	45	45	25	5
Maximum Induced Stress (MPa)	59	59	62	58	96
Unconfined Compressive Strength (MPa)	67	67	67	67	67
Q'	9.0	9.0	9.0	9.0	9.0
RQD	73.0	73.0	73.0	73.0	73.0
J_r	1.1	1.1	1.1	1.1	1.1
J_a	1.0	1.0	1.0	1.0	1.0
J_n	9.0	9.0	9.0	9.0	9.0
Jw	1.0	1.0	1.0	1.0	1.0
A Factor	0.1	0.1	0.1	0.1	0.1
B Factor	0.2	0.2	0.5	0.85	0.25
C Factor	5.8	6.1	8	8	2
N' Stability Number	1.0	1.1	3.6	6.1	0.5
Hydraulic Radius (m)	3.7	3.8	2.5	3.7	2.4
Peridotite Concentration (%)	66	51	61	35	-
Surface Condition	Stable	Stable	Stable	Stable	Unstable
Exposure Time	> 1 day	> 1 day	> 1 day	> 1 day	< 1 day

Table C.2 30-848.1 Rock Mass Classification Data

30-848.1 (Raise Failure)	N. Shoulder	S. Shoulder	Hanging Wall	Footwall	Back	Raisebore
Critical Joint Orientation (^{o})	81	81	81	81	8	81
Maximum Induced Stress (MPa)	74	63	82	78	91	74
Unconfined Compressive Strength (MPa)	67	67	67	67	67	67
Q'	9.3	9.3	9.3	9.3	9.3	9.3
RQD	70.0	73.0	73.0	73.0	73.0	73.0
J_r	1.2	1.2	1.2	1.2	1.2	1.2
J_a	1.0	1.0	1.0	1.0	1.0	1.0
J_n	9.0	9.0	9.0	9.0	9.0	9.0
Jw	1.0	1.0	1.0	1.0	1.0	1.0
A Factor	0.1	0.1	0.1	0.1	0.1	0.1
B Factor	0.3	0.3	0.2	0.2	0.2	0.2
C Factor	7.1	7.1	8	8	2	8
N' Stability Number	2.0	2.0	1.5	1.5	0.4	1.5
Hydraulic Radius (m)	4.3	3.5	3.7	3.5	3.2	1.7
Peridotite Concentration (%)	-	-	-	-	-	-
Surface Condition	Stable	Stable	Stable	Stable	Stable	Unstable
Exposure Time	> 3 days	> 3 days	> 3 days	> 3 days	> 3 days	< 3 days

Table C.3 32-872.1 Rock Mass Classification Data

32-872.1	N. Shoulder	S. Shoulder	Hanging Wall	Footwall	Back
Critical Joint Orientation (^{o})	81	75	75	81	22
Maximum Induced Stress (MPa)	66	66	83	72	104
Unconfined Compressive Strength (MPa)	67	67	67	67	67
Q'	7.0	7.0	7.0	7.0	7.0
RQD	49.0	49.0	49.0	49.0	49.0
J_r	1.3	1.3	1.3	1.3	1.3
J_a	1.0	1.0	1.0	1.0	1.0
J_n	9.0	9.0	9.0	9.0	9.0
Jw	1.0	1.0	1.0	1.0	1.0
A Factor	0.1	0.1	0.1	0.1	0.1
B Factor	0.02	0.3	0.25	0.2	0.2
C Factor	5.8	6.3	6.1	8	2
N' Stability Number	0.8	1.3	1.1	1.1	0.3
Hydraulic Radius (m)	2.8	3.9	3.2	3.3	2.4
Peridotite Concentration (%)	40	68	56	64	-
Surface Condition	Stable	Unstable	Stable	Stable	Stable
Exposure Time	> 3days	< 3days	> 3days	> 3days	> 3days

Table C.4 33-840.1 Rock Mass Classification Data

33-840.1	N. Shoulder	S. Shoulder	Hanging Wall	Footwall	Back
Critical Joint Orientation (^{o})	71	61	71	59	59
Maximum Induced Stress (MPa)	60	62	58	57	103
Unconfined Compressive Strength (MPa)	67	67	67	67	67
Q'	9.1	9.1	9.1	9.1	9.1
RQD	63.0	63.0	63.0	63.0	63.0
J_r	1.3	1.3	1.3	1.3	1.3
J_a	1.0	1.0	1.0	1.0	1.0
J_n	9.0	9.0	9.0	9.0	9.0
Jw	1.0	1.0	1.0	1.0	1.0
A Factor	0.1	0.1	0.1	0.1	0.1
B Factor	0.3	0.2	0.2	0.2	0.8
C Factor	6.2	6.5	8	8	2
N' Stability Number	1.7	1.2	1.5	1.5	1.5
Hydraulic Radius (m)	3.1	3.2	3.7	4.3	2.9
Peridotite Concentration (%)	27	43	28	41	-
Surface Condition	Stable	Unstable	Stable	Unstable	Stable
Exposure Time	> 1 day	< 1 day	> 1 day	> 1 day	> 1 day

Table C.5 33-848.1 Rock Mass Classification Data

33-848.1	N. Shoulder	S. Shoulder	Hanging Wall	Footwall	Back
Critical Joint Orientation (^{o})	71	61	71	59	59
Maximum Induced Stress (MPa)	75	52	75	93	125
Unconfined Compressive Strength (MPa)	67	67	67	67	67
Q'	9.5	9.5	9.5	9.5	9.5
RQD	66.0	66.0	66.0	66.0	66.0
J_r	1.3	1.3	1.3	1.3	1.3
J_a	1.0	1.0	1.0	1.0	1.0
J_n	9.0	9.0	9.0	9.0	9.0
Jw	1.0	1.0	1.0	1.0	1.0
A Factor	0.1	0.1	0.1	0.1	0.1
B Factor	0.2	0.2	0.2	0.2	0.8
C Factor	5.2	6.5	8	8	2
N' Stability Number	1.0	1.2	1.5	1.5	1.5
Hydraulic Radius (m)	2.6	2.7	2.7	3.4	2.5
Peridotite Concentration (%)	61	66	33	51	-
Surface Condition	Stable	Stable	Stable	Unstable	Stable
Exposure Time	> 1 day	> 1 day	> 1 day	< 1 day	> 1 day

Table C.6 33-848.2 Rock Mass Classification Data

33-848.2	N. Shoulder	S. Shoulder	Hanging Wall	Footwall	Back
Critical Joint Orientation (^{o})	71	61	71	59	59
Maximum Induced Stress (MPa)	51	53	0	94	127
Unconfined Compressive Strength (MPa)	67	67	67	67	67
Q'	6.5	6.5	6.5	6.5	6.5
RQD	45.0	45.0	45.0	45.0	45.0
J_r	1.3	1.3	1.3	1.3	1.3
J_a	1.0	1.0	1.0	1.0	1.0
J_n	9.0	9.0	9.0	9.0	9.0
Jw	1.0	1.0	1.0	1.0	1.0
A Factor	0.1	0.1	1	0.1	0.1
B Factor	0.3	0.2	0.2	0.2	0.8
C Factor	6	6.9	8	8	2
N' Stability Number	1.2	0.9	10.4	1.0	1.0
Hydraulic Radius (m)	3.8	3.6	3.1	2.8	3.0
Peridotite Concentration (%)	55	70	-	28	-
Surface Condition	Stable	Stable	Stable	Stable	Unstable
Exposure Time	> 1 day	> 1 day	> 1 day	> 1 day	< 1 day

Table C.7 33-936.2 Rock Mass Classification Data

33-936.2	N. Shoulder	S. Shoulder	Hanging Wall	Footwall	Back
Critical Joint Orientation (^{o})	70	63	59	59	10
Maximum Induced Stress (MPa)	92	123	35	35	87
Unconfined Compressive Strength (MPa)	67	67	67	67	67
Q'	12.9	12.9	12.9	12.9	12.9
RQD	58.0	58.0	58.0	58.0	58.0
J_r	2.0	2.0	2.0	2.0	2.0
J_a	1.0	1.0	1.0	1.0	1.0
J_n	9.0	9.0	9.0	9.0	9.0
Jw	1.0	1.0	1.0	1.0	1.0
A Factor	0.1	0.1	0.1	0.1	0.1
B Factor	0.25	0.23	0.2	0.2	0.2
C Factor	6	5.8	5.9	5.9	2
N' Stability Number	1.9	1.7	1.5	1.5	0.5
Hydraulic Radius (m)	4.4	3.7	3.3	2.8	3.2
Peridotite Concentration (%)	-	-	-	-	-
Surface Condition	Stable	Stable	Stable	Stable	Unstable
Exposure Time	> 1 day	> 1 day	> 1 day	> 1 day	< 1 day

Table C.8 33-916.2 Rock Mass Classification Data

33-916.2	N. Shoulder	S. Shoulder	Hanging Wall	Footwall	Back
Critical Joint Orientation (^{o})	71	61	71	59	59
Maximum Induced Stress (MPa)	200	152	0	35	138
Unconfined Compressive Strength (MPa)	67	67	67	67	67
Q'	4.8	4.8	4.8	4.8	4.8
RQD	33.0	33.0	33.0	33.0	33.0
J_r	1.3	1.3	1.3	1.3	1.3
J_a	1.0	1.0	1.0	1.0	1.0
J_n	9.0	9.0	9.0	9.0	9.0
Jw	1.0	1.0	1.0	1.0	1.0
A Factor	0.1	0.1	1.0	0.1	0.1
B Factor	0.3	0.2	0.2	0.2	0.8
C Factor	6.0	5.8	8.0	8.0	2.0
N' Stability Number	0.9	0.6	7.6	0.8	0.8
Hydraulic Radius (m)	3.3	3.2	3.4	3.5	3.2
Peridotite Concentration (%)	-	-	-	-	-
Surface Condition	Unstable	Stable	Stable	Stable	Stable
Exposure Time	< 6 days	> 6 days	> 6 days	> 6 days	> 6 days

Table C.9 32-928.1 Rock Mass Classification Data

32-928.1	N. Shoulder	S. Shoulder	Hanging Wall	Footwall	Back
Critical Joint Orientation (^{o})	81	75	81	81	20
Maximum Induced Stress (MPa)	75	79	68	68	79
Unconfined Compressive Strength (MPa)	67	67	67	67	67
Q'	9.0	9.0	9.0	9.0	9.0
RQD	60.0	60.0	60.0	60.0	60.0
J_r	1.3	1.3	1.3	1.3	1.3
J_a	1.0	1.0	1.0	1.0	1.0
J_n	9.0	9.0	9.0	9.0	9.0
Jw	1.0	1.0	1.0	1.0	1.0
A Factor	0.1	0.1	0.1	0.1	0.1
B Factor	0.25	0.3	0.3	0.2	0.2
C Factor	6.5	6.4	7.2	7.2	2.0
N' Stability Number	1.5	1.7	1.9	1.3	0.4
Hydraulic Radius (m)	3.2	2.8	2.1	3.5	2.5
Peridotite Concentration (%)	2.0	14	4.0	22	-
Surface Condition	Stable	Stable	Stable	Stable	Stable
Exposure Time	> 16 days	> 16 days	> 16 days	> 16 days	> 16 days

Table C.10 33-916.3 Rock Mass Classification Data

33-916.3	N. Shoulder	S. Shoulder	Hanging Wall	Footwall	Back
Critical Joint Orientation (^{o})	81	75	75	81	22
Maximum Induced Stress (MPa)	125	100	0	45	125
Unconfined Compressive Strength (MPa)	67	67	-	67	67
Q'	7.0	7.0	-	7.0	7.0
RQD	48.0	48.0	-	48.0	48.0
J_r	1.3	1.3	-	1.3	1.3
J_a	1.0	1.0	-	1.0	1.0
J_n	9.0	9.0	-	9.0	9.0
Jw	1.0	1.0	-	1.0	1.0
A Factor	0.1	0.1	-	0.1	0.1
B Factor	0.2	0.2	-	0.3	0.3
C Factor	4.5	5.3	-	8.0	2.0
N' Stability Number	0.6	0.7	-	1.6	0.4
Hydraulic Radius (m)	2.9	2.3	3.6	4.1	3.0
Peridotite Concentration (%)	33.0	39	55.0	8.0	-
Surface Condition	Stable	Stable	Stable	Stable	Stable
Exposure Time	> 10 days	> 10 days	> 10 days	> 10 days	> 10 days